PL-TR--
94-1044

ADVANCED REGENERATORS FOR VERY LOW TEMPERATURE CRYOCOOLERS

Woody Ellison

General Pneumatics Corporation
Western Research Center
7662 E. Gray Road, Suite 107
Scottsdale, AZ 95260-6910

February 1994

Final Report

PHILLIPS LABORATORY
Space and Missiles Technology Directorate
AIR FORCE MATERIEL COMMAND
KIRTLAND AIR FORCE BASE, NM 87117-5776

AD NUMBER

AD-B205 138

NEW LIMITATION CHANGE

TO

DISTRIBUTION STATEMENT A -
Approved for public release; Distribution unlimited.

Limitation Code: 1

FROM

DISTRIBUTION STATEMENT -

Limitation Code:

AUTHORITY

Janet E. Mosher, Phillips Lab., Kirtland AFB, N.M.

PL-TR-94-1044

This final report was prepared by General Pneumatics Corporation, Scottsdale, AZ, under Contract F29601-93-C-0085 Job Order, 9991SBIR, with Phillips Laboratory, Kirtland Air Force Base, New Mexico. The Laboratory Project Officer-in-Charge was Brian Whitney, (VTPT).

If your address has changed, if you wish to be removed from the mailing list, or if your organization no longer employs the addressee, please notify PL/VTPT, 3550 Aberdeen Ave SE, Kirtland AFB, NM 87117-5776 to help maintain a current mailing list.

This report has been reviewed and is approved for publication.

BRIAN WHITNEY
Project Officer

FOR THE COMMANDER

DAVID KRISTENSEN, Lt Col, USAF
Chief, Space Power and Thermal Management Division

HENRY L. PUGH, JR., Col, USAF
Director of Space and Missiles Technology

DO NOT RETURN COPIES OF THIS REPORT UNLESS CONTRACTUAL OBLIGATIONS OR NOTICE ON A SPECIFIC DOCUMENT REQUIRES THAT IT BE RETURNED.

The following notice applies to any unclassified (including originally classified and now declassified) technical reports released to "qualified U.S. contractors" under the provisions of DoD Directive 5230.25, Withholding of Unclassified Technical Data From Public Disclosure.

NOTICE TO ACCOMPANY THE DISSEMINATION OF EXPORT-CONTROLLED TECHNICAL DATA

1. Export of information contained herein, which includes, in some circumstances, release to foreign nationals within the United States, without first obtaining approval or license from the Department of State for items controlled by the International Traffic in Arms Regulations (ITAR), or the Department of Commerce for items controlled by the Export Administration Regulations (EAR), may constitute a violation of law.

2. Under 22 U.S.C. 2778 the penalty for unlawful export of items or information controlled under the ITAR is up to two years imprisonment, or a fine of $100,000, or both. Under 50 U.S.C., Appendix 2410, the penalty for unlawful export of items or information controlled under the EAR is a fine of up to $1,000,000, or five times the value of the exports, whichever is greater; or for an individual, imprisonment of up to 10 years, or a fine of up to $250,000, or both.

3. In accordance with your certification that establishes you as a "qualified U.S. Contractor", unauthorized dissemination of this information is prohibited and may result in disqualification as a qualified U.S. contractor, and may be considered in determining your eligibility for future contracts with the Department of Defense.

4. The U.S. Government assumes no liability for direct patent infringement, or contributory patent infringement or misuse of technical data.

5. The U.S. Government does not warrant the adequacy, accuracy, currency, or completeness of the technical data.

6. The U.S. Government assumes no liability for loss, damage, or injury resulting from manufacture or use for any purpose of any product, article, system, or material involving reliance upon any or all technical data furnished in response to the request for technical data.

7. If the technical data furnished by the Government will be used for commercial manufacturing or other profit potential, a license for such use may be necessary. Any payments made in support of the request for data do not include or involve any license rights.

8. A copy of this notice shall be provided with any partial or complete reproduction of these data that are provided to qualified U.S. contractors.

D E S T R U C T I O N N O T I C E

For classified documents, follow the procedures in DoD 5200.22-M, Industrial Security Manual, Section II-19 or DoD 5200.1-R, Information Security Program Regulation, Chapter IX. For unclassified, limited documents, destroy by any method that will prevent disclosure of contents or reconstruction of the document.

DRAFT SF 298

1. Report Date (dd-mm-yy) February 1994	2. Report Type Final	3. Dates covered (from... to) 4/93 to 11/93
4. Title & subtitle Advanced Regenerators for Very Low Temperature Cryocoolers		5a. Contract or Grant # F29601-93-C-0085
		5b. Program Element # 62601F
6. Author(s) Woody Ellison		5c. Project # 9991
		5d. Task # SB
		5e. Work Unit # 1R
7. Performing Organization Name & Address General Pneumatics Corporation Western Research Center 7662 E. Gray Road, Suite 107 Scottsdale, AZ 95260-6910		8. Performing Organization Report # 8427W
9. Sponsoring/Monitoring Agency Name & Address Phillips Laboratory 3550 Aberdeen Ave SE Kirtland AFB, NM 87117-5776		10. Monitor Acronym
		11. Monitor Report # PL-TR-94-1044

12. Distribution/Availability Statement
Distribution authorized to DoD components only; Proprietary Information; February 1994. Other requests shall be referred to AFMC/STI.

13. Supplementary Notes

14. Abstract This SBIR project is Phase I in the development of a new form of high effectiveness regenerators which are critically needed to develop efficient, long-life cryocoolers for producing temperatures to below 10 K. Regenerator ineffectiveness can overwhelmingly increase required drive power and impose limits on highest operating speed and lowest refrigeration temperature. Due to the fundamental nature of matter and heat, current regenerators do not allow cryocoolers to operate new 10 K at speeds above 5 to 10 Hz. Increase in regenerator effectiveness would allow increase in operating speed and reductions in machine power consumption, size, and drive loads. Higher operating speed is essential to employing flexure suspension, linear drive systems for prolonged operating life. This Phase I research defines the analytical modeling, thermofluid trade-offs, material properties, production and test methods, and feasibility for developing regenerators for higher effectiveness and operating speed in 10 K cryocoolers. These results provide the basis for the design, fabrication, and testing of prototype regenerators in Phase II of the development.

15. Subject Terms Cryocooler, Stirling, Regenerator, effectiveness, enthalpy, heat capacity, diffusivity, porosity

Security Classification of			19. Limitation of Abstract	20. # of Pages	21. Responsible Person (Name and Telephone #)
16. Report Unclassified	17. Abstract Unclassified	18. This Page Unclassified	Limited	116	Brian Whitney (505) 846-1867

GOVERNMENT PURPOSE LICENSE RIGHTS
(SBIR PROGRAM)

Contract Number: F29601-93-C-0085
Contractor: General Pneumatics Corporation
Western Research Center
Scottsdale, AZ

For a period of four (4) years after delivery and acceptance of the last deliverable item under the above contract, this technical data shall be subject to the restrictions contained in the definition of "Limited Rights" in DFARS clause at 252.227-7013. After the four-year period, the data shall be subject to the restrictions contained in the definition of "Government Purpose License Rights" in DFARS clause at 252.227-7013. The Government assumes no liability for unauthorized use or disclosure by others. This legend shall be included on any reproduction thereof and shall be honored only as long as the data continues to meet the definition on Government purpose license rights.

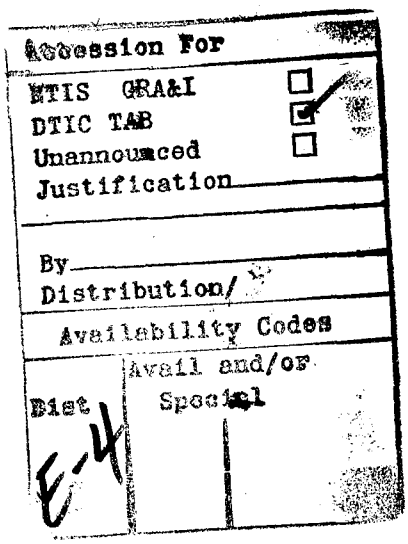

PROJECT SUMMARY

The subject Small Business Innovation Research project is Phase I in the development of a new form of high effectiveness regenerators which are critically needed to develop efficient, long-life cryocoolers for producing temperatures to below 10 K, such as for spaceborne instrumentation. The best current 10 K cryocoolers are impractically large, inefficient, and unreliable for aerospace applications. This is largely due to fundamental problems with regenerator ineffectiveness at very low temperatures.

High regenerator effectiveness is critical to optimizing the power, speed, weight, size, and service life of Stirling cryocoolers, and, even with multiple stages, is essential to reaching temperatures much below 65 K. Regenerator ineffectiveness can overwhelmingly increase required drive power and impose limits on highest operating speed and lowest refrigeration temperature. Increase in the currently achievable effectiveness of regenerators for 10 K cryocoolers would allow increase in operating speed and reductions in machine power consumption, size, and drive loads. Higher operating speed is essential to employing flexure suspension, linear drive systems for prolonged operating life.

Regenerator ineffectiveness results from deficient heat transfer between the matrix and the working fluid due to insufficient matrix heat capacity or heat transport rate, and heat dissipation due to compression/expansion of working fluid in the regenerator void volume. Heat flow resulting from regenerator ineffectiveness directly subtracts from the refrigeration produced in a cryocooler, thereby necessitating a larger machine and greater power input for a given amount of refrigeration. Regenerators must trade flow restriction, axial heat conduction, and void volume for adequate heat transfer and storage capacity. These parameters are intimately interrelated and must be carefully balanced to minimize ineffectiveness and other parasitic losses.

The heat capacity and conductivity of solids fall off steeply while gas density rises with decreasing temperature below 100 K, making it difficult to provide sufficient effective regenerator heat capacity and necessitating a slow operating speed. Due to the fundamental nature of matter and heat, known regenerator materials and forms do not allow cryocoolers to operate near 10 K at speeds above 5 to 10 Hz, and thus preclude employing linear resonant drives and nonrubbing piston suspensions and seals for prolonged service.

The Phase I research reported herein defines the analytical modeling, thermofluid trade-offs, material properties, production and test methods, and feasibility for developing a new type of regenerator for higher effectiveness and operating speed in very low temperature cryocoolers. These results provide the basis and methods for the design, fabrication, and testing of prototype regenerators in Phase II of the development.

ACKNOWLEDGEMENT

The work reported herein was carried out at the Western Research Center of General Pneumatics Corporation, Scottsdale, Arizona during the period April 1993 through November 1993. The work was performed under a Small Business Innovation Research (SBIR) Phase I contact, F29601-93-C-0085, sponsored by the Strategic Defense Initiative Organization (now Ballistic Missile Defense Organization), and monitored by the Air Force Phillips Laboratory.

The analyses of very low temperature cryocooler regenerator requirements presented in Appendix II were performed for this project by Dr. Ray Radebaugh of the National Institute of Standards and Technology, Boulder, Colorado.

The analyses of the very low temperature thermal properties of fullerenes reported in Appendix III were conducted for this project by Drs. John Page and Otto Sankey of Arizona State University, Tempe, Arizona.

The discussions of technology and methods for producing and testing candidate fullerenes described in Appendix IV were prepared for this project by Drs. Tapesh Yadav and Prakash Arya of the Materials and Electrochemical Research Corporation, Tucson, Arizona.

We also wish to gratefully acknowledge the ongoing consultation from Dr. Donald Huffman of the University of Arizona, Tucson, who is one of the foremost pioneers in the research and synthesis of fullerenes.

USE AND EXPRESSION OF UNITS

The values in this report are expressed primarily in the International System of Units (SI) and customary units are provided in parentheses as appropriate for clarity.

CERTIFICATION OF TECHNICAL DATA CONFORMITY

The contractor, General Pneumatics Corporation, Western Research Center, hereby certifies that, to the best of its knowledge and belief, the technical data delivered herein under contract F29601-93-C-0085 is complete, accurate, and complies with all requirements of the contract.

17 February 1994
Date

Steven G. Zylstra, General Manager,
Western Research Center

CONTENTS

NOMENCLATURE

Symbol	Definition	Units
A_g	gas flow cross-section area	m^2
A_{ht}	total gas-to-matrix ('wetted') heat transfer area	m^2
A_m	matrix material cross-section area	m^2
Al	aluminum	----
c_m	matrix specific heat	J/kg·K
c_p	gas constant pressure specific heat	J/kg·K
c_v	gas constant volume specific heat	J/kg·K
C_g	gas heat capacity	J/K
C_m	matrix heat capacity	J/K
C_{60}	fullerene molecule of 60 carbon atoms	----
D	diameter	m
De	effective screen wire diameter = $L A_g/(A_g + A_m)$	m
F	flow friction factor	----
G	actual/ideal gross refrigeration	----
h_H	gas specific enthalpy at warm end of regenerator	J/kg
h_L	gas specific enthalpy at cold end of regenerator	J/kg
h_{HTHP}	gas specific enthalpy at high temperature, high pressure	J/kg
h_{HTLP}	gas specific enthalpy at high temperature, low pressure	J/kg
h_{LTHP}	gas specific enthalpy at low temperature, high pressure	J/kg
h_{LTLP}	gas specific enthalpy at low temperature, low pressure	J/kg
H_T	gas-to-matrix heat transfer coefficient	$W/m_2·K$
i	regenerator inefficiency = $1 - \epsilon$	----
k_a	matrix axial thermal conductivity	W/m·K
k_g	gas thermal conductivity	W/m·K
k_m	matrix material conductivity	W/m·K
K	temperature on Kelvin scale, or potassium	----

NOMENCLATURE (CONT'D)

Symbol	Definition	Units
L	regenerator length along flow axis	m
ℓn	natural logarithm	----
m	mass	kg
$\dot{m}_a$	gas cyclic mass flow rate amplitude	kg/s
$\dot{m}_H$	gas mass flow rate at warm end of regenerator	kg/s
$\dot{m}_L$	gas mass flow rate at cold end of regenerator	kg/s
m_{ge}	gas mass displacement of expansion space	kg
m_{gr}	gas mass displaced through regenerator	kg
Mg	magnesium	----
Na	sodium	----
P	pressure	Pa
P_a	pressure cycle amplitude	Pa
P_H	pressure cycle maximum	Pa
P_L	pressure cycle minimum	Pa
P_o	pressure cycle average	Pa
Pr	Prandtl number = $\mu c_P/k$	----
ΔP	pressure change	Pa
PC	power coefficient = input power per unit gross refrigeration	----
PC_c	Carnot power coefficient = $(T_H - T_L)/T_L$	----
PC_3	Carnot power coefficient for each of 3 equal stages	----
PC_{1e}	equivalent power coefficient for single stage	----
PC_{3e}	effective power coefficient for each of 3 equal stages	----
$\dot{Q}_c$	conducted heat rate	W/s
Q_E	heat absorbed in expansion space	W
$\dot{Q}_P$	refrigeration rate reduction due to flow pressure loss	W/s
Q_R	heat exchanged in regenerator	W

NOMENCLATURE (CONT'D)

Symbol	Definition	Units
Q_{net}	refrigeration available after losses	W
r_h	hydraulic radius = LA_g/A_{int}	m
R	gas constant per unit mass	J/kg·K
Re	Reynolds number = $4\rho v r_h/\mu$	----
t	time	s
t_g	gas gap thickness	m
t_m	matrix material thickness	m
T	temperature	K
T_E	expansion space temperature	K
T_g	gas temperature	K
T_H	high temperature	K
T_L	low temperature	K
T_m	matrix temperature	K
T_o	temperature cycle average	K
T_{in}	gas temperature entering regenerator	K
T_{out}	gas temperature exiting regenerator	K
T_1	first-stage regenerator cold-end temperature	K
T_2	second-stage regenerator cold-end temperature	K
ΔT	temperature change	K
ΔT_m	matrix temperature change	K
U	internal energy	J
v	velocity	m/s
V_E	expansion space volume displacement	m^3
V_m	matrix material volume = LA_m	m^3
V_{rg}	regenerator gas (void) volume = LA_g	m^3
δ_t	thermal penetration depth = $(2\ k_m/\rho_m c_m \omega)^{1/2}$	m

NOMENCLATURE (CONT'D)

Symbol	Definition	Units
ϵ	regenerator effectiveness = actual/perfect heat exchange	----
μ	gas dynamic viscosity (Pa·s)	kg/m·s
θ	pressure cycle phase angle	rad
ϕ	temperature cycle phase angle	rad
ω	angular frequency	rad/s
π	geometric constant pi	----
ρ_g	gas density	kg/m^3
ρ_m	matrix material density	kg/m^3

1.0 INTRODUCTION

Currently the mission lives of spacecraft requiring cryogenic cooling for instrumentation are seriously limited by dependence on stored cryogens such as liquid helium. Cryocoolers capable of 5 to 10 years of continuous orbital operation are needed to cool the focal planes, optics, baffles, etc., of infrared sensor systems. But the power, weight, size, and life penalties of current 10 K cryocoolers are prohibitive for spacecraft applications. Development of compact, lightweight, power efficient, high reliability, long life cryocoolers capable of producing temperatures down to 10 K while rejecting heat at temperatures in the range of 300 K has become a critically pacing technology.

Proposals for new and innovative approaches for cryogenic cooling of space-based sensors and their associated systems were invited under Topic No. SDIO93-003, Sensors, in the Department of Defense Small Business Innovation Research Program Solicitation 93.1. In response, research was proposed to employ the new carbon materials, fullerenes, in an innovative concept for high effectiveness regenerative heat exchangers which are critically needed to develop efficient cryocoolers for operation at temperatures of 10 K and below, such as for spaceborne instrumentation. Phase I of the subject research was to analyze the potential thermofluid properties of candidate forms of fullerenes as related to the feasibility and prospective advantages of using them in high effectiveness regenerators for Stirling cryorefrigerators, and to define methods for producing and testing candidate materials and representative regenerators in Phase II. Phase I was conducted under Contract F29601-93-C-0085 (effective April 23, 1993) administered by the Directorate of Space and Missile Technology of the Air Force Phillips Laboratory, and is reported herein.

2.0 STIRLING CRYOCOOLERS

The Carnot cycle defines the theoretic minimum work required per unit of refrigeration, which is equal to $(T_H - T_L)/T_L$ where T_H and T_L are, respectively, the cycle maximum

(sink) and minimum (refrigeration) absolute temperatures. However, the Carnot cycle is an unimplementable mathematical ideal. The cycle most closely approaching the performance of the Carnot cycle, upon which to base a cryorefrigerator with a sink temperature in the range of 300 K, is the Stirling cycle.

Progressively smaller, lighter Stirling cryocoolers have been developed over the past 40 years, principally for infrared night vision equipment and missile guidance systems requiring cooling in the range of 80 K. In competition with many other types of cryocoolers, including Vuilleumier, Linde-Hampson, Brayton, Claude, Gifford-McMahon, and Solvay, Stirling cryocoolers have emerged as the choice for small systems, being smaller, lighter, lower in cost, and more efficient.

Recently, a new generation of miniature Stirling cryocoolers, typified by the Oxford cryocooler (Bib. 18) and the Standard Spacecraft Cooler, has been developed employing nonrubbing clearance seals, flexure suspensions, and resonant linear motors for greatly improved life and reliability. But there are fundamental problems in reaching temperatures much below 65 K with these machines.

3.0 REGENERATORS

3.1 Function

A regenerator cyclically absorbs heat from and releases heat back to the working fluid. In the ideal Stirling refrigeration cycle, diagrammed in Figure 1 of Appendix I, the working fluid takes on heat at constant volume as it passes through a regenerator from a cold expansion space to a warmer compression space. Heat is rejected from the system by isothermal compression in the compression space. The working fluid then passes back through the regenerator for constant volume regenerative cooling. Heat is stored in the regenerator for transport out in the next cycle. Finally, refrigeration occurs by isothermal expansion in the expansion space where heat is absorbed by the working fluid.

In a real Stirling machine the flow surges back and forth so that little or none of the working fluid (typically helium) passes completely through the regenerator matrix. This, combined with the axial temperature gradient, complicates the energy flows so the incremental details are not well understood and theories of regenerator operation in Stirling machines are highly idealized. It is common, for example, to assume a linear axial temperature gradient and to ignore the local temperature variations in both matrix and gas that must occur. Ideally, the regenerator should have high heat capacity and heat transport capabilities such that heat exchange with the helium working fluid at a high rate does not cause significant temperature fluctuation in the regenerator. Also, the regenerator should introduce minimal axial heat conduction, flow restriction, void (compressible gas) volume, and clogging susceptibility in the helium flow path. Void volume is volume in the working space, e.g., in the heat exchangers, which does not vary cyclically and therefore reduces compression ratio while causing power losses due to heat flows resulting from compression and expansion of the gas in the void. For ideal Stirling machines, void volume increases the size required for a given power or refrigeration capacity by reducing the cycle pressure ratio but does not reduce the power efficiency or coefficient of performance below the Carnot value. In real Stirling machines, void volume causes thermal and pressure power losses.

Regenerator ineffectiveness results from deficient heat transfer between the matrix and the working fluid due to insufficient matrix heat capacity or heat transport rate, and heat dissipation due to compression/expansion of working fluid in the regenerator void volume. Heat flow resulting from regenerator ineffectiveness directly subtracts from the refrigeration produced in a cryocooler, thereby necessitating a larger machine and greater power input for a given amount of refrigeration. The requirement for a larger machine compounds the reduction in power efficiency by proportionately increasing the void volume and heat transfer losses.

Conventional regenerators have contained stacked fine wire mesh, coiled foil, porous sintered powder, or, in the coldest stages, snugly packed lead/antimony microspheres. Heat capacity is a serious problem in very low temperature regenerators because the specific heat and thermal conductivity of solids decrease with temperature while density remains constant, whereas the specific heat and density of helium increase with decreasing temperature. This makes it very difficult to effectively couple enough regenerator heat capacity to the helium working fluid. The specific heat capacity of materials falls off steeply with decreasing temperature below 100 K. This is due to the inherent decrease, with temperature, in lattice vibration energy, which is the primary form of thermal energy, and to a lesser degree in electron energy. Thus, as atomic freedom is diminished by decreasing temperature, so is a material's capacity to store thermal energy. As depicted in Figure 2 of Appendix I, a few materials undergo magnetic moment transitions in internal energy over narrow temperature changes below 20 K, which has the effect of a spike in heat capacity. Because such transitions occur over only a few degrees in temperature change, they are of limited value in providing a small supplemental heat capacity. Various combinations of these magnetic transition compounds are being researched for very cold regenerators but offer marginal benefits and are very difficult to produce in suitable forms, quantities, or uniformity.

Helium at only 1 MPa pressure has a higher specific heat capacity than virtually all other materials below 12 K. For size and weight practicality, cryocoolers typically have helium charge pressures of 1 to 2 MPa. Consequently, a relatively large amount of regenerator material is required to provide more heat capacity than the helium working fluid itself. Adding regenerator material creates problems with flow restriction, void volume, axial conduction losses, and time required to transfer heat into and out of the regenerator matrix. The last factor necessitates a low flow rate which, in Stirling machines, results in slow operating speed and high drive mechanism loads for a given power level (torque x rad/sec).

Currently, 10 K cryocoolers are limited to operating speeds in the range of 0.5 to 5 Hz and consequently weigh several hundred kilograms and require 1.5 kW or more of power per watt of refrigeration, because of the very poor effective heat capacity and transport rate of conventional regenerators. In contrast, 80 K cryocoolers operate at speeds of 30 to 60 Hz and weigh on the order of a kilogram per watt of refrigeration. Increases in the effectiveness of regenerators for 10 K cryocoolers would allow proportionate increases in operating speed, which would allow more than proportionate reduction in machine size and weight, since parasitic losses also decrease with machine size.

Since refrigeration is produced in proportion to the rate of doing work, operation at higher speed and power efficiency corresponds with much lower drive forces and bearing loads. Higher operating speed is also essential to employing flexure suspension, linear resonant drive systems, which require very short strokes of less that 1 mm (for flexure life) and resonant operating frequency in the range of 30 to 60 Hz (for weight and power efficiency). Such systems have been found to be key to extending the operating life of 80 K cryocoolers from a few 1000s of hours to several 10,000s of hours.

3.2 Effectiveness

The heat absorbed (gross refrigeration produced) Q_E by isothermal expansion of mass m_{ge} of an ideal gas from high pressure P_H to low pressure P_L at expansion temperature T_E is

$$Q_E = m_{ge} R T_E \ell n (P_H/P_L).$$

In real Stirling machines, expansion and compression are due to sinusoidal volume changes and are not purely isothermal, which reduces Q_E by the product of factors of 0.6 to 0.8 and approximately 0.5, respectively, so that

$$Q_E = G\, m_{ge} R T_E \ell n\, (P_H/P_L)$$

where G is approximately 0.3 to 0.4.

Ideally, the heat Q_R exchanged in a regenerator by a mass m_{gr} of gas with constant specific heat c_p passing through between high temperature T_H and low temperature T_L is

$$Q_R = m_{gr}\, c_p\, (T_H - T_L).$$

If $m_{gr} = m_{ge}$ (i.e., there is no void volume) and $T_L = T_E$, then the ratio of heat cycled in the regenerator per unit of gross refrigeration produced is

$$\frac{Q_R}{Q_E} = \frac{c_p (T_H - T_E)}{G\, R T_E \ell n\, (P_H/P_L)}.$$

Noting that the gas constant $R = c_p - c_v$, where c_p and c_v are the gas specific heats at constant pressure and constant volume, respectively, then

$$\frac{Q_R}{Q_E} = \left(\frac{c_p}{c_p - c_v}\right)\left(\frac{T_H - T_E}{T_E}\right) / \; G \ell n\, (P_H/P_L).$$

For helium, $c_p/(c_p - c_v)$ is approximately 2.5 for temperatures from about 300 K to below 30 K, and typically for Stirling refrigerators, P_H/P_L is approximately 2 and G is approximately 0.36, so that

$$\frac{Q_R}{Q_E} = 10 \left(\frac{T_H - T_E}{T_E}\right).$$

Thus, with a heat sink temperature $T_H = 300$ K, the ratio of heat cycled in a perfect regenerator per unit of gross refrigeration produced at temperature T_E is 27.5 at 80 K, 140 at 20 K, and 290 at 10 K. (The values given in Appendix I are from an idealized Schmidt analysis which did not correct for nonisothermal expansion.)

Regenerator effectiveness is defined as

$$\epsilon = \frac{actual\ heat\ exchange}{perfect\ heat\ exchange} = \frac{Q_R\ actual}{Q_R\ maximum}.$$

Since c_p for real gases varies with temperature and pressure, for alternating flows of m_{gr} at different pressures, P_H and P_L, between fixed temperatures, T_H and T_L, the maximum heat available for exchange is $m_{gr}\ c_p\ (T_H - T_L)$ for the flow with the lower overall c_p.

Regenerator ineffectiveness, the relative heat exchange deficiency, is

$$1 - \epsilon = \frac{Q_R\ maximum - Q_R\ actual}{Q_R\ maximum}.$$

The heat not transferred, due to regenerator ineffectiveness, directly subtracts from the gross refrigeration produced. The net possible refrigeration available is then

$$Q_{net} = Q_E - (1 - \epsilon)\, Q_{R,max} = Q_E \left[1 - (1 - \epsilon) \frac{Q_{R,max}}{Q_E}\right].$$

For $Q_R/Q_E = 10(T_H - T_E)/T_E$ as previously derived,

$$Q_{net} = Q_E \left[1 - (1 - \epsilon)\, 10 \left(\frac{T_H - T_E}{T_E}\right)\right].$$

The minimum effectiveness required for a regenerator to reach from T_H = 300 K to T_E (at which Q_{net} = 0) is 0.964 for 80 K, 0.993 for 20 K, and 0.997 for 10 K. As the lowest achievable temperature for a given regenerator effectiveness is approached, the net available refrigeration diminishes to zero and the power input required per unit of useful refrigeration increases prohibitively. It is therefore evident why single-stage

Stirling cryocoolers operating with a heat sink near 300 K do not reach much below 65 K.

3.3 Multiple Stages

Stirling cryocoolers with multiple stages of expansion spaces and regenerators can reach temperatures near 10 K from 300 K, although with very high power input required per unit of net refrigeration. Multiple stages reduce the regenerator effectiveness required as follows.

Designate power input required per unit of refrigeration as the power coefficient PC. Between temperatures T_H and T_L, the Carnot power coefficient is $PC_C = (T_H - T_L)/T_L$.

Choose T_1 and T_2 to be intermediate temperatures between T_H and T_L such that there are 3 stages of equal PC_Cs:

$$\frac{T_H - T_1}{T_1} = \frac{T_1 - T_2}{T_2} = \frac{T_2 - T_L}{T_L}$$

$$T_2 (T_H - T_1) = T_1 (T_1 - T_2) \longrightarrow T_1^2 = T_2 T_H$$
$$T_L (T_1 - T_2) = T_2 (T_2 - T_L) \longrightarrow T_2^2 = T_1 T_L$$
$$T_1^4 = T_2^2 T_H^2 = T_1 T_L T_H^2 \longrightarrow T_1^3 = T_L T_H^2$$
$$T_2^4 = T_1^2 T_L^2 = T_2 T_H T_L^2 \longrightarrow T_2^3 = T_H T_L^2.$$

For T_H = 300 K and T_L = 10 K, T_1 = 96.55 K and T_2 = 31.07 K. The PC_C for 1 stage from 300 K to 10 K is (300 - 10)/10 = 29. The PC_C for each of 3 equal stages is (31.07-10)/10 = 2.107. Since these are all Carnot PCs, the heat loads and power inputs to the 3 stages must combine to equal 29, the PC_C for 1 stage from T_H to T_L.

Stage	Heat Load	x	PC_C	=	Power Input
10 K	1	x	2.107	=	2.107
31.07 K	(1 + 2.107)	x	2.107	=	6.546
96.55 K	(1 + 2.107 + 6.546)	x	2.107	=	20.339
	Total PC_C from 10 K to 300 K			=	28.992

From the above example, if $PC_1 = PC_C$ for the single stage, and PC_3 = the PC_C for each of 3 equal stages, then:

$$PC_1 = PC_3 (1) + PC_3 (1 + PC_3) + PC_3 [1 + PC_3 + PC_3 (1 + PC_3)]$$

$$PC_1 = 3\, PC_3 + 3\, PC_3^2 + PC_3^3.$$

Check: $3(2.107) + 3\,(2.107)^2 + (2.102)^3 = 28.993 \approx 29$ within rounding error.

Recall from Section 3.2, $Q_R/Q_E \approx 10(T_H - T_E)/T_E = 10\, PC_C$. If i = regenerator ineffectiveness, $(1 - \epsilon)$, then net refrigeration $Q_{net} = Q_E - iQ_R = Q_E\,(1 - i10PC_C)$, and (power input/$Q_{net}$) = $Q_E PC_C/Q_{net} = PC_C/(1 - i10PC_C)$.

For the maximum allowable i for a single stage from 300 K to 10 K, $(1 - i10PC_1) \geq 0$, $i \leq 1/10(29) = 0.0034$, $\epsilon \geq 1 - 0.0034 = 0.9966$. If $i = 0.003$, $\epsilon = 0.997$, then (power input/Q_{net}) = $29/[1 - 0.003(10)29] = 223$.

For each of the 3 stages of equal PCs from 300 K to 10 K, $(1 - i10PC_3) \geq 0$, $i \leq 1/10(2.107) = 0.047$, $\epsilon \geq 0.953$ (compared to allowable $i \leq 0.0034$, $\epsilon \geq 0.9966$ for the single stage). For each stage, (power input/Q_{net}) = $PC_3/1 - i10\, PC_3$), which is the effective PC per stage, PC_{3e}. The equivalent overall PC is $PC_{1e} = 3\, PC_{3e} + 3\, PC^2_{3e} + PC^3_{3e}$. For $i = 0.003$, $\epsilon = 0.997$, total (power input/Q_{net}) = $PC_{1e} = 33.3$ (compared to 223 for the single stage). For $i = 0.03$, $\epsilon = 0.97$, $PC_{1e} = 303$. For $i = 0.04$, $\epsilon = 0.96$, $PC_{1e} = 2987$.

It is apparent that as the maximum allowable ineffectiveness is approached, the power input required per unit net refrigeration (at T_L) increases rapidly. It can also be seen that ineffectiveness in the lower stages, where it is most difficult to minimize, compounds the heat load on upper stages, increasing the need for effectiveness in them.

The foregoing simplistic example of multiple stages is based on equal PC_Cs and ϵs among the stages and no other parasitic loads. It illustrates the greater regenerator ineffectiveness allowable in multiple stages compared to a single stage, although the allowance is still quite tight (0.047 maximum ineffectiveness or an overall effectiveness of about 0.96) to reach from 300 K to 10 K in 3 stages. Another major advantage of multiple stages is the interception of parasitic heat loads, such as conducted and radiated heat, before they get to lower temperatures and require more input power for removal.

In actuality, multiple stages probably would not have equal PCs and ϵs due to trade-offs in axial conduction, pressure drops, and decreasing matrix volumetric heat capacity with lower temperature. Also, although heat capacity is easier to provide in upper stages, they must have the capacity to handle the gas and heat flows from the lower stages. These factors increase the requirement for high regenerator effectiveness.

Thus, multiple stages allow distributing the regenerators to operate over smaller temperature differentials, which lowers the effectiveness required and provides more power efficient interception of heat loads.

3.4 Real Regenerators and Real Gas

In a perfect regenerator there is no heat transfer with the surroundings, no heat conduction or pressure loss along the length, and no net heat gain or loss over a

complete cycle. The gas exits either end at the same temperature it had entered that end. This requires infinite heat transfer area and conductance into the heat storage matrix so that there is no temperature difference between the gas and the matrix, and infinite matrix heat capacity, so that there is no temperature change in the matrix as it exchanges heat with the gas. Otherwise, in a real regenerator, the matrix must be colder than the gas to absorb heat from it and warmer than the gas to return heat to it. This results in a temperature deficit, $\Delta T = T_{out} - T_{in}$, at each end as shown in Figure 1. At the cold end, the gas enters colder (T_L, in) than the matrix, absorbing heat from the matrix, and exits (later in the cycle) warmer (T_L, out) than the matrix, having returned heat to the matrix. At the cold end, the enthalpy transferred into the regenerator from the expansion space is $m_{ge}c_p$ (T_L, in). Later in the cycle, the enthalpy returned to the expansion space is $m_{ge}c_p$ (T_L, out). The net enthalpy transferred into the expansion space each cycle is $m_{ge}c_p$ (T_L, out - T_L, in) = $m_{ge}c_p\Delta T$. With ideal gas and no other heat leaks, it can be shown by conservation of energy that this enthalpy flow must be the same at each end of the regenerator and results in a net enthalpy flow each cycle from the warm end to the cold end. Such an enthalpy flow is the heat exchange deficit from regenerator ineffectiveness, which directly subtracts from the gross refrigeration produced in the expansion space. Thus, regenerator ineffectiveness is due to limited heat transfer area, conductance, and heat capacity in the matrix, even with ideal gas.

For real gases, enthalpy is a function of temperature and pressure. This can result in an additional enthalpy flow in a Stirling refrigerator because the gas enters and exits each end of the regenerator at different points in the pressure cycle. Gas flows toward the expansion space during the high pressure part of the cycle and an equal gas mass flows away from the expansion space during the low pressure part of the cycle.

Let the specific enthalpy, h, of the gas at each end of a perfect regenerator be designated as follows:

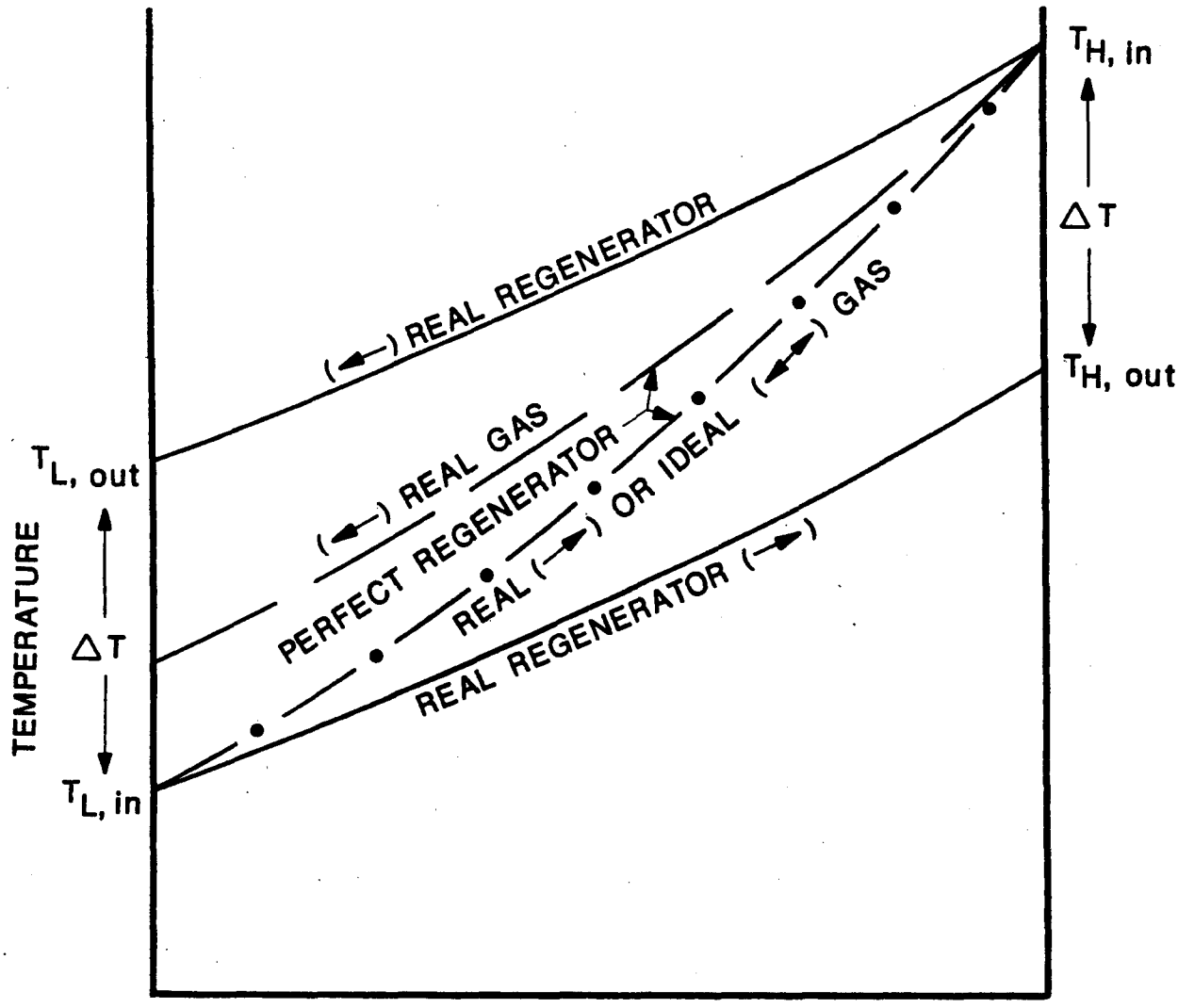

FIGURE 1. TEMPERATURE PROFILES FOR THE ALTERNATING FLOW OF IDEAL OR REAL GAS THROUGH A PERFECT OR REAL REGENERATOR

h_{HTHP} at high temperature, high pressure

h_{HTLP} at high temperature, low pressure

h_{LTHP} at low temperature, high pressure

h_{LTLP} at low temperature, low pressure.

Per unit mass, the enthalpy difference in the gas entering and leaving the expansion space at T_L is $(h_{LTHP} - h_{LTLP})$, and the imbalance in the enthalpy changes in the high and low pressure flows between T_H and T_L (the lack of capacity in the low pressure flow to cool the high pressure flow from T_H to T_L) is $(h_{HTHP} - h_{LTHP}) - (h_{HTLP} - h_{LTLP})$. The net enthalpy flow per unit mass towards the expansion space is

$$(h_{LTHP} - h_{LTLP}) + (h_{HTHP} - h_{LTHP}) - (h_{HTLP} - h_{LTLP}) = h_{HTHP} - h_{HTLP}.$$

For helium, enthalpy variation with pressure at constant temperature is significant at temperatures below 30 K but is negligible (more like an ideal gas) at warmer temperatures for pressures below about 4 MPa. Therefore, the nonideal gas effect, $(h_{HTHP} - h_{HTLP})$, of helium on net refrigeration is negligible with heat sink temperatures above 30 K and pressures below 4 MPa. The refrigeration added to the isothermal expansion by the enthalpy change from high pressure to low pressure at T_L, $(h_{LTHP} - h_{LTLP})$, is balanced out by the excess enthalpy change, $(h_{HTHP} - h_{LTHP}) - (h_{HTLP} - h_{LTLP})$, required to cool the high pressure flow to T_L. However, the enthalpy excess in the high pressure flow may affect the apparent performance of a real regenerator since it results in a temperature excess at the cold end, which represents heat that must be absorbed by the expansion-induced enthalpy change.

3.5 Regenerator Trade-Offs

Real regenerators must trade flow restriction, axial heat conduction, and void volume for matrix heat capacity, conductance into the matrix, and heat transfer area. There must be sufficient effective heat capacity to store the required amount of heat within an

allowable matrix temperature fluctuation each cycle. Adequate heat transfer and conductance into the matrix must be provided to transfer the required heat within a half cycle with an acceptable temperature differential. Temperature differentials between the matrix and gas, arising from limited matrix heat capacity, heat transfer area, and conductance, result in an enthalpy flow, $m_{ge}c_p\Delta T$ each cycle, which directly subtracts from the gross refrigeration produced. The matrix must also have enough porosity to pass the required gas flow without excessive pressure drop and to provide adequate heat transfer area without excessive void volume. These parameters are intimately interrelated and must be carefully balanced to minimize regenerator ineffectiveness and other parasitic losses.

Overall, the regenerator performance objective is to provide adequate heat capacity and transfer rate with minimal gas versus matrix temperature differential, void volume, flow pressure loss, and axial heat conduction.

Axial heat conduction along the length of the regenerator is a parasitic heat load on the refrigeration produced. The axial heat conduction rate is given by

$$\dot{Q}_C = (A_m/L)\int_{T_L}^{T_H} k_a dT$$

where A_m = cross-sectional area of matrix material (i.e., total cross-sectional area minus gas flow cross-sectional area A_g)

L = regenerator length

k_a = matrix axial conductivity.

For given regenerator heat capacity, heat transfer area, and flow area, void volume and flow pressure drop could be made small by using a short, large diameter regenerator, except that axial heat conduction would become excessive. Axial conduction imposes trade-offs in providing sufficient material volume LA_m (for heat

capacity) and flow area A_g (to limit pressure drop) without excessive void volume $V_{rg} = LA_g$.

Flow pressure drop through the regenerator adds to the compressor work input required for a given cycle pressure ratio P_H/P_L in the expansion space. For laminar flow with negligible end effects, as is typical in regenerators (Bib. 21), the average pressure drop is approximately

$$\Delta P = F\, L(\dot{m}_{gr}/A_g)^2/2\rho_g\, r_h$$

where F = Fanning friction factor
$\dot{m}_{gr}$ = average gas mass flow rate
ρ_g = average gas density
r_h = hydraulic radius = $LA_g/A_{ht} = V_{rg}/A_{ht}$
A_{ht} = gas-to-matrix heat transfer ('wetted') area.

Substituting $r_h = LA_g/A_{ht}$, then $\Delta P = F\, \dot{m}_{gr}^2\, A_{ht}/2\rho_g A_g^3$.

It can be seen that large heat transfer area A_{ht} for high effectiveness to limit the heat transfer losses (enthalpy flows) causes flow pressure loss, which is limited by providing flow area A_g resulting in void volume LA_g. However, pressure-cycle-induced enthalpy flow increases with void volume, so that performance improvement requires that A_{ht} can be increased more than LA_g, or there is an overriding need to reduce temperature-gradient-induced enthalpy flow at the cost of increased flow pressure drop, axial conduction, and/or pressure-cycle-induced enthalpy flow.

The dependence of pressure drop on flow velocity v, regenerator length L, and flow gap (characterized by r_h) is seen by substituting $\dot{m}_{gr} = \rho_g v A_g$:

$$\Delta P = F\, \rho_g\, v^2\, A_{ht}/2A_g = F\, L\, \rho_g\, v^2/2r_h.$$

Radebaugh (Bib. 21) has shown that ΔP can be equated to a loss $\dot{Q}_p$ in gross refrigeration rate $\dot{Q}_E$ by

$$\dot{Q}_p = \pi \dot{Q}_E \Delta P/(P_H - P_L)$$

where ΔP is the average flow pressure loss for a sinusoidal pressure cycle of $(P_H - P_L)$ peak-to-peak amplitude. This shows that $\dot{Q}_p$ can become relatively large for small pressure ratio P_H/P_L, which trades off against decreasing pressure-cycle-induced enthalpy flow for decreasing P_H/P_L.

Void volume in the regenerator is necessary to provide flow passage and heat transfer area. Void volume must be limited so that the cyclic compression and expansion of the gas occur largely in the compression and expansion spaces where the associated heat transfers are intended. Compression and expansion of gas in the regenerator void volume, V_{rg}, cause heat transfers to and from the matrix and attendant temperature differentials between the gas and the matrix. These temperature differentials result in an enthalpy flow in addition to that previously described arising from the imperfect heat exchange of the cyclic gas mass flow through the temperature gradient $(T_H - T_L)$ of the regenerator. Thus, regenerator effectiveness ϵ decreases with increasing pressure ratio P_H/P_L due to the enthalpy flow arising from compression/expansion of gas in the void volume.

Minimizing these enthalpy flows is not a simple matter of minimizing regenerator void volume since void volume is required for flow and heat transfer areas, which are essential to regenerator effectiveness. The enthalpy flow induced by the pressure cycle increases proportionately with void volume, but that associated with the temperature gradient does not. The resultant of these enthalpy flows, and the reduction in the refrigeration produced, depends on the relative magnitudes and phasing of the pressure cycle (P_H/P_L) and mass flow, as determined by the proportioning of the expansion, void, and compression volumes, the phasing between the expansion and compression swept volumes, and the temperature ratio (T_H/T_L).

Although ideally the maximum gross refrigeration is produced with the expansion volume leading the compression volume by 90°, the resultant of the above enthalpy flows varies with the phase angle such that the maximum net refrigeration (gross refrigeration minus resultant enthalpy flow) occurs at a smaller phase angle. Radebaugh (Bib. 20, 21) derived the analytic relationships among these parameters, as simplified below, and cited examples of the maximum net refrigeration occurring with expansion/compression spaces phase angles of 70° to 80°.

With constant regenerator void volume V_{rg}, gas mass flow rates $\dot{m}_H$ at the warm (T_H) end and $\dot{m}_L$ at the cold (T_L) end, respective specific enthalpies h_H and h_L, and internal energy U, the heat transfer rate from the gas is

$$\dot{Q}_R = \frac{dQ_R}{dt} = \dot{m}_H h_H - \dot{m}_L h_L - \frac{dU}{dt}.$$

Assuming ideal gas: $U = mc_vT = c_vPV_{rg}/R$, $dU/dt = (c_v/R)\, V_{rg}\, (dP/dt)$,

$$\dot{m}_H - \dot{m}_L = dm/dt = (V_{rg}/RT_g)(dP/dt), \text{ and}$$

$$\dot{Q}_R = \dot{m}_L\, c_P\, (T_H - T_L) + (V_{rg}/R)(c_pT_H/T_g - c_v)\, (dP/dt).$$

With sinusoidal pressure $P = P_o + P_a \cos(\omega t + \theta)$ and mass flow $\dot{m}_L = \dot{m}_a \cos(\omega t)$ at an operating frequency $\omega/2\pi$:

$$\dot{Q}_R = c_p\, (T_H - T_L)\, \dot{m}_a \cos(\omega t) - (V_{rg}/R)(c_pT_H/T_g - c_v)\, P_a\, \omega \sin(\omega t + \theta)$$

where $\dot{m}_a = \dot{m}_{ge}\, \pi/2$ and $P_a = (P_H - P_L)/2$.

The first component of $\dot{Q}_R$ is the heat exchange due to mass flow across the temperature gradient ($T_H - T_L$), which is proportional to the rate of refrigeration produced. The second component is parasitic heat exchange due to compression/ expansion of gas in the regenerator void volume V_{rg}. Both components induce temperature differentials which contribute to regenerator ineffectiveness.

The heat transfer rate between the gas and matrix is $\dot{Q}_R = H_t A_{ht} (T_g - T_m)$, where H_t is the heat transfer coefficient, A_{ht} is the total heat transfer (wetted) area between the gas and matrix, and T_g and T_m are the corresponding local gas and matrix temperatures, respectively, along the regenerator length between T_H and T_L.

The heat stored or returned by the regenerator matrix each half cycle is $Q_R = C_m \Delta T_m$, where C_m is the effective matrix heat capacity and ΔT_m is the matrix temperature fluctuation. The stored heat exchange rate is $\dot{Q}_R = C_m \, dT_m/dt$. Assuming $T_m = T_o + \Delta T_m \cos(\omega t + \phi)$, then $\dot{Q}_R = - C_m \Delta T_m \, \omega \sin(\omega t + \phi)$.

The heat transfer with the gas must equal that with the regenerator matrix:

$$\dot{Q}_R = H_t A_{ht} (T_g - T_m) = - C_m \, \Delta T_m \, \omega \sin(\omega t + \phi).$$

As heat is absorbed or returned by the matrix, the local temperature must change by ΔT_m. The gas versus matrix temperature differential to transfer the heat is then $T_g - T_m + \Delta T_m$, which results in regenerator ineffectiveness. To minimize this temperature differential requires large $H_t A_{ht}$ and C_m.

The effective heat capacity of the regenerator matrix is $C_m = \rho_m c_m A_{ht} \delta_t$, where ρ_m is matrix density, c_m is matrix mass specific heat, and δ_t is the thermal penetration depth, i.e., the effective depth to which heat can penetrate within a half cycle. For sinusoidally alternating flow over a semi-infinite flat surface, the thermal penetration depth is

$$\delta_t = (2 k_m/\omega \rho_m c_m)^{1/2},$$

where k_m is the effective thermal conductivity into the matrix.

The effective regenerator heat capacity is then

$$C_m = A_{ht} (2 k_m \rho_m c_m/\omega)^{1/2}.$$

As previously discussed, k_m and c_m of solids fall off steeply while gas density rises with decreasing temperature below 100 K, making it difficult to provide sufficient effective regenerator heat capacity and necessitating a slow operating speed to avoid excessive void volume.

It has been shown (Bib. 20, 21) by first-order analysis that the ratio of regenerator void volume to expansion space swept volume, V_{rg}/V_E, is minimized when $C_m/C_g \approx 1.8$. However, first-order analysis neglects the effects of void volume on regenerator and system performance trade-offs, such as pressure-cycle-induced enthalpy flow and phasing with temperature-gradient-induced enthalpy flow. Void volume is necessary for flow passage and heat transfer area, and greater C_m/C_g tends to reduce ΔT_m, a contributor to ineffectiveness. As Radebaugh notes in Appendix II, "for temperatures of about 20 K and below the void volumes in practical regenerators become rather large and the simplification (of first-order analysis) is no longer accurate." The value of $C_m/C_g \approx 1.8$ may not be optimum for overall regenerator performance.

The primary design objective of a cryocooler is to produce net refrigeration at a specified rate and temperature. Gross refrigeration is produced at a rate proportional to $\dot{m}_{ge} \ell n\ (P_H/P_L)$. For a given pressure ratio, the mass displacement rate required per unit of gross refrigeration rate is independent of operating frequency. Operation at a different frequency requires an inversely proportional expansion space displacement V_E such that $V_E\omega$ = constant. An increase in frequency requires a decrease in expansion space volume, resulting in a decreased ratio of expansion space to void volume for the same mass flow rate.

In the range of pressure ratios, 1.5 to 3, typical of regenerative cycle cryocoolers, the $\ell n\ (P_H/P_L)$ varies closely with P_H/P_L [e.g., $\ell n\ (2P_H/P_L) \approx 2\ell n\ (P_H/P_L)$]. A decrease in pressure ratio would require a proportionate increase in mass flow rate and void volume, along with the relatively larger loss in gross refrigeration rate for small pressure ratio described previously.

Consolidating and summarizing the simplified governing relationships, with material properties approximated as constant over the temperature range of the regenerator:

Net refrigeration rate: $\dot{Q}_{net} \approx \dot{Q}_E - (1 - \epsilon)\dot{Q}_R - \dot{Q}_C - \dot{Q}_P$

Gross refrigeration rate: $\dot{Q}_E \approx 0.3\, \dot{m}_{ge} R T_E \ell n\, (P_H/P_L)$

Regenerator heat exchange rate:

$$\dot{Q}_R = (\dot{m}_{ge}\pi/2)c_p(T_H - T_L)\cos(\omega t) - (V_{rg}/R)(P_H - P_L)(\omega/2)[(c_p T_H/T_g) - c_v]\sin(\omega t + \theta)$$
$$= H_t A_{ht}(T_g - T_m) = A_{ht}(2\omega\, k_m \rho_m c_m)^{1/2}\, \Delta T_m \sin(\omega t + \phi)$$

Regenerator ineffectiveness: $(1 - \epsilon)\,\dot{Q}_R = \dot{m}_{ge}\, c_p(T_g - T_m + \Delta T_m)$

Axial conduction: $\dot{Q}_c = (k_e A_m/L)(T_H - T_L)$

Flow pressure loss: $\dot{Q}_p = \pi \dot{Q}_E F\, \dot{m}_{gr}^2\, A_{ht}/2\rho_g A_g^3\, (P_H - P_L)$

It would seem that $\dot{Q}_{net}$ could be maximized with high P_H/P_L, ω, and long L, except for the component of $\dot{Q}_R$ due to compression/expansion of gas in the regenerator void volume $V_{rg} = LA_g$. $H_t A_{ht}$ is required in proportion to $\dot{m}_{ge}$ to limit $(T_g - T_m)$. High P_H/P_L would increase $\dot{Q}_E/\dot{m}_{ge}$, which would reduce $H_t A_{ht}(T_g - T_m)$, $\dot{m}_{ge}(T_g - T_m + \Delta T_m)$, $\dot{m}_{gr}^2/(P_H - P_L)$ and $\dot{Q}_p$. High ω would decrease the matrix volume, $V_m = LA_m$, required for a given volumetric heat capacity $\rho_m c_m$ and ΔT_m. This along with long L would reduce $\dot{Q}_C$. However, the parasitic increase in $\dot{Q}_R$, arising from V_{rg}, increases with the product of V_{rg}, $(P_H - P_L) = P_L(P_H/P_L - 1)$, and ω, and can only be moderated within narrow limits by optimizing phasing as previously described.

The effect of the product $V_{rg}(P_H - P_L)\,\omega$ is to convert drive power input into heat which is transported to the cold end of the regenerator. Lowering the pressure ratio requires more mass flow rate per unit gross refrigeration, which increases flow pressure drop and the need for matrix heat transfer area and heat capacity. Lowering operating

speed increases the machine size and drive loads. The escalating increase in regenerator ineffectiveness with increasing speed, pressure ratio, and matrix coarseness has been methodically demonstrated by testing of stacked-screen regenerators (Bib. 14). The key then is to minimize the V_{rg} per unit $\dot{m}_{ge}$, A_{ht}, and A_g without excessive $k_m A_m/L$.

It can be seen by the dependence on H_t, A_{ht}, $A_g{}^3$, and $(k_m \rho_m c_m)^{1/2}$ that the matrix form governing the relationship of heat transfer, fluid flow, and void volume is at least as important as the material thermal conductivity and volumetric heat capacity.

Determination of H_t is highly empirical and is usually based on established correlations with basic heat exchanger types and flow conditions. The relationship of H_t to the heat exchanger and flow parameters may be expressed in various ways, depending on the parameter of particular interest, as illustrated below for the common forms of regenerator matrices with laminar flow, Reyonlds number Re, gas thermal conductivity k_g, and Prandtl number Pr ≈ 0.7.

Packed spheres of diameter $D = 18\ r_h$:

$$H_t \approx 0.3\ Re^{2/3}\ k_g/D \approx 0.5\ \dot{m}_g c_p/A_g Re^{1/3}$$

Stacked screens of $De = L\ A_g/(A_g + A_m)$:

$$H_t \approx 0.8\ Re^{2/3}\ k_g/De \approx 1.3\ \dot{m}_g c_p/A_g Re^{1/3}$$

Parallel plates or concentric cylinders separated by flow gap t_g:

$$H_t \approx 3\ k_g/t_g \approx 1.3\ \dot{m}_g\ c_p/A_g\ Re^{1/2}$$

For the low Re's (in the range of 100) typical of cryocooler regenerators, H_t is primarily due to gas conductivity across the effective flow gap t_g and can be reasonably approximated for all of the typical matrix forms as $H_t \approx 3\ k_g/t_g$. (Accurate confirmation of actual H_ts requires testing.) With smaller flow gaps and more tortuous flow paths,

packed spheres and stacked screens may have higher H_ts than parallel plates. However, as shown in Appendix II, parallel plates provide the highest ratio $H_t A_g Pr^{2/3}/\dot{m}_g c_p F$, a measure of heat transfer versus pressure drop.

A high ratio of heat transfer versus pressure drop alone does not resolve all of the void volume trade-offs. At very low temperature the primary problem is providing enough effective matrix heat capacity C_m without excessive void volume or axial conduction. The need for volumetric heat capacity decreases as $\omega^{1/2}$ increases, but the loss due to void volume increases directly with ω. Falling volumetric heat capacity with temperature requires adding matrix volume $V_m = LA_m$. If added by increasing length L, then void volume $V_{rg} = LA_g$ increases unless flow area A_g can be reduced at the cost of pressure drop increasing with $1/A_g^3$. Adding matrix cross section A_m increases axial conduction and is ineffective if the material thickness t_m is greater than twice the thermal penetration depth, i.e., $t_m > 2\delta_t$. Thus it is critical that matrix volume be fully utilized as effective heat capacity, which requires that $A_{ht}\delta_t = LA_m$ with $t_m = 2\delta_t$. For given $\dot{m}_{gr}$, this results in minimum adequate A_{ht}/A_g to limit pressure loss, A_m/L to limit axial conduction, and void volume. Since $C_m = A_{ht}(2 k_m \rho_m c_m/\omega)^{1/2}$, at very low temperature (low $k_m c_m$) and practical operating speed, the required A_{ht} provides ample $H_t A_{ht}$ for heat transfer.

4.0 FULLERENES

Regenerator ineffectiveness not only increases the drive power requirement of a cryocooler, it limits the lowest temperature and highest speed at which the cryocooler can operate. Reaching temperatures below 20 K, even with multiple stages, using currently available materials requires problematically slow operating speed and high drive forces. Combinations of rare-earth magnetic transition materials offer only marginal improvements and are very expensive and difficult to produce in the forms and uniformity required.

The analyses in the preceding section and in Appendix II show that maximizing regenerator effectiveness and operating speed requires providing a high ratio of effective matrix heat capacity [= $A_{ht}(2\ k_m\rho_m c_m/\omega)^{1/2}$] to void volume (= $L\ A_g$) while limiting axial conduction (~$k_a A_m/L$) and pressure loss (~ A_{ht}/A_g^3). At low temperature, where c_m and k_m are low, a finely divided, low porosity [$A_g/(A_m + A_g)$] matrix with a high ratio of $A_{ht}/(A_m + A_g)$ is required such that the material thicknesses t_m between flow passages are approximately twice the thermal penetration depth ($\delta_t \approx (2\ k_m/\rho_m c_m \omega)^{1/2}$) and A_g is the minimum necessary to suitably limit pressure loss. Also, it is highly desirable that the conductivity k_m into the matrix be higher than the effective axial conductivity k_a in the flow direction through the matrix.

In Appendix II it is shown that for a regenerator operating over a temperature span of 10 K to 20 K a porosity of 0.13 is required for reasonably good performance (i.e., loss due to ineffectiveness is less than 50% of the gross refrigeration rate produced). It is further shown that losses might be minimized with a porosity as low as 0.02. The fixed porosity of 0.38 for packed spheres of uniform size results in very little if any net refrigeration remaining after ineffectiveness and other losses, which explains why current 10 K cryocoolers using packed lead microspheres require 1.5 kW or more of drive power per watt of refrigeration. A porosity of about 0.25 can be approached with packed spheres of different sizes, but proper mixing for even flow distribution is difficult to ensure. Stacked screens are even less suitable with typical porosities greater than 0.6.

Low porosity can be achieved with parallel plates, concentric cylinders, or coiled foil, for which porosity equals $t_g/(t_m + t_g)$. At an average regenerator temperature of 15 K and speed of 10 Hz, thermal penetration depths δ_t of suitable materials vary from about 0.3 mm for G-10 fiberglass/epoxy to about 0.9 mm for lead. For a porosity of 0.13 with $t_m = 2\delta_t$, the respective flow gaps t_g would be 0.09 mm and 0.27 mm. Such thin sections and close spacing are somewhat difficult to fabricate, control, and maintain. Operation at 50 Hz (to employ resonant linear drives with nonrubbing piston

suspensions and seals) would require a porosity approaching 0.02 with material thicknesses and flow gaps of approximately t_m = 0.3 mm and t_g = 0.007 mm for G-10, and t_m = 0.8 mm and t_g = 0.02 mm for lead, which are probably not practicable.

The prospective advantages of using fine powders for the matrices of very low temperature regenerators are described in Bib. 21. Very high surface area to volume ratio, small particle size, and low porosity can be easily achieved, and the ratio of k_m/k_a is inherently much higher in a matrix of discrete particles than in a continuous matrix such as parallel plates. However, it is noted that suitable materials having high volumetric heat capacity at low temperature, such as lead, tend to be soft and have low melting points so that the powder readily sinters together and loses the high surface area and k_m/k_a advantages.

As described in Appendix I, the objective of the current project was to investigate the possibility that helium-impregnated fullerene carbon (probably as a compressed powder) might be used to form an effective, high heat capacity, very low temperature regenerator matrix. The very low temperature heat capacity of fullerenes was analyzed for this project at Arizona State University (ASU), Tempe, as reported in Appendix III, using computer models developed especially for the study of the quantum molecular dynamics of fullerenes. Methods for producing, purifying, forming, and testing impregnated fullerenes were defined for this project, as described in Appendix IV, by the Materials and Electrochemical Research (MER) Corporation, Tucson, Arizona, the leading producer of fullerenes.

The ASU study confirmed that the carbon-carbon bonds make fullerenes very incompressible and allow efficient transmission of thermal energy into endohedral (impregnated) fullerenes. However, it was found that encapsulation of a single helium atom in C_{60} (the most common fullerene molecule) probably would not offer a volumetric heat capacity approaching that of lead. (Encapsulation of 2 helium atoms, which is thought to occur, would provide more heat capacity enhancement but is very

complex to analyze and better left to test.) Rather, it was determined that encapsulation of a metal ion, such as that of Na, K, Mg, or Al, in C_{60} could result in a volumetric heat capacity approximately equal to that of lead at 10 K and about half that of lead at 15 K. Considering the dependence of regenerator effectiveness on A_{ht}, porosity, and $(k_m \rho_m c_m)^{1/2}$, some compromise in $\rho_m c_m$ would still be advantageous to achieve a simple matrix form which provides a high ratio of A_{ht} to porosity and of k_m/k_a.

MER has demonstrated the production and test of high purity fullerenes in various forms, dimensions, controlled porosities, and with impregnants such as helium and metal ions. The MER report (Appendix IV) describes established methods for producing and concentrating helium-impregnated fullerenes in suitable quantities. In consultations with MER subsequent to the ASU analyses, it was learned that impregnation with metal ions is easier and produces higher yields than with inert gases (e.g., helium), and concentration/purification is facilitated by greater molecular weight and solubility differences. The theoretical voidage of 48% and lattice porosity of 12% referred to in the MER report do not correspond to regenerator void volume or porosity, which would be controlled by particle size and compressing and would have to be tested.

5.0 CONCLUSIONS AND RECOMMENDATIONS

High regenerator effectiveness is critical to optimizing the power, speed, weight, size, and service life of Stirling cryocoolers, and, even with multiple stages, is essential to reaching temperatures much below 65 K. Because of the high ratio of heat cycled in a regenerator per unit of gross refrigeration produced, regenerator ineffectiveness can overwhelmingly increase required drive power and impose limits on highest operating speed and lowest refrigeration temperature. Increase in the currently achievable effectiveness of regenerators for 10 K cryocoolers would allow more than proportionate increase in operating speed and reductions in machine power

consumption, size, and weight. Operating at higher speed and power efficiency corresponds with lower drive forces and mechanism loads.

The effect of the product of regenerator void volume, cycle pressure swing, and operating frequency is to convert drive power into heat which is transported to the cold end of the regenerator. To provide effective regenerator heat capacity at very low temperature with minimal void volume and allow increased operating frequency, the matrix must be finely divided such as to optimize the required material and flow cross-sections and thereby minimize void volume without excessive axial conduction or flow pressure loss. The material thicknesses must be approximately 2 times the thermal penetration depth and the flow gaps must be much smaller to provide sufficient material and flow cross-sections with minimum necessary porosity. Low porosity, to minimize void volume, inherently entails a high ratio of material/flow cross-section, even if finely divided, making a high ratio of material/axial thermal conductivity important and favoring powder rather than plates for very low temperature regenerators.

Due to the fundamental nature of matter and heat, known regenerator materials and forms apparently do not offer the prospect of cryocoolers operating near 10 K at speeds above 5 to 10 Hz, and thus preclude employing linear resonant drives and nonrubbing piston suspensions and seals for prolonged service.

Metal-ion-impregnated fullerenes are a new form of material which offers the prospect of providing an adequate volumetric heat capacity, comparable to that of lead in the 10 to 15 K temperature range, without the proclivity to fuse together in powder form, such as when compressed or subjected to the cyclic pressure and flow in a Stirling regenerator. As such, fullerenes may make possible matrices which provide intimate thermal coupling to the working gas and a high ratio of effective heat capacity to compressible void volume, axial conduction, and pressure loss, allowing higher regenerator effectiveness and operating speed than other currently known materials.

Further development of fullerene-based high-effectiveness regenerators for very low temperature will require making material and matrix samples and complete regenerators for testing as outlined below using methods described in Appendix IV. Therefore, Phase II of the development will be to determine:

- Most suitable impregnant, raw materials, and as-produced material form.
- Production, concentration, verification, and matrix forming methods.
- Matrix density, helium permeability, compressible gas void volume, and helium flow resistance.
- Matrix volumetric heat capacity, thermal diffusivity and conductivity at 10 K.
- Matrix cohesive strength, resistance to breakdown by cyclic helium flow, and coefficient of thermal expansion from 300 K to 10 K.

Basic heat capacity will be measured by calorimeter test for standard reference to other materials. However, calorimeter tests are not representative of the effective matrix heat capacity in a cryocooler regenerator. For measurement of regenerator effectiveness near 10 K, agreement will be sought for testing in the National Institute of Standards and Technology's Regenerator Test Facility, Boulder, Colorado, (described in Bib. 21), in continuing collaboration with Dr. Radebaugh. Finally, regenerator performance in an actual Stirling cryocooler will be tested in General Pneumatics' four-stage Stirling test-bed cryocooler, which is capable of variable operating speed and pressure.

BIBLIOGRAPHY

1. Bar-Cohen, A., et al., 1986, "Research Needs in Electronic Cooling," National Science Foundation and Purdue Univ., Andover, MA

2. Barron, R., 1984, Cryogenic Systems, 2nd Ed., Oxford University Press, Oxford, U.K.

3. Bradshaw, T. W., 1986, "First Results on a Prototype Two Stage Miniature Stirling Cycle Cooler for Spaceflight Applications," Fourth International Cryocoolers Conf., Easton, MD

4. Castles, S. H., 1988, "Current Developments in NASA Cryogenic Cooler Technology," Advances in Cryogenic Engineering, Vol. 33

5. Chan, C. K., 1987, "Survey of Cooling Techniques for Electronic and Sensor Devices," Symposium on Low Temperature Electronics and High Temperature Superconductors, Honolulu, HI

6. Chan, C. K., 1989, Survey of Cooling Techniques, JPL Invention Report NPO-17457/6964, NASA Jet Propulsion Laboratory, Pasadena, CA

7. Fieldhouse, I. B., Porter, R. W., 1986, Cryogenic Cooling of Infrared Electronics, GACIAC SOAR-86-02, IIT Research Institute, Chicago, IL

8. Gasser, M. (Ed.), 1983, Refrigeration for Cryogenic Sensors, NASA Conference Publication 2287

9. Green, G., et al., 1986, "Low Temperature Ribbon Regenerator," Second Interagency Meeting on Cryocoolers, Easton, MD

10. Hands, G. A., 1986, Cryogenic Engineering, Academic Press, San Diego, CA

11. Hargreaves, C. M., 1991, The Philips Stirling Engine, Elsevier Science Publishers B.V., Amsterdam, The Netherlands

12. Keung, C. S., Lindale, E., 1984, "Effect of Leakage Through Clearance Seals on the Performance of a 10 K Stirling-Cycle Refrigerator," Third Cryocooler Conf., Boulder, CO

13. Knox, L., et al., 1984, "Design of a Flight Qualified Long-Life Cryocooler," Third Cryocooler Conf., Boulder, CO

14. Kush, P. K., Thirumaleshwar, M., 1989, "Design of regenerators for a Gifford-McMahon cycle cryorefrigerator," Cryogenics, Vol. 29

15. Ledford, O., 1986, "Cryogenics for Space Systems," Advanced Technology International, Los Angeles, CA

16. Marsden, D., 1986, "System Design Requirements for Infra-Red Detector Cryocoolers," Fourth International Cryocoolers Conf., Easton, MD

17. McFarlane, R., et al., 1988, "Long Life Stirling Cryocooler for Space Applications," Fifth International Cryocooler Conf., Monterey, CA

18. Orlowska, A. H., Davey, G., 1987, "Measurements of Losses in a Stirling Cycle Cooler," Cryogenics, Vol. 27

19. Radebaugh, R., Louie, B., 1984, "A Simple, First Step to the Optimization of Regenerator Geometry," Third Cryocooler Conf., Boulder, CO

20. Radebaugh, R., 1986, "Ineffectiveness of Powder Regenerators in the 10 K Temperature Range," Second Interagency Meeting on Cryocoolers, Easton, MD

21. Radebaugh, R., et al., 1992, Measurement and Calculation of Regenerator Ineffectiveness for Temperatures of 5 to 40 K, Report WL-TR-92-3074, March 1992, Wright Laboratory, Wright-Patterson AFB, OH

22. Smith, J., et al., 1984, "Survey of the State of the Art of Miniature Cryocoolers for Superconducting Devices," Mass. Institute of Tech., Cambridge, MA

23. Walker, G., 1983, Cryocoolers, Plenum Press, New York, NY

24. Walker, G., 1989, Miniature Refrigerators for Cryogenic Sensors and Cold Electronics, Oxford University Press, Oxford, U.K.

25. Walker, G., et al., 1988, "Microcomputer Simulation of Stirling Cryocoolers," Twelfth International Cryogenic Engineering Conference, Southampton, UK

26. Walker, G., Urieli, I., 1990, "An Ideal Adiabatic Analysis of a Stirling Cryocooler with Multiple Expansion Stages," Low Temperature Engineering and Cryogenics Conf., Southampton, UK

27. Walker, G., Bingham, E. R., 1993, Low Capacity Cryogenic Refrigeration, University of Calgary, Alberta, Canada (to be published in 1994)

APPENDIX I

PHASE I SBIR PROPOSAL FOR ADVANCED REGENERATORS FOR VERY LOW TEMPERATURE CRYOCOOLERS

U.S. DEPARTMENT OF DEFENSE

SMALL BUSINESS INNOVATION RESEARCH (SBIR) PROGRAM

PROPOSAL COVER SHEET

Failure to use a RED Copy as the original for each proposal and to fill in all appropriate spaces may cause your proposal to be disqualified

TOPIC NUMBER: AF93-065

PROPOSAL TITLE: Advanced Regenerators for Very Low Temperature Cryocoolers

FIRM NAME: General Pneumatics Corporation, Western Research Center

MAIL ADDRESS: 7662 E. Gray Road, Suite 107

CITY: Scottsdale, STATE: AZ ZIP: 85260-6910

PROPOSED COST: $61,992.20 PHASE I OR II: PROPOSAL I PROPOSED DURATION: IN MONTHS 6

BUSINESS CERTIFICATION:

	YES	NO
▶ Are you a small business as described in paragraph 2.2?	[X]	[ ]
▶ Are you a minority or small disadvantaged business as defined in paragraph 2.3? (Collected for statistical purposes only)	[ ]	[X]
▶ Are you a woman-owned small business as described in paragraph 2.4? (Collected for statistical purposes only)	[ ]	[X]
▶ Has this proposal been submitted to other US government agency/agencies; or DoD components, or other SBIR Activity? If yes, list the name(s) of the agency, DoD component or other SBIR office in the spaces to the left below. If it has been submitted to another SBIR activity list the Topic Numbers in the spaces to the right below:	[X]	[ ]

Strategic Defense Initiative Organization — SDI093-003

▶ Number of employees including all affiliates (average for preceding 12 months) 40

PROJECT MANAGER/PRINCIPAL INVESTIGATOR	CORPORATE OFFICIAL (BUSINESS)
NAME: Mr. Woody Ellison	NAME: Mr. Steven G. Zylstra
TITLE: Engineering Manager	TITLE: General Manager, WRC
TELEPHONE: 602-998-1856	TELEPHONE: 602-998-1856

For any purpose other than to evaluate the proposal, this data except Appendix A and B shall not be disclosed outside the Government and shall not be duplicated, used or disclosed in whole or in part, provided that if a contract is awarded to this proposer as a result of or in connection with the submission of this data, the Government shall have the right to duplicate, use or disclose the data to the extent provided in the funding agreement. This restriction does not limit the Government's right to use information contained in the data if it is obtained from another source without restriction. The data subject to this restriction is contained on the pages of the proposal listed on the line below.

PROPRIETARY INFORMATION: 8 thru 12

Woody Ellison — SIGNATURE OF PRINCIPAL INVESTIGATOR — 12/23/92 DATE

Steven G. Zylstra — SIGNATURE OF CORPORATE BUSINESS OFFICIAL — 12/23/92 DATE

Nothing on this page is classified or proprietary information/data

Proposal page No. 1

U.S. DEPARTMENT OF DEFENSE

SMALL BUSINESS INNOVATION RESEARCH (SBIR) PROGRAM

PROJECT SUMMARY

Failure to use a RED Copy as the original for each proposal and to fill in all appropriate spaces may cause your proposal to be disqualified

TOPIC NUMBER: AF93-065

PROPOSAL TITLE: Advanced Regenerators for Very Low Temperature Cryocoolers

FIRM NAME: General Pneumatics Corporation, Western Research Center

PHASE I or II PROPOSAL: I

Technical Abstract (Limit your abstract to 200 words with no classified or proprietary information/data.)

Proposed is a new concept for high effectiveness regenerative heat exchangers which are critically needed to develop efficient cryocoolers for operation at temperatures of 10 K and below. Development of light weight, power efficient, long life cryocoolers capable of providing refrigeration at and below 10 K has become a critically-pacing technology for spaceborne instrumentation. The best current 10 K cryocoolers are impractically large, inefficient, and unreliable for aerospace applications. This is largely due to fundamental problems with regenerator ineffectiveness at very low temperature.

The new type of regenerators proposed offers for 10 K cryocoolers the prospect of reductions of 100's of watts of power and kilograms of weight per watt of refrigeration, and extension of operating life by 10,000's of hours. The proposed research will define the analytical modeling, thermofluid performance trade-offs, material properties, production and test methods for such high effectiveness regenerators.

Anticipated Benefits/Potential Commercial Applications of the Research or Development

The proposed new type of regenerators offers major advances in the efficiency, size, reliability, and life of cryocoolers for operation down to temperatures of 10 K and below. These advances are critical to the development of practical, long-life cryocoolers for spacecraft as well as various superconductor, medical imaging, and research applications.

List a maximum of 8 Key Words that describe the Project.

cryorefrigerators	Stirling
regenerators	thermofluid

Nothing on this page is classified or proprietary information/data

U. S. DEPARTMENT OF DEFENSE
DEPARTMENT OF THE AIR FORCE
SMALL BUSINESS INNOVATION RESEARCH PROGRAM

Topic No. AF93-065:

Advanced Cryocooler Components

Proposal Title:

Advanced Regenerators for Very Low Temperature Cryocoolers

Prepared for:

United States Air Force
PL/XPP
(SBIR Program Manager)
Bldg 592, Rm 24
Kirtland AFB, NM 97117-6008

Submitted by:

Western Research Center
General Pneumatics Corporation
7662 E. Gray Road, Suite #107
Scottsdale, AZ 85260
(602) 998-1856

Principal Investigator: Mr. Woody Ellison

December 1992

TABLE OF CONTENTS

C) IDENTIFICATION AND SIGNIFICANCE OF THE PROBLEM OR OPPORTUNITY

1) Introduction

Proposals were sought to develop advanced components for cryogenic refrigerators for spacecraft applications under Topic No. AF93-065, Advanced Cryocooler Components, in the Department of Defense Small Business Innovation Research Program Solicitation 93.1. In response, research is proposed to employ fullerenes in an innovative concept for high effectiveness regenerative heat exchangers which are critically needed to develop efficient cryocoolers for operation at temperatures of 10 K and below such as for spaceborne instrumentation.

Currently the mission lives of spacecraft requiring cryogenic cooling for instrumentation are seriously limited by dependence on stored cryogens such as liquid helium. Cryocoolers capable of 5 to 10 years of continuous orbital operation are needed to cool the focal planes, optics, baffles, etc. of infrared sensor systems. But the power, weight, size, and life penalties of current 10 K cryocoolers are prohibitive for spacecraft applications. Development of compact, light weight, power efficient, high reliability, long life cryocoolers capable of producing temperatures down to 10 K while rejecting heat at temperatures in the range of 300 K has become a critically-pacing technology.

2) Stirling Cryocoolers

To absorb heat at a low temperature and reject it to a higher temperature, i.e. generate refrigeration, requires the application of work on a thermodynamic medium. The medium may be fluid, elastic, magnetic, or electric, but in general only fluids (specifically gasses) allow sufficient operating range to achieve a temperature change of more than a few tens of degrees Kelvin. Therefore, to generate cryogenic refrigeration with a heat sink in the range of 300 K requires the cyclic compression and expansion of a gas having a suitably low boiling point.

The Carnot cycle defines the theoretic minimum work required per unit of refrigeration. The Carnot cycle, however, is an unimplementable mathematical ideal. The cycle most closely approaching the performance of the Carnot cycle, upon which to base a cryorefrigerator with a sink temperature in the range of 300 K, is the Stirling cycle.

For applications where thermodynamic efficiency, mechanical simplicity, and minimum weight and size are priorities, Stirling cryocoolers offer the best potential.

Progressively smaller, lighter Stirling cryocoolers have been developed over the past 40 years, principally for infrared night vision equipment and missile guidance systems requiring cooling in

the range of 80 K. Stirling cryocoolers have been developed in vigorous competition with many other types of cryocoolers, including Vuilleumier, Linde-Hampson, Joule-Brayton, Claude, Gifford-McMahon, Solvay and Postle. Stirling cryocoolers have emerged as the system of choice for miniature systems, being smaller, lighter, lower in cost, and more efficient than the competitive systems.

Recently, a new generation of miniature Stirling cryocoolers, typified by the Oxford cryocooler (Orlowska and Davey, 1987) and the Standard Spacecraft Cooler, have been developed employing non-rubbing clearance seals, flexure suspensions, and resonant linear motors for greatly improved life and reliability. But there are still fundamental problems in reaching temperatures much below 65 K with these machines.

3) **Regenerators**

Figure 1 shows the ideal Stirling refrigeration cycle. In process A-B the working fluid takes on heat at constant volume as it passes through the regenerator from a cold space (at temperature T_R) to a warm space (at temperature T_C). A regenerative heat exchanger is comprised of a single channel filled with a porous heat storage medium in which a fluid cyclically reverses flow. The regenerator may be thought of as thermodynamic sponge cyclically absorbing heat from and releasing heat back to the working fluid. The heat absorbed from the regenerator is the area A-B-H-F. Heat Q_C, corresponding to area B-C-G-H, is rejected from the system in the isothermal compression process B-C. The working fluid then passes back through the regenerator in the constant volume regenerative cooling process C-D. Heat corresponding to the area C-D-E-G is stored in the regenerator for transport out next time around in process A-B. Finally, refrigeration occurs in the isothermal compression process D-A where heat Q_R, corresponding to area D-A-F-E, is absorbed by the working fluid.

Two factors critical to a Stirling cryocooler's power efficiency and ability to reach low temperature are the dead volume and the thermofluid performance of the regenerator. Dead volume is volume in the working space, e.g. in the heat exchangers, which does not vary cyclically and therefore reduces compression ratio. Favorable thermofluid characteristics are low fluid friction and thermal conductivity in the flow (axial) direction, and high radial conductivity, surface area, and heat capacity to promote heat transfer with minimum temperature difference between the matrix and the working fluid.

Providing effective regenerator heat capacity is a fundamental problem in achieving temperatures below 15 K with regenerative cycle cryocoolers (e.g. Stirling, Gifford-McMahan, etc.). Ideally, the regenerator should have high heat capacity and heat transport capabilities such that heat exchange with the helium working fluid

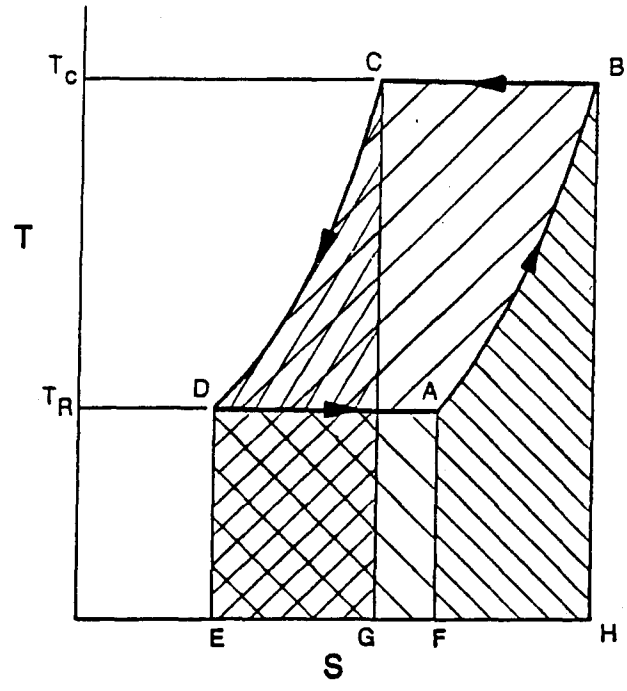

FIGURE 1A. IDEAL STIRLING CYCLE

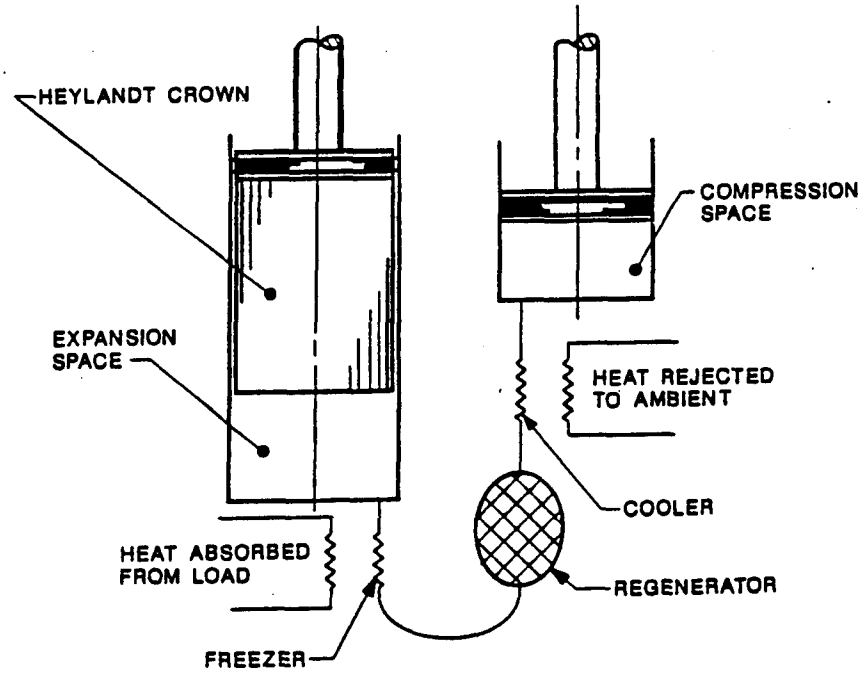

FIGURE 1B. TWO PISTON, PARALLEL CYLINDER STIRLING REFRIGERATOR

at a high rate does not cause significant temperature fluctuation in the regenerator. Also, the regenerator should introduce minimal axial heat conduction, flow restriction, and void (compressible) volume in the helium flow path.

Regenerators have typically contained fine wire screen, gauze, wool, or lead shot. Heat capacity is a serious problem in very low temperature regenerators because the specific heat of solids decreases with temperature while density remains constant, whereas the specific heat and density of helium increase with decreasing temperature. The specific heat capacity of materials falls off steeply with decreasing temperature below 100 K. This is due to the inherent decrease, with temperature, in lattice vibration energy, which is the primary form of thermal energy, and to a lesser degree in electron energy. Thus, as atomic freedom is diminished by decreasing temperature, so is a material's capacity to store thermal energy. As depicted in Figure 2, a few materials undergo magnetic moment transitions in internal energy over narrow temperature changes below 20 K, which has the effect of a spike in heat capacity. Because such transitions occur over only a few degrees in temperature change, they are of limited value in providing a small supplemental heat capacity and are not very effective during start-up from ambient temperature.

Making matters worse, helium at only 1 MPa pressure (10 atm) has a higher specific heat capacity than virtually all other materials below 12 K. For size and weight practicality, cryocoolers typically have helium charge pressures of 1 to 2 MPa. Thus, a large amount of regenerator material is required to provide more heat capacity than the helium working fluid itself. Adding regenerator material creates problems with flow restriction, void volume, axial conduction losses, and time required to transfer heat into and out of the regenerator matrix. The last factor necessitates a low flow rate which, in Stirling machines, results in slow operating speed and high drive mechanism loads for a given power level (torque x rpm).

A means of achieving increased heat capacity in a very low temperature regenerator would be to use helium itself as the heat storage medium. But to do so, the heat storage helium must be mechanically uncoupled from the working fluid helium so as not to increase the volume of compressible gas (void volume) in the regenerator. Compressible gas in the regenerator lowers the refrigerator's compression ratio and causes power losses due to dissipating heat of compression in the regenerator. A prior concept was to use a packed bed of tiny helium-filled glass beads for a regenerator. But such has not been widely implemented, if at all, perhaps due to problems in producibility or in encapsulating helium at sufficiently high density (pressure) in the beads.

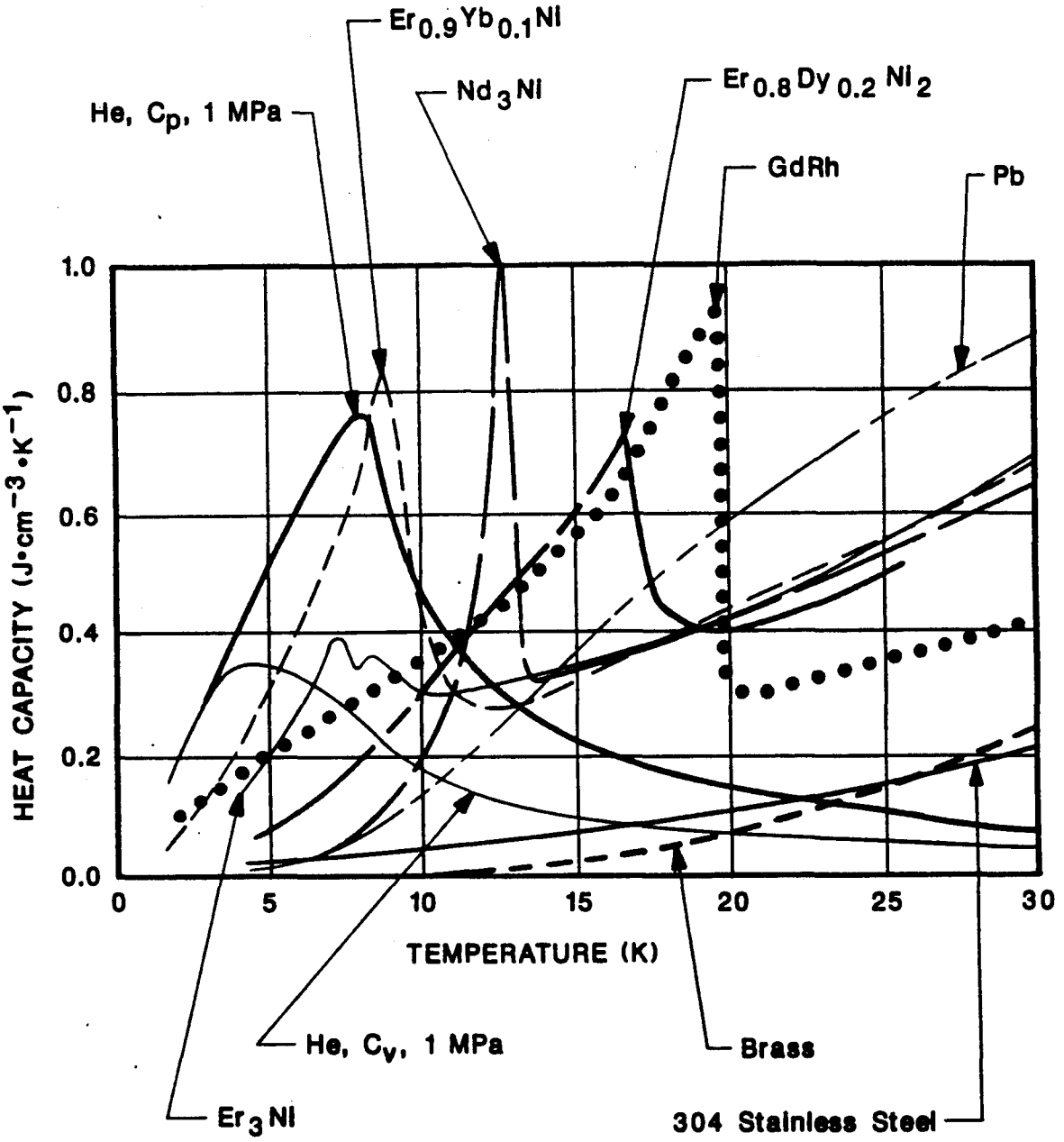

FIGURE 2. VOLUMETRIC HEAT CAPACITIES OF VARIOUS MATERIALS

The proposed new concept for entraining helium in a regenerator is to encapsulate helium atoms in fullerene carbon molecular cages. Fullerenes are large, closed, carbon molecules (e.g. C_{60}, C_{70}, etc.) which are described as hollow, geodesic, microscopic balls or cages. It has been shown that atoms of various elements, notably helium, can be inserted and confined inside fullerene molecules. It is also known that fullerenes can form a highly permeable bulk mass. It is proposed here that helium-impregnated fullerene molecules could be used to form a regenerator matrix which would effectively be a packed bed of microscopic helium-filled carbon balls. It is expected that, because of their discrete, closed, geodesic, carbon-carbon bonds structure, the fullerene balls would be extremely rigid (incompressible) with good thermal conductivity from exterior to interior, but not from ball to ball.

Such a regenerator matrix would preclude the compressibility of the heat storage helium from the working fluid helium, while providing intimate thermal coupling between the two, without introducing high conducted heat losses through the regenerator.

4) **Advancement Prospects**

Power

Two primary forms of regenerator ineffectiveness are deficient heat transfer between the matrix and the working fluid due to insufficient matrix heat capacity or heat transport rate, and heat dissipation due to compression/expansion of working fluid in the regenerator void volume. Regenerator ineffectiveness directly subtracts from the refrigeration produced in a cryocooler, thereby necessitating a larger machine and greater power input for a given amount of refrigeration. The requirement for a larger machine compounds the reduction in power efficiency by proportionately increasing the void volume and heat transfer losses.

The criticality of regenerator ineffectiveness in cryocoolers is illustrated by noting that, with a heat sink temperature of 300 K, the ratio of heat cycled in a perfect regenerator per unit of refrigeration produced at various temperatures is: 14 at 77 K, 70 at 20 K, and 140 at 10 K. Thus, for each watt of refrigeration at 10 K, a 0.5% regenerator inefficiency causes a 0.5% X 140 = 0.7 watt refrigeration loss requiring increased size and power input by a factor of more* than 1/(1 - 0.7) = 3.3 (*due to the compounding effect of increasing size).

To translate this into terms of input power required, the minimum theoretical (Carnot) input power required per watt of refrigeration at 10 K, with a 300 K heat sink, is (300 - 10)/10 = 29 watts/watt. Real cryocoolers have typically achieved less than 1 to 2% of Carnot efficiency at 10 K, requiring 1500 to 3000 watts/watt, largely due to regenerator inefficiency.

A regenerator inefficiency of only 1/140 ≈ 0.7% would result in zero power efficiency, i.e. no refrigeration producible at 10 K. An improvement of only 0.1% in regenerator efficiency might well double power efficiency, reducing input power required by 750 to 1500 watts/watt.

Size and Weight

In addition to size and weight savings associated with increased power efficiency, improved regenerators offer the prospect of higher operating speed with proportionate reduction in system size and weight. Currently, 10 K cryocoolers are limited to operating speeds in the range of 0.5 to 5 Hz, and consequently weigh several hundred kg per watt of refrigeration, because of the very poor specific heat capacity and transport rate of conventional regenerators. In contrast, 80 K cryocoolers operate at speeds of 30 to 60 Hz and weigh on the order of a kg per watt of refrigeration. Improvements in the specific heat capacity or transport rate of regenerators for 10 K cryocoolers would allow proportionate increases in operating speed. For the same amount of refrigeration, this would allow more than proportionate reduction in machine size and weight, since parasitic losses also decrease with machine size.

Reliability and Life

Since refrigeration is produced in proportion to the rate of doing work, operation at higher speed and power efficiency corresponds with much lower drive forces and bearing loads. Higher operating speed is also essential to employing flexure suspension, resonant linear drive systems, which require very short strokes of less than 1 mm (for flexure life) and resonant frequency in the range of 30 to 60 Hz (for weight and power efficiency). Such systems have been found to be key to extending the operating life of 80 K cryocoolers from a few 1000's of hours to several 10,000's of hours.

Thus, improvements in regenerators for 10 K cryocoolers are critically fundamental to reductions of 100's of watts of power and kilograms of weight per watt of refrigeration, and extension of operating life by 10,000's of hours.

D) PHASE I TECHNICAL OBJECTIVES

The objectives of the proposed Phase I research are to analyze the potential thermofluid properties of helium-impregnated fullerenes as related to the feasibility and prospective advantages of using them in high effectiveness regenerators for Stirling cryorefrigerators, and to define methods for producing and testing candidate materials and representative regenerators in Phase II.

Factors to be evaluated include: the density to which helium atoms can be encapsulated in fullerenes and the effect on the molecular vibration modes; the thermal transfer effectiveness into and between the fullerene molecules in a pressurized helium medium; and the achievable combination of heat capacity, transfer rate, flow restriction, and void volume for operation in a Stirling cryocooler down to temperatures reaching 10 K.

E) PHASE I WORK PLAN

The tasks for Phase I of the proposed research for fullerene-based regenerators for very low temperature cryocoolers will consist of the following:

1. Define specific performance requirements and relationships in terms of heat capacity, transfer rate, conductivity, fluid flow restriction, and void volume for prospective cryogenic applications using the REGEN series of regenerator analysis computer models in collaboration with Dr. Radebaugh of NIST.

2. Analyze the vibrational modes of prospective fullerene molecules, which are the principal means for transferring and storing thermal energy, as affected by the encapsulation of helium atoms, using computer models developed especially for the study of the quantum molecular dynamics of fullerenes at Arizona State University.

3. Translate the results of Task 2 into terms of thermal properties, e.g. heat capacity, conductivity, temperature and pressure dependency, and correlate with the findings of Task 1 to determine the most suitable candidate fullerene/helium combinations and physical forms.

4. Compose a plan for making candidate helium - impregnated fullerenes, in collaboration with Dr. Withers of MER Corp. (the sole licensee for the production of fullerene materials), for testing in Phase II.

5. Define the equipment and procedures for testing the key thermofluid and mechanical properties of the helium-impregnated fullerene material as related to regenerators, e.g. heat capacity, conductivity, porosity.

6. Devise a regenerator test apparatus for testing the performance of helium-impregnated fullerene regenerators at temperatures in the range of 10 K in Phase II.

7. Prepare a final report describing the results of each of the foregoing tasks, and the feasibility and prospective performance of helium/fullerene regenerators for very low temperature cryocoolers.

The schedule for completing the Phase I tasks is given below:

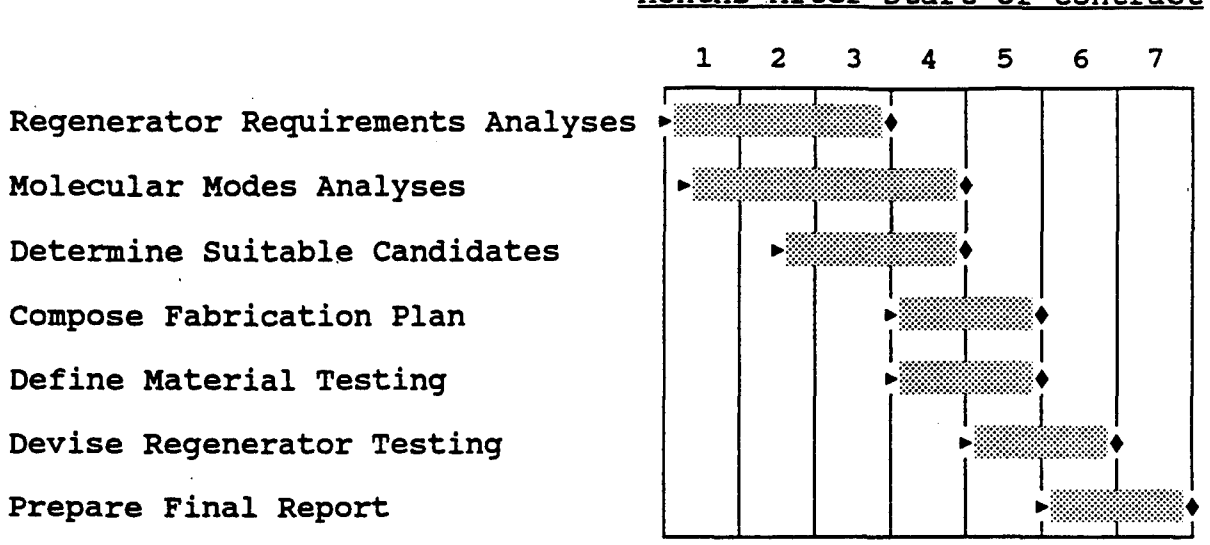

All of the work for the proposed fullerene-based cryogenic regenerators Phase I research will be performed at the General Pneumatics Western Research Center in Scottsdale, Arizona. The Principal Investigator will be Mr. Woody Ellison, who has nineteen years of research experience in heat transfer, thermal analysis, cryogenics and development of high precision electromechanical and thermal control devices for aerospace applications. The program will be fully supported by the extensive experience of the Western Research Center staff in cryocooler development, and by the consulting services of Dr. Graham Walker and Dr. Ray Radebaugh, both leading authorities on cryorefrigerators, and Dr. James Withers, an expert in materials science and the production and analysis of fullerenes. Resumes for the program team are presented in Section I, Key Personnel, and Section K, Consultants.

F) RELATED WORK

1) Related R & D at General Pneumatics

The Western Research Center of General Pneumatics was specifically established to research and develop cryorefrigerators, Stirling engines and refrigerators, and new approaches for thermal management and energy conversion. Previous and current development projects, in addition to internal research and development, include:

- A methane or radioisotope fuelled Ross-Stirling engine/ generator for use as a battery charger for remote, unattended data gathering and communication systems for DARPA (N00014-85-C-0856, Sept. 1985)

- A Ross-Stirling refrigerator for NASA-MSFC to refrigerate food and biological stores in spacecraft using the cabin atmosphere as the working fluid to preclude any hazardous leakage to the crew (NAS8-36260, Dec. 1985)

- A compact high-pressure gas compressor and a low-temperature helium rotary expander for a closed-cycle cryorefrigerator for DOE (DE-AC02-80271-85ER80271, Oct. 1985 and DE-AC02-85ER80272, Sept. 1985)

- A nitrogen-cycle Linde-Hampson cryorefrigerator, featuring a non-clogging, variable-flow cryostat, for condensing liquid oxygen boil-off in a distillation column for NASA-KSC (NAS10-11144, Jan. 1985 and NAS10-11322, Aug. 1986)

- A combined Stirling/Linde-Hampson cryorefrigerator for reliquefying helium boil-off from spacecraft cryogen storage tanks for SDIO (FO4611-88-C-0003, Nov. 1987 and FO4611-89-C-0055, Jan. 1990)

- A natural-gas-powered duplex Stirling cryorefrigerator to liquefy natural gas for automotive fuel for DOE (DE-AC03-89ER80730, Aug. 1989 and DE-FG03-90ER80860, Mar. 1990)

- A triple-fluid, closed-cycle, Linde-Hampson helium liquefier to cool spaceborne sensors and stored cryogens for NASA-ARC (NAS2-12990, Feb. 1989)

- A Stirling cryocooler for direct circulation of refrigerant to instruments, shields, and dewars without need for a cryogenic pump for NASA-MSFC (NAS8-39321, Jan. 1992)

The above work involves thermal, flow, materials, heat exchanger and Stirling system design experience which is directly applicable to the proposed advanced cryogenic regenerators research.

2) **Related References**

Bar-Cohen, A., et al, 1986, "Research Needs in Electronic Cooling", National Science Foundation and Purdue Univ., Andover, MA

Barron, R., 1984, Cryogenic Systems, 2nd Ed., Oxford University Press, Oxford, U.K.

Bradshaw, T. W., 1986, "First Results on a Prototype Two Stage Miniature Stirling Cycle Cooler for Spaceflight Applications", Fourth International Cryocoolers Conf., Easton, MD

Castles, S. H., 1988, "Current Developments in NASA Cryogenic Cooler Technology", Advances in Cryogenic Engineering, Vol. 33

Chan, C. K., 1987, "Survey of Cooling Techniques for Electronic and Sensor Devices", Symposium on Low Temperature Electronics and High Temperature Superconductors, Honolulu, HI

Chan, C. K., 1989, "Survey of Cooling Techniques", JPL Invention Report NPO-17457/6964

Fieldhouse, I. B., Porter, R. W., 1986, "Cryogenic Cooling of Infrared Electronics", GACIAC SOAR-86-02

Gasser, M. (Ed.), 1983, Refrigeration for Cryogenic Sensors, NASA Conference Publication 2287

Green, G., et al, 1986, "Low Temperature Ribbon Regenerator", Second Interagency Meeting on Cryocoolers, Easton, MD

Hands, G. A., 1986, Cryogenic Engineering, Academic Press, San Diego, CA

Keung, C. S., Lindale, E., 1984, "Effect of Leakage Through Clearance Seals on the Performance of a 10 K Stirling-Cycle Refrigerator", Third Cryocooler Conf., Boulder, CO

Knox, L., et al, 1984, "Design of a Flight Qualified Long-Life Cryocooler", Third Cryocooler Conf., Boulder, CO

Ledford, O., 1986, "Cryogenics for Space Systems", Advanced Technology International, Los Angeles, CA

Marsden, D., 1986, "System Design Requirements for Infra-Red Detector Cryocoolers", Fourth International Cryocooler Conf., Easton, MD

McFarlane, R., et al, 1988, "Long Life Stirling Cryocooler for Space Applications", Fifth International Cryocooler Conf., Monterey, CA

Orlowska, A. H. and Davey, G., 1987, "Measurements of Losses in a Stirling Cycle Cooler", Cryogenics, Vol. 27

Radebaugh, R., 1986, "Ineffectiveness of Powder Regenerators in the 10 K Temperature Range", Second Interagency Meeting on Cryocoolers, Easton, MD

Radebaugh, R., Louie, B., 1984, "A Simple, First Step to the Optimization of Regenerator Geometry", Third Cryocooler Conf., Boulder, CO

Smith, J., et al, 1984, "Survey of the State of the Art of Miniature Cryocoolers for Superconducting Devices", Mass. Institute of Tech., Cambridge, MA

Walker, G., 1983, Cryocoolers, Plenum Press, New York, NY

Walker, G., 1989, Miniature Refrigerators for Cryogenic Sensors and Cold Electronics, Oxford University Press, Oxford, U.K.

Walker, G., et al, 1988, "Microcomputer Simulation of Stirling Cryocoolers", Twelfth International Cryogenic Engineering Conference, Southampton, UK

Walker, G., Urieli, I., 1990, "An Ideal Adiabatic Analysis of a Stirling Cryocooler with Multiple Expansion Stages", Low Temperature Engineering and Cryogenics Conf., Southampton, UK

G) RELATIONSHIP WITH FUTURE RESEARCH OR RESEARCH AND DEVELOPMENT

The results of the proposed Phase I research will define the analytical modeling, thermofluid trade-offs, material properties, production and test methods, and establish the feasibility and advantages for employing fullerenes to develop high effectiveness regenerative heat exchangers for very low temperature cryorefrigerators. The results will provide the basis and methods for the design, fabrication, and testing of representative fullerene-based regenerators in Phase II, which in turn will provide for experimental refinement of the modeling and design approaches for practical applications.

H) POTENTIAL POST APPLICATIONS

The effectiveness of regenerative heat exchangers is essential to the efficiency of cryorefrigerators. For numerous applications the best currently available cryocoolers are impractically inefficient, heavy, large, and short-lived. Development of fullerene-based regenerators offers the prospect for major advances in cryocooler power, size, weight, reliability, and operating life. These advances are critical to the development of practical, long-life cryocoolers for spacecraft as well as various superconductor, medical (e.g. magnetic resonance imaging), and research applications.

I) **KEY PERSONNEL**

1) **Staff**

Mr. Woody Ellison is Engineering Manager. Prior to joining General Pneumatics in 1987, Mr. Ellison acquired fifteen years experience at Sperry Space Systems Division in the development of high-precision electromechanical devices and magnetic suspensions for spacecraft applications, which included extensive experience in thermal control, vibration, and vacuum effects analysis, design, and test. Mr. Ellison graduated from Arizona State University with a BSME degree in 1972.

Mr. Ernest E. Atkins is a Senior Development Engineer. Prior to this, he was employed by Goodyear Aerospace Corporation as Sr. Design Engineer where he worked on various defense programs. Earlier, he was a Mechanical Engineer for Sperry Flight Systems, Defense Systems and Space Development (DSSD). Mr. Atkins has been engaged in research and development on Stirling engines and advanced cryogenic systems since 1983. He has acted as Program Manager on various projects to develop Stirling engine cogeneration systems, Stirling refrigerators and oil-free high-pressure compressors for closed-cycle Linde-Hampson cryocoolers. Mr. Atkins has completed engineering courses at the following colleges and universities towards his BSME: University of Maine, 1975-1979, Mesa Community College, 1980-1983, Arizona State University, 1984, Scottsdale Community College, 1985-1988, Paradise Valley Community College, 1989-1990.

Mr. Randall Kohuth is a Senior Development Engineer in the research and development of advanced Stirling systems. Prior to joining General Pneumatics he was employed at McDonnell Douglas Helicopter Company in the design of conventional control actuation systems, research and development of advanced integrated actuators, and as an aerothermal analyst provided thermodynamic and fluid dynamics analysis for turbine engine installation performance, environmental control systems and other related energy systems. Before joining McDonnell Douglas, he was a research assistant at Arizona State University and designed mechanical, optical, and electronic test equipment. Mr. Kohuth was also responsible for interfacing computers to fluid dynamics test systems and developing software for data acquisition and reduction. Mr. Kohuth graduated from Arizona State University with a B.S. (1984) and M.S. (1986) in mechanical engineering.

Mr. Steven G. Zylstra is General Manager of the Western Research Center and Director of Engineering for General Pneumatics Corporation. He was previously employed as Technical Manager on several space programs with Bendix Guidance Systems Division. Prior to that, he acted as Responsible Engineer with Ford Aerospace on the AIM-9M Sidewinder missile program. Before joining FA, he was a Design Engineer with Ford Motor Company. He obtained his

bachelor's degree in engineering from Western Michigan University and has graduate credits toward a MBA from California State University at Fullerton. Mr. Zylstra is Chairman of the Arizona Innovation Network, an organization to help stimulate the growth of small high technology businesses in the State. He also serves on the Arizona Governer's Science and Technology Council and the U. S. Chamber of Commerce, Small Business Council.

2) **Publications and Patents**

Atkins, E., Walker, G., Zylstra, S., "Miniature Multistage High-Pressure Gas Compressor for Linde-Hampson Cryocoolers", Fourth International Cryocoolers Conference, Easton, MD, Sept 1986

Ellison, W., Walker, G., Zylstra, S., "Low Capacity Helium Reliquefier", Interagency Meeting on Cryocoolers, Monterey, CA, Aug 1988

Ellison, W., Atkins, E., Walker, G., Zylstra, S., "A Gas-Fired Duplex-Stirling Cryorefrigerator to Liquefy Natural Gas for Automotive Fuel", Sixth International Cryocooler Conference, Plymouth, MA, Oct 1990

Hedegard, K., Walker, G., Zylstra, S., "A Non-Clogging, Temperature-Sensitive, Closed-Cycle Linde-Hampson Cryocooler, Fifth International Cryocooler Conference, Monterey, CA, Aug 1988

Hedegard, K., Walker, G., Zylstra, S., "Temperature Sensitive Variable Area Flow Regulator for Joule-Thomson Nozzles", Fourth International Cryocoolers Conference, Easton, MD, Sept 1986

Prentice, J., Walker, G., Zylstra, S., "Advancements in Clog Resistant and Demand Flow Joule-Thomson Cryostats", Cryogenic Engineering Conference, Huntsville, AL, Jun 1991

Walker, G., Stirling Cycle Machines, Oxford University Press, Oxford, UK, 1973

Walker, G., Stirling Engines, Oxford University Press, Oxford, UK, 1980

Walker, G., Cryocoolers, 2 Vols., Plenum Publishing Corp., New York, NY, 1983

Walker, G., Senft, J. R., Free Piston Stirling Engines, Springer-Verlag, Berlin, 1983

Walker, G., Ellison, W., Zylstra, S., "Cryocoolers for the New High-Temperature Superconductors", Journal of Superconductivity, Vol. 1, No. 2, Plenum Publishing Corp., 1988

Walker, G., Scott, M., Zylstra, S., "Ross-Stirling Spacecraft Refrigerator", Journal of Spacecraft and Rockets, Vol. 25, No. 5, American Institute of Aeronautics and Astronautics, Sept-Oct 1988

Walker, G., Miniature Refrigerators for Cryogenic Sensors and Cold Electronics, Oxford University Press, New York, NY, 1989

Walker, G., "Micro and Nanno Cryocoolers: Speculations on Future Development", Sixth International Cryocooler Conference, Plymouth, MA, Oct 1990

Walker, G., Radebaugh, R., Low Capacity Cryogenic Refrigerators, Plenum Publishing Corp., New York, NY (in press for publication mid 1991)

Walker, G., "Joule-Thomson Apparatus with Temperature Sensitive Annular Expansion Passageway", U.S. Patent #4,631,928, General Pneumatics Corporation, Dec. 30, 1985, 5 pp

Walker, G., "Refrigerant Expansion Device with Means for Capturing Condensed Contaminants to Prevent Blockage", U.S. Patent #4,738,122, General Pneumatics Corporation, Apr. 19, 1988, 5 pp

J) **FACILITIES/EQUIPMENT**

The Western Research Center (WRC) of General Pneumatics Corporation (GPC) is situated in a 5,600 sq. ft. building on the Scottsdale Airpark in Scottsdale, Arizona. The facility is divided into three distinct areas as follows: engineering, laboratory and machine shop.

The engineering department is equipped with all the necessary tools to research, analyze, design and draft novel engineering concepts. There is a technical library with engineering reference materials, military standards and supplier catalogs. The computing capability consists of two Hewlett-Packard Vectra computers each with 640K of internal memory and 40 meg hard disk drives. The software library consists of Lotus 1-2-3, Wordperfect, Advance Link, Auto-Cad, MS-DOS, HP-Basic, DOS-Basic, Isothermal 2nd Order Stirling Engine Simulator and numerous internally written programs.

The machine shop is equipped with all the necessary machine tools and equipment to fabricate the innovative devices which are designed at WRC. These include two milling machines, four lathes, surface grinder, band saw, belt sander, welding equipment, heat treat oven, drill press, 5-ton mechanical press, inspection equipment, etc.

The laboratory is set-up with all the necessary instrumentation and equipment to assemble and test the various devices which are designed and fabricated at the Center. This equipment includes

motors, power supplies, function generators, bridge amplifiers, temperature analyzers, high speed recorders, load cells, tachometers, oscilloscopes, digital multimeters, pressure gauges and transducers, pressure regulators, vacuum gauges, flow meters (turbine and rotameter), gas pressure boost pump, vacuum pumps, vacuum chambers, hand tools, etc. The facility is almost totally self-sufficient in nature and requires minimal use of outside services with the exception of special processes, such as anodizing, plating, brazing, etc.

The Western Research Center is in close proximity to the expertise and facilities for the processing and analysis of fullerenes at the University of Arizona and the MER Corp. in Tucson, and for the research into the quantum molecular dynamics of fullerenes at Arizona State University in Tempe.

The company headquarters is located in Orange, New Jersey in three buildings totaling about 20,000 sq. ft. The facility is an engineering and production manufacturing entity and is recognized as the leading producer of pneumatic control valves and pressure regulators for the emergency raft and slide evacuation systems on commercial and military aircraft. These components are supplied to literally every aircraft manufacturer and airline in the free world.

The company also supplies hydraulic and pneumatic valves (relief, check, exhaust and regulatory) for the military aerospace industry. GPC produces components for the Sidewinder, Chaparral, Hawk, Patriot, and Sparrow missiles and supplies these products to prime-contractors such as General Dynamics, Loral Aeronutronic, Raytheon Company, Kollsman Instruments Company, etc.

The Company employs forty persons, ten of whom are located at the Western Research Center.

K) **CONSULTANTS**

Dr. Ray Radebaugh is a Research Physicist and Project Leader at the National Institute of Standards and Technology, Boulder, Colorado. Dr. Radebaugh is a specialist in cryogenics, with over twenty years experience in the research of He^3-He^4 dilution, electrocaloric, thermoelectric, Stirling, and pulse-tube refrigerators and regenerative heat exchangers. His pioneering work in computer modeling and analysis of regenerators for cryorefrigerators has made him a leading authority in the field. Dr. Radebaugh is an advisory editor for the international journal, Cryogenics, serves on the boards for the International Cryocooler Conference and the Cryogenic Engineering Conference, and is regularly an invited speaker at various international conferences.

Dr. Graham Walker is the Director of Advanced Research and Development for General Pneumatics Corporation (GPC) and a Professor of Mechanical Engineering at the University of Calgary, Alberta, Canada. Dr. Walker joined GPC's Western Research Center (WRC) in January 1984 on a one-year unpaid leave of absence from the university. He returned to the University of Calgary in January 1985 and he presently acts as a consultant exclusively to GPC.

Walker has been engaged in research and development of power equipment, heat exchangers, refrigeration systems, and Stirling engines since 1956. He is the author of 8 books and over 180 papers to the scientific and engineering journals, national and international conferences, including the Cryogenic Engineering Conference, Cryogenics, the Intersociety Energy Conversion Engineering Conference, the International Stirling Conference, and the ASME and SAE Annual Meetings.

Walker is the inventor of the novel non-clogging General Pneumatics cryostat, Patent No. 4,631,928, and 4,738,122 presently used on several of the previously mentioned cryocooler programs. He has given short courses on Stirling engines and cryocoolers at the University of California, Los Angeles, the University of Maryland, various U.S. companies and government agencies, and many foreign universities, companies and government agencies.

Dr. Walker has project and consulting experience on Stirling engines and cryocoolers for: the Night Vision Laboratory; U.S. Army, Fort Belvoir; the U.K. Ministry of Defense Royal Armament Research and Development Establishment, Fort Halstead; the Canadian Defense Research Board, Quebec; the Canadian Department of National Defense, Ottawa; Honeywell Research Center, Minneapolis; Martin Marietta Corporation, Orlando, Florida; Raytheon Missile Systems Division, Bedford, Massachusetts; Argonne National Laboratory, Argonne, Illinois; Oak Ridge National Laboratory, Oak Ridge, Tennessee; Sunpower, Athens, Ohio; Mechanical Technology Inc., Latham, New York; and the National Aeronautics and Space Administration, Lewis Research Center.

Dr. Walker holds the degree of B.S. (1st Class Honors), 1957 and Ph.D., 1961 in Mechanical Engineering from the University of Durham, United Kingdom.

Dr. James C. Withers is a Research Scientist and the CEO of MER Corporation of Tucson, Arizona. Dr. Withers is an expert in materials science with over 35 years of experience in the fields of process development, chemical vapor deposition, plasma technology/processing and electrochemistry. Dr. Withers has authored 25 U.S. patents, 30 publications in trade magazines, technical journals & books, and served as principal investigator or otherwise participated in over 65 SBIR and other government contracts including several projects involving fullerenes. While

the process for synthesizing fullerenes was discovered at the University of Arizona (Dr. Donald R. Huffman and Dr. Kratschmer from Max Plank Institute), their representative Research Corporation Technologies (RCT) has applied for a number of patents. MER has the only license, from RCT, to produce and sell fullerenes. Dr. Withers and MER have an ongoing, collaborative relationship with Dr. Huffman and his associates at the U of A.

L) PRIOR, CURRENT OR PENDING SUPPORT

A like proposal, titled "High Effectiveness Regenerators for Very Low Temperature Cryocoolers", is being submitted concurrently to SDIO/TNI/SBIR, in response to DOD SBIR Solicitation 93.1, Topic SDIO 93-003, Sensors. The Principal Investigator is designated to be Mr. Woody Ellison, Engineering Manager. Submission of similar proposals to different agencies is to find the most suitable match with Federal Government development objectives. There is no intention of accepting duplicate funding for similar projects. Otherwise, no other prior or current similar project has been funded or is pending funding by any agency of the Federal Government.

APPENDIX II

Report on

ADVANCED REGENERATORS FOR CRYOCOOLERS

performed for General Pneumatics Corporation
for the USAF Phillips Laboratory Contract No. F29601-93-C-0085

ADVANCED REGENERATORS FOR CRYOCOOLERS

Ray Radebaugh
Fluid Systems Group
Process Measurements Division
National Institute of Standards and Technology
325 Broadway
Boulder, CO 80303
Phone (303) 497-3710
FAX (303) 497-5044

Prepared for:

Woody Ellison
General Pneumatics Corporation
Western Research Center
7662 E. Gray Road, Suite 107
Scottsdale, AZ 85260
Phone (602) 998-1856
FAX (602) 951-1934

INTRODUCTION

As part of a Phase I SBIR study being conducted by General Pneumatics for the Air Force Phillips Laboratory on the use of fullerenes for regenerators, we were asked to study the fundamental relationships and parameters that determine the performance of regenerators for temperatures below about 20 K. An ideal regenerator has the following characteristics:

1. Infinite matrix heat capacity
2. Infinite surface area for heat transfer
3. Infinite radial thermal conductivity
4. Zero axial thermal conductivity
5. Zero void volume
6. Zero pressure drop

None of these conditions will be true in practical regenerators, but it is often possible to come close to meeting some of these requirements. Most often, changing parameters to meet one requirement results in a sacrifice to another requirement. An optimized regenerator is usually one designed to maximize the coefficient of performance of the refrigerator. This optimization procedure can be very complex in the most general case, but it becomes simplified in some limiting cases.

Radebaugh and Louie[1] were the first to describe a relatively simple procedure for the optimization of regenerators for the case where the void volume is relatively small. This case is closely approximated for regenerators with cold ends of about

80 K and above. They used a first order analysis in which void volume is neglected in the regenerator performance. By inverting the normal performance calculation they arrived at simple analytical expressions for the regenerator geometry that gave the specified performance with the minimum void volume. This analysis was then incorporated into the NIST software known as REGEN for the optimization of regenerator geometry. However, for temperatures of about 20 K and below the void volumes in practical regenerators become rather large and the simplification of the Radebaugh and Louie method is no longer accurate. A finite difference model using the conservation of energy, mass, and momentum equations was developed at NIST to accurately predict the performance of regenerators at all temperatures, even when the void volumes are large.[2] The latest version of this code is known as REGEN3.1.[3] Because it is a numerical model rather than an analytical model the physics of the regenerator behavior is not apparent. In this report we discuss some simplifications that relate to the behavior of practical regenerators in the region of 20 K and below. We derive some simple equations that show the importance of various regenerator parameters and material properties. With these equations we then give some guidelines for the design of regenerators for this low temperature range.

MATRIX HEAT CAPACITY

Figure 1 shows the primary reason why the performance of regenerators generally decreases significantly for temperatures below about 20 K. As this figure shows, the volumetric heat capacity of the helium gas passing through the regenerator begins to exceed that of the regenerator matrix for temperatures below about 20 K. In order to achieve a sufficiently high total matrix heat capacity to prevent a significant temperature oscillation, the volume of matrix material must be made relatively large. For a fixed porosity the void volume then becomes large also. This void volume may become much larger than the volume of gas that passes through the regenerator. This large void volume has a significant effect an the performance of the regenerator.

Figure 2 compares the regenerator ineffectiveness in a regenerator with no void volume (dashed line) to that of a regenerator with a finite void volume (solid lines). The two solid lines are for two different pressure ratios. This particular example was calculated using REGEN3.1 for a regenerator operating between 10 and 15 K. The ratio of void volume V_{rg} to the volume of gas V_e the passes by the cold end of the regenerator is closely related to the ratio of the heat capacity C_{void} of the gas in the void space to the heat capacity C_f of the gas that passes by the cold end of the regenerator. This example was for a case of $N_{tu} = 84$, where N_{tu} is the number of heat transfer units. As Figure 2 shows, the ineffectiveness of regenerators decreases as the ratio of total matrix heat capacity C_r to C_f increases. However, the presence of the void volume greatly increases the ineffectiveness for values of C_r/C_f greater than about 1. That increase is a result of the additional heat that must be transferred when the gas in the void space is undergoing an oscillating pressure. For very low values of matrix heat capacity the heat capacity of the void volume gas begins to take over as the effective regenerator matrix. Any reasonable regenerator would need to be operating in the region of $C_r/C_f > 1$. So far we have shown only qualitative

features of regenerator design and performance. To quantify the relationships between regenerator performance and the various regenerator parameters it is necessary to develop some analytical equations pertaining to regenerator performance.

THEORY OF REGENERATOR PERFORMANCE

We begin the analysis by using the conservation of energy equation for an element of gas in the regenerator. When the axial thermal conduction in the gas is neglected, the equation for the heat transferred to the gas per unit volume of gas becomes

$$\frac{\dot{Q}}{V_{rg}} = \frac{\partial}{\partial x}\left(\frac{\dot{m}h}{A_g}\right) + \frac{\partial(\rho u)}{\partial t}$$
$$= h\frac{\partial}{\partial x}\left(\frac{\dot{m}}{A_g}\right) + \left(\frac{\dot{m}}{A_g}\right)\frac{\partial h}{\partial x} + \rho\frac{\partial u}{\partial t} + u\frac{\partial \rho}{\partial t}. \tag{1}$$

The relationship between specific internal energy and specific enthalpy is given by

$$u = h - P/\rho. \tag{2}$$

Substituting Eq. (2) into Eq. (1) gives

$$\frac{\dot{Q}}{V_{rg}} = h\frac{\partial}{\partial x}\left(\frac{\dot{m}}{A_g}\right) + \left(\frac{\dot{m}}{A_g}\right)\frac{\partial h}{\partial x} + \rho\frac{\partial u}{\partial t} + h\frac{\partial \rho}{\partial t} - \frac{P}{\rho}\frac{\partial \rho}{\partial t}. \tag{3}$$

The conservation of mass for an element of gas is expressed as

$$\frac{\partial}{\partial x}\left(\frac{\dot{m}}{A_g}\right) = -\frac{\partial \rho}{\partial t}. \tag{4}$$

Eq. (4) is substituted into Eq. (3) to yield

$$\frac{\dot{Q}}{V_{rg}} = \left(\frac{\dot{m}}{A_g}\right)\frac{\partial h}{\partial x} + \rho\frac{\partial u}{\partial t} - \frac{P}{\rho}\frac{\partial \rho}{\partial t}. \tag{5}$$

At this point we use the ideal gas equation of state to keep the equations simple. For an ideal gas

$$u = c_v T, \tag{6}$$

$$h = c_p T, \tag{7}$$

and

$$\rho = P/RT. \tag{8}$$

Differentiating Eq. (8) with time gives

$$\frac{\partial \rho}{\partial t} = \dot{\rho} = \left(\frac{1}{RT}\right)\dot{P} - \left(\frac{P}{RT^2}\right)\dot{T}. \tag{9}$$

Substituting Eqs. (6), (7), and (8) into Eq. (5) gives

$$\frac{\dot{Q}}{V_{rg}} = \left(\frac{\dot{m}c_p}{A_g}\right)\frac{\partial T}{\partial x} + \frac{P}{T}\left(\frac{c_v}{R}+1\right)\dot{T} - \dot{P}. \tag{10}$$

Because an ideal gas has the relation

$$\frac{c_v}{R} + 1 = \frac{c_p}{R}, \tag{11}$$

Eq. (10) can be written as

$$\begin{aligned} \frac{\dot{Q}}{V_{rg}} &= \frac{\dot{m}c_p}{A_g}\frac{\partial T}{\partial x} + \frac{c_p P}{R T}\dot{T} - \dot{P} \\ &= \frac{\dot{m}c_p}{A_g}\frac{\partial T}{\partial x} + \rho c_p \dot{T} - \dot{P}. \end{aligned} \tag{12}$$

We now equate this heat transfer to the gas to the change in internal energy of the matrix. The resulting equation becomes

$$\frac{\dot{m}c_p}{A_g}\frac{\partial T}{\partial x} + \rho c_p \dot{T} - \dot{P} = -\frac{(1-n_g)}{n_g}\rho_m c_m \dot{T}_m. \tag{13}$$

For temperatures below about 20 K we have found that there is usually little difference between T and T_m. This situation occurs when C_r/C_f is small and N_{tu} is large. These conditions are quantified in Appendix A. For this case when $T \approx T_m$, Eq. (13) is approximated by

$$[\rho c_p + \frac{(1-n_g)}{n_g}\rho_m c_m]\dot{T} = -\frac{\dot{m}c_p}{A_g}\frac{\partial T}{\partial x} + \dot{P}. \tag{14}$$

Solving Eq.(14) for $\dot{T}$ yields

$$\dot{T} = \frac{-\frac{\dot{m}c_p}{A_g}\frac{\partial T}{\partial x} + \dot{P}}{\rho c_p + \frac{(1-n_g)}{n_g}\rho_m c_m}. \tag{15}$$

To integrate Eq. (15) we assume sinusoidal behavior for $\dot{m}$, P, and T. In addition, we assume that the amplitudes of P and T are small compared with the average values, P_0 and T_0. For instance, with a pressure ratio of 1.5 (typical in most Stirling and pulse tube refrigerators) the amplitude of the pressure is only 20% of the average pressure. In a regenerator the relative amplitude of the temperature oscillation is usually much less than 20%, although the temperature-vs.-time curve deviates from sinusoidal behavior near the ends of the regenerator. With this approximation Eq. (15) integrates to

$$T = \frac{-\frac{mc_p}{A_g}\frac{\partial T_0}{\partial x} + P}{\rho_0 c_p + \frac{(1-n_g)}{n_g}\rho_m c_m}, \tag{16}$$

where m is the mass of gas that passes by a cross-section of the regenerator. The regenerator loss is given by the time-averaged enthalpy flow through the regenerator, which for an ideal gas is expressed as

$$\langle \dot{H} \rangle = \langle \dot{m}c_p T \rangle = (1/2)c_p \dot{m}_1 T_1 \cos\theta, \tag{17}$$

where the subscripts 1 refer to the amplitudes of the sinusoidal oscillations and θ is the phase angle between $\dot{m}$ and T. Substituting Eq. (16) into Eq. (17) results in

$$\langle \dot{H} \rangle = \frac{-\frac{\langle \dot{m}m \rangle c_p^2}{A_g}\frac{\partial T_0}{\partial x} + c_p\langle \dot{m}P \rangle}{\rho_0 c_p + \frac{(1-n_g)}{n_g}\rho_m c_m}. \tag{18}$$

Because the phase angle between $\dot{m}$ and m is 90°, the term $\langle \dot{m}m \rangle = 0$. Therefore,

$$\langle \dot{H} \rangle = \frac{c_p \langle \dot{m} P \rangle}{\rho_0 c_p + \frac{(1-n_g)}{n_g} \rho_m c_m}. \tag{19}$$

Dividing numerator and denominator by $\rho_0 c_p$ gives

$$\langle \dot{H} \rangle = \frac{\langle (\dot{m}/\rho_0) P \rangle}{1 + \frac{(1-n_g)}{n_g} \frac{\rho_m c_m}{\rho_0 c_p}}. \tag{20}$$

We note that $\dot{m}/\rho_0 = \dot{V}$, where $\dot{V}$ is the volume flow rate. Since the hydrodynamic work flow is given by

$$\langle \dot{W}_h \rangle = \langle \dot{V} P \rangle, \tag{21}$$

Eq. (20) can be expressed as

$$\langle \dot{H} \rangle = \frac{\langle \dot{W}_h \rangle}{1 + \frac{(1-n_g)}{n_g} \frac{\rho_m c_m}{\rho_0 c_p}}. \tag{22}$$

Eq. (22) shows that as $\rho_m c_m \rightarrow 0$, $\langle \dot{H} \rangle = \langle \dot{W}_h \rangle$. In this limit the enthalpy flow reaches its maximum value. For an ideal, reversible expansion in any regenerative refrigerator using an ideal gas, the maximum gross refrigeration power is simply

$$\dot{Q}_{rm} = \langle \dot{W}_h \rangle_c, \tag{23}$$

where the subscript c on the hydrodynamic work flow means that it is evaluated at the cold end of the regenerator. For any real refrigerator where the expansion process is not entirely reversible, the actual gross refrigeration power $\dot{Q}_r$ may be only 50 to 85% of the maximum value.

Because the time-averaged enthalpy flow through the regenerator must be constant (no net heat transfer occurs to the surrounding along the length of the regenerator) Eq. (22) should use work flow, porosity, and heat capacity values that are averaged over the volume of the regenerator. For an ideal gas the work flow varies linearly with temperature because of the linear dependence of the specific volume on temperature. Thus, we should use the average regenerator temperature T_a as the temperature to evaluate the average properties. The average work flow becomes

$$\langle \dot{W}_h \rangle_a = (T_a/T_c)\langle \dot{W}_h \rangle_c . \tag{24}$$

The time-averaged enthalpy flow in Eq. (22) can now be expressed as

$$\langle \dot{H} \rangle = \frac{(T_a/T_c)\langle \dot{W}_h \rangle_c}{1 + \dfrac{(1-n_g)}{n_g}\dfrac{\rho_m c_m}{\rho_0 c_p}}, \tag{25}$$

where the volumetric heat capacities are evaluated at the average temperature. Since the heat capacities are averaged over the entire regenerator volume, we can express Eq. (25) as

$$\langle \dot{H} \rangle = \frac{(T_a/T_c)\langle \dot{W}_h \rangle_c}{1 + \dfrac{C_r}{C_{void}}}, \tag{26}$$

where C_r is the matrix heat capacity and C_{void} is the heat capacity of the gas in the regenerator void space. Equation (25) shows that for a given matrix volumetric heat capacity the only geometrical parameter that can effect the regenerator performance is the porosity. A small regenerator loss requires a low porosity.

To determine a typical porosity that is necessary for a low temperature regenerator, we consider the case of a regenerator operating between 10 and 20 K, which gives an average temperature of 15 K. For a reasonably good regenerator performance we desire $\langle \dot{H} \rangle \leq 0.2\ \dot{Q}_{rm}$. Figure 3 shows the volumetric heat capacities for helium at various pressures and three typical regenerator materials used for these temperatures. For a pressure of 2 MPa we use the typical value $(\rho_m c_m/\rho_0 c_p) = 1$. Solving Eq. (25) for the porosity gives $n_g = 0.13$. For the case of packed spheres $n_g = 0.38$. For the same matrix heat capacity, the regenerator loss becomes $0.57\dot{Q}_{rm}$, which is so high that there is little net refrigeration power remaining after other losses are considered.

As the porosity is made smaller the axial thermal conduction is increased. Here we determine the lower limit for the porosity to prevent an abnormally large axial conduction. The ratio of axial conduction to the hydrodynamic work flow at the cold end is given by

$$\frac{\dot{Q}_c}{\langle \dot{W}_h \rangle_c} = \frac{(A_m/L)\int k dT}{(1/2)RT_c \dot{m}_{c1}(P_1/P_0)\cos\theta} = \frac{(1-n_g)\int k dT}{(1/2)n_g LRT_c(\dot{m}_{c1}/A_g)(P_1/P_0)\cos\theta}, \tag{27}$$

where L is the regenerator length, $\int k dT$ is the thermal conductivity integral in the axial direction, and θ is the phase angle between $\dot{m}_c$ and P. The maximum value of $(\dot{m}_{c1}/A_g)$ that can be passed through the regenerator is determined by pressure-drop considerations. The term $(\dot{m}_{c1}/A_g)$ is related to the average pressure drop ΔP in a half-cycle by

$$\frac{\dot{m}_1}{A_g} = \frac{\pi}{2}\left[\frac{2\alpha\rho\Delta P}{N_{tu}N_{pr}^{2/3}}\right]^{1/2}, \tag{28}$$

where $\dot{m}_1$ is the average between $\dot{m}_{c1}$ and $\dot{m}_{h1}$, N_{pr} is the Prandlt number and α is a measure of the ratio of heat transfer to pressure drop and is defined as

$$\alpha \equiv \frac{N_{st}N_{pr}^{2/3}}{f}, \tag{29}$$

where N_{st} is the Stanton number and f is the Fanning friction factor. Figure 4 shows values of α for various geometries. These values are only weak functions of the Reynolds number N_r. With the ideal gas approximation for ρ, Eq. (28) becomes

$$\frac{\dot{m}_1}{A_g} = \frac{\pi}{2}P_0\left[\frac{2\alpha(\Delta P/P_0)}{RT_0N_{tu}N_{pr}^{2/3}}\right]^{1/2}. \tag{30}$$

We consider a typical case of $P_0 = 2$ MPa, $\alpha = 0.28$ (holes), $\Delta P/P_0 = 0.005$, $T_0 = 15$ K, $N_{tu} = 200$, and $N_{pr} = 0.7$. For this case $(\dot{m}_1/A_g) \approx 7.5$ g/(s·cm^2). This flow rate is an average over the length of the regenerator and is the maximum that can be passed through the regenerator per unit area. The flow rate at the cold end is usually less than this value. For this example we will use the value $(\dot{m}_{c1}/A_g)\cos\theta \approx 5$ g/(s·cm^2) in Eq. (27). In addition we use typical values of $k_{ave} = 9$ mW/(cm·K) (value for Er_3Ni), $L = 5$ cm, $P_1/P_0 = 0.2$, and $\dot{Q}_c/\langle \dot{W}_h \rangle_c = 0.1$. According to Eq. (27) the minimum value of porosity then becomes $n_g \approx 0.02$. For $n_g \ll 1$, $n_g \propto k_{ave}$. With a porosity of 0.02, Eq. (25) gives $\langle \dot{H} \rangle / \dot{Q}_{rm} = 0.03$. This low value of relative regenerator loss is about the lowest that could be achieved if all of the above conditions could be met. In practice the minimum loss will usually be somewhat higher. For example, to achieve a low porosity the matrix volume is usually increased because the void volume must remain sufficiently large to achieve the desired N_{tu}. As the matrix volume increases the ratio

C_f/C_f increases to the point where it is no longer small compared with N_{tu}. Thus, the analysis presented here is no longer valid at very low porosities. However, the use of very low porosities does allow the regenerator loss to be reduced while still using a matrix that has a somewhat lower volumetric heat capacity. Such materials may be considerably cheaper than the high heat capacity rare earth materials.

With very low porosities, there may be problems with typical radial heat flow paths in the matrix exceeding the thermal penetration depth. The thermal penetration depth in a semi-infinite plate is given by

$$\delta_t = \left[\frac{k_m}{\pi f \rho_m c_m}\right]^{1/2} . \tag{31}$$

Figure 5 shows this thermal penetration depth as a function of thermal conductivity for the case of a semi-infinite plate with $\rho_m c_m$ = 0.4 J/(cm^3·K). With a thermal conductivity of 9 mW/(cm·K) the thermal penetration depth at 10 Hz is only about 0.25 mm. This length represents the maximum distance an element of matrix can be from a helium flow channel and still be effective in contributing its heat capacity. In the case of parallel plates with a gap thickness of 15 μm (typical minimum gap thickness for this temperature and pressure) a porosity of 0.02 requires a plate thickness of 0.74 mm. The center part of this plate is then 0.37 mm from the helium channel, which exceeds the thermal penetration depth. As shown by Eq. (31) and by Fig. 5 the thermal penetration depth can be increased by increasing the thermal conductivity in the radial direction. That increase can be accomplished by the use of a composite with such things as high thermal conductivity fibers. The large thermal penetration depth then permits lower porosities to be used.

Another practical problem with very low porosities is the void volumes associated with the manifold necessary to connect a large diameter, low porosity regenerator to a small diameter, high porosity expander or pulse tube. Thus, in practice it may not be possible to effectively use porosities less than about 0.10. However, even this porosity is much less than the 0.38 porosity of packed spheres of one size.

COMPARISON OF ANALYTICAL AND NUMERICAL MODELS

In order to verify our simple analytical model we compare the value of regenerator loss calculated by this model with that calculated from the numerical model that has very few assumptions. We should point out that the numerical model uses the real gas properties whereas the analytical model discussed here considers an ideal gas. Three of the examples being compared are taken from the work of Radebaugh et al.[4] These three cases are evaluated with the regenerator operating between approximately 10 and 15 K. The fourth example (case D) is for temperatures between 10 and 35 K. The comparison between the analytical model and the numerical model is given in Table 1. Cases A, B, and C satisfy the condition $C_f/C_f \ll N_{tu}$. Those three cases show very good agreement between the analytical and numerical models, as

indicated by the last two rows of the table. Case D does not meet the condition $C_r/C_f \ll N_{tu}$ very well. As a result, Eq. (26) of the analytical model underestimates the regenerator loss by about a factor of 2. The additional loss is due to the limited heat transfer area which gives rise to a sizeable temperature difference between the gas and matrix temperatures. For example, Fig. 6 shows the gas and matrix temperatures as a function of time in the center of the regenerator for Case A. There is almost no difference between the gas and matrix temperatures in this case. Figure 7 shows the same comparison for Case D. Here there is a significant difference between the gas and matrix temperatures. For this case some reduction in the regenerator loss could be made by increasing N_{tu}. However, that can only be done at the expense of increasing the pressure drop, the conduction loss, or the void volume. An optimized regenerator considers all of these losses. The Case D does represents an optimized design for a 40 Hz frequency. Cases A, B, and C were for a frequency of about 2.5 Hz, but not fully optimized.

Even for Case D the analytical model shows that the porosity has a significant effect on the regenerator performance. Though the model will not always give accurate results for all cases for the temperature range below about 20 K, it does show the parameters that have the largest effect on the regenerator performance.

Table 1. Comparison between analytical model and numerical model.

Parameter	Case A	Case B	Case C	Case D
Matrix	Pb+5%Sb	GdRh	Brass	User defined
T_h (K)	15.3	15.0	14.6	35
T_c (K)	10.0	9.8	11.0	10
n_g	0.38	0.52	0.46	0.38
N_{tu}	117	57.8	58.3	167
C_r (J/K)	0.898	1.37	0.063	0.635
C_f (J/K)	0.654	0.72	1.31	0.0245
C_{void} (J/K)	1.76	2.44	1.80	0.0837
C_r/C_f	1.37	1.90	0.048	25.9
C_r/C_{void}	0.510	0.561	0.035	7.59
$\langle \dot{H} \rangle / \langle \dot{W}_h \rangle$ Eq. (26)	0.84	0.81	1.12	0.26
$\langle \dot{H} \rangle / \langle \dot{W}_h \rangle$ REGEN3.1	0.86	0.72	1.33	0.56

CONCLUSION

For temperatures below about 20 K with matrix volumetric heat capacities of the order of the best currently known materials, the regenerator loss can only be reduced by decreasing the porosity or increasing the volumetric heat capacity of the matrix. Until we find a regenerator material with a significantly higher volumetric heat capacity in this temperature range, the only way to significantly improve regenerator performance in this low temperature range is to reduce the porosity of the matrix. By reducing the porosity from 0.38 (typical of packed spheres) to 0.10 the regenerator loss can be reduced by a factor of about 4 with existing regenerator materials. In order to fully realize this improvement, considerable care is necessary in the design of the regenerators to prevent excessively large losses due to pressure drops, axial conduction, and finite thermal penetration depth. All of the necessary design equations to optimize the regenerator geometry for low porosity have been presented here. The use of low porosity regenerators could permit the use of inexpensive matrix materials that have somewhat lower volumetric heat capacities than those of the rare earth materials commonly used now for this temperature region.

REFERENCES

[1] R. Radebaugh and B. Louie, "A Simple, First Step to the Optimization of Regenerator Geometry," NBS Special Publication 698, 177 (1985).

[2] J. Gary, D. E. Daney, and R. Radebaugh, "A Computational Model for a Regenerator," NBS Special Publication 698, 199 (1985).

[3] J. Gary and R. Radebaugh, "An Improved Numerical Model for Calculation of Regenerator Performance (REGEN3.1)," Proceedings of the Fourth Interagency Meeting on Cryocoolers, DTRC-91/003 (1991), p. 165.

[4] Ray Radebaugh, J. Gary, E. Marquardt, B. Louie, D. Daney, V. Arp, and D. Linenberger, "Measurement and Calculation of Regenerator Ineffectiveness for Temperatures of 5 to 40 K," Air Force Report WL-TR-92-3074 (1992).

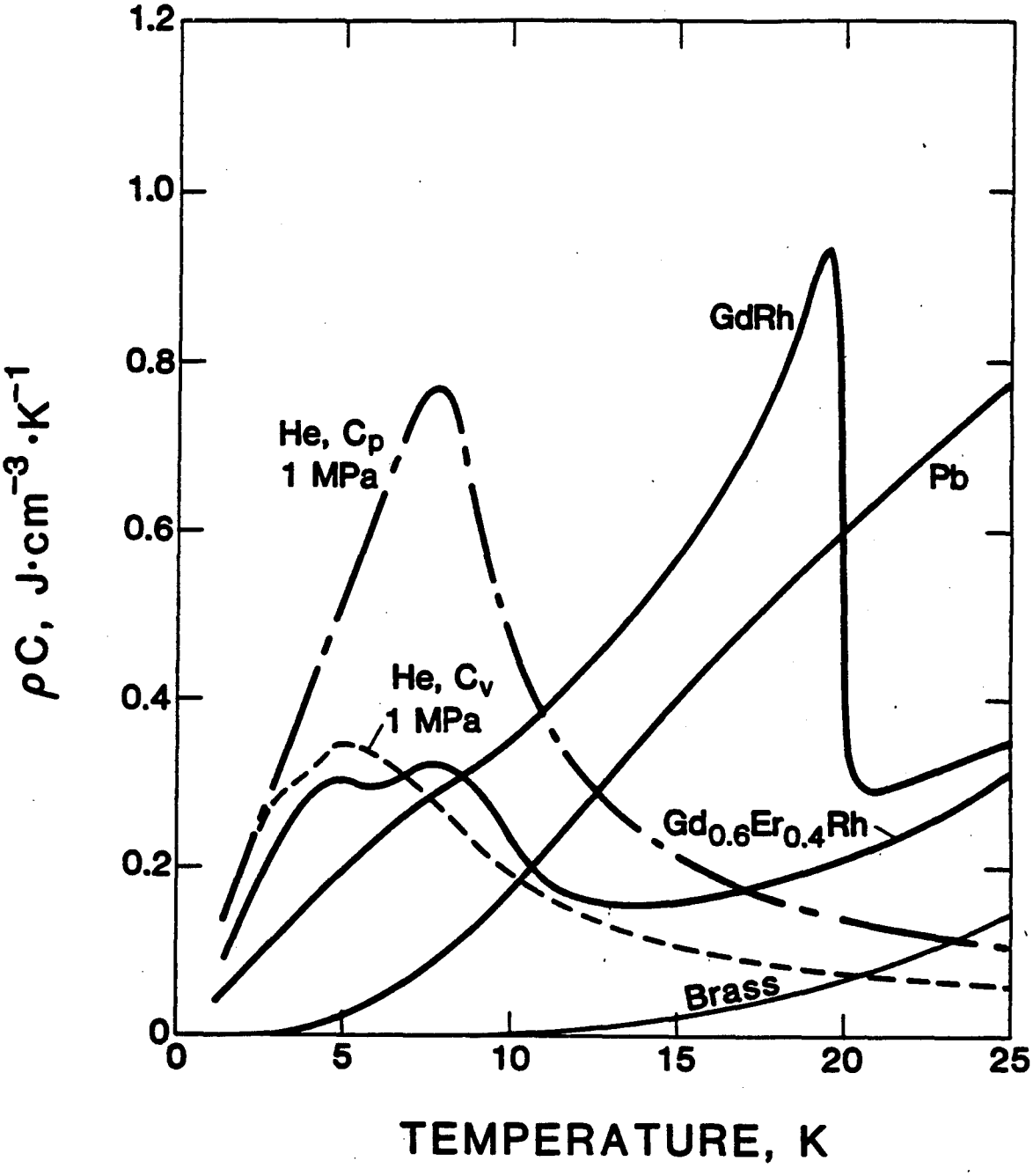

Fig. 1. Volumetric heat capacity of several regenerator materials for temperatures below 25 K.

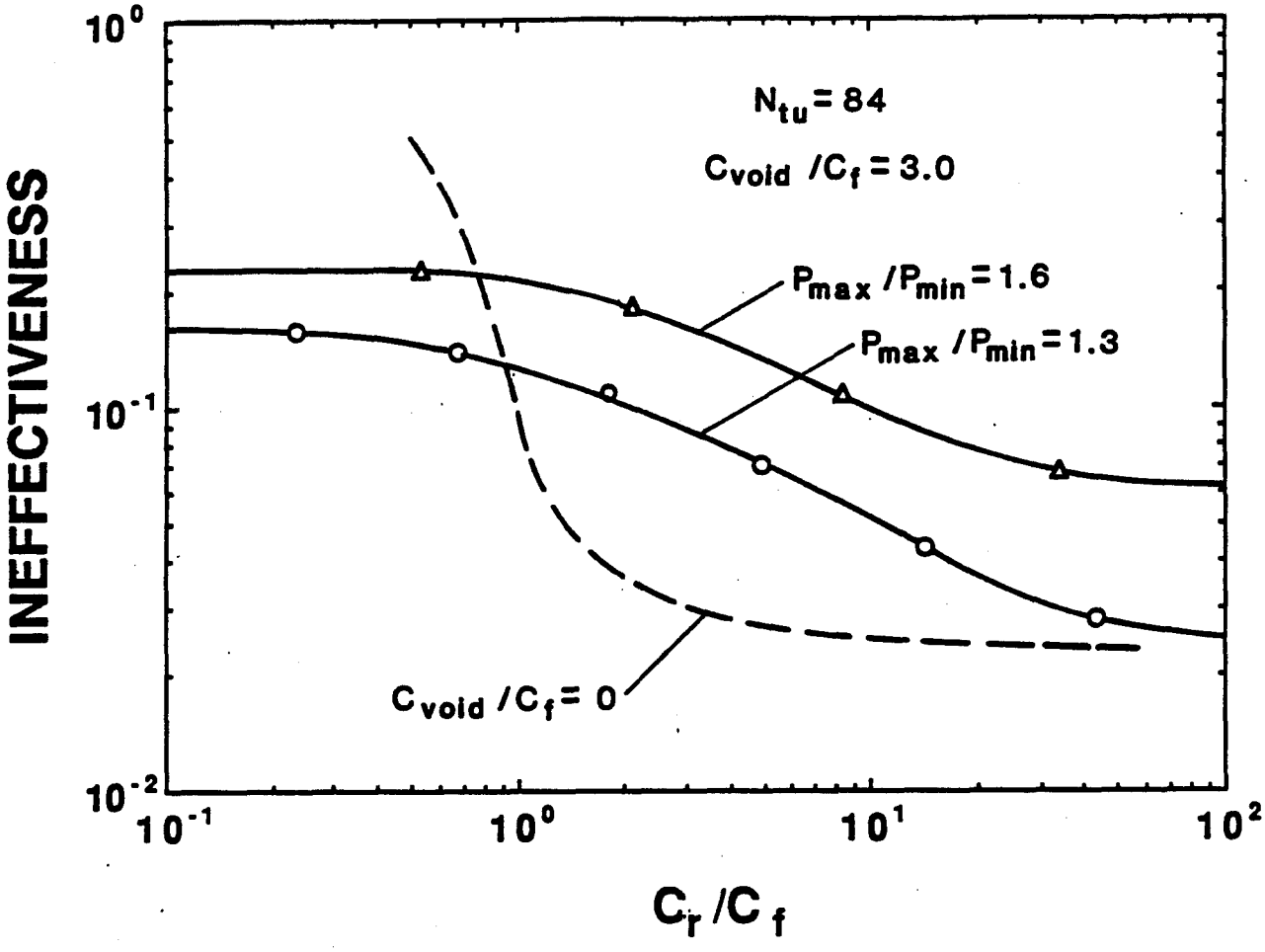

Fig. 2. Ineffectiveness as a function of heat capacity ratio calculated for zero void volume and for finite void volume.

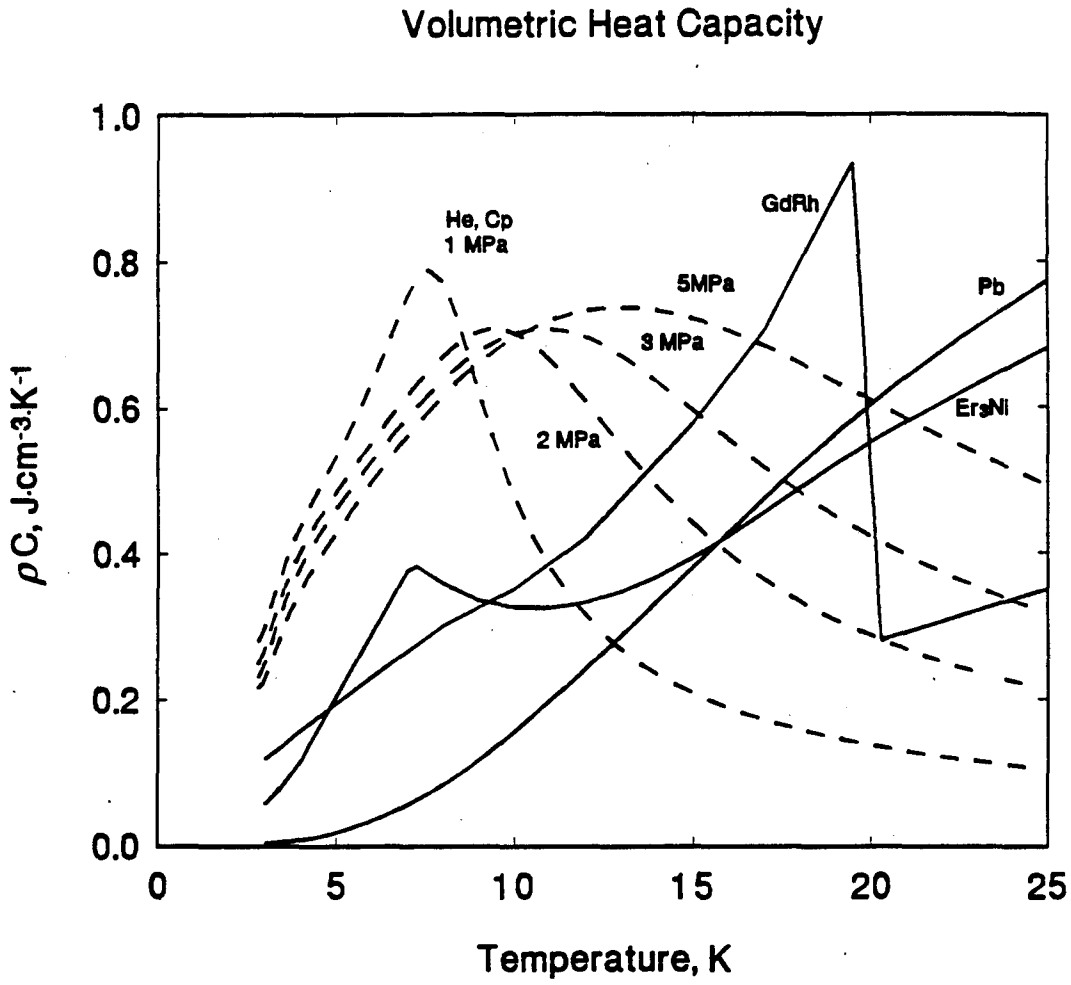

Fig. 3. Volumetric heat capacity of helium at various pressures and of common matrix materials.

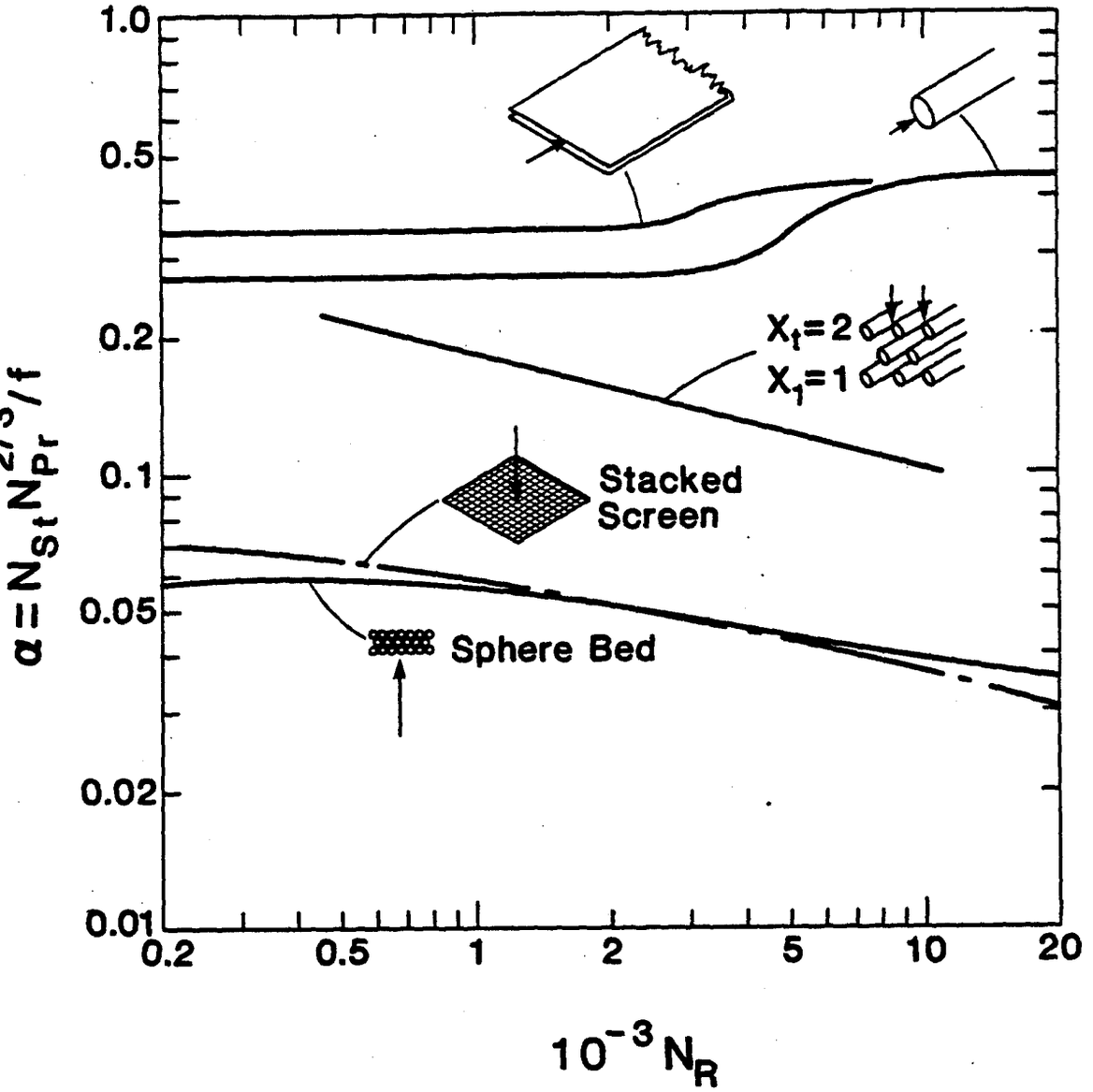

Fig. 4. Ratio of heat transfer and friction factor as a function of Reynolds number for several configurations.

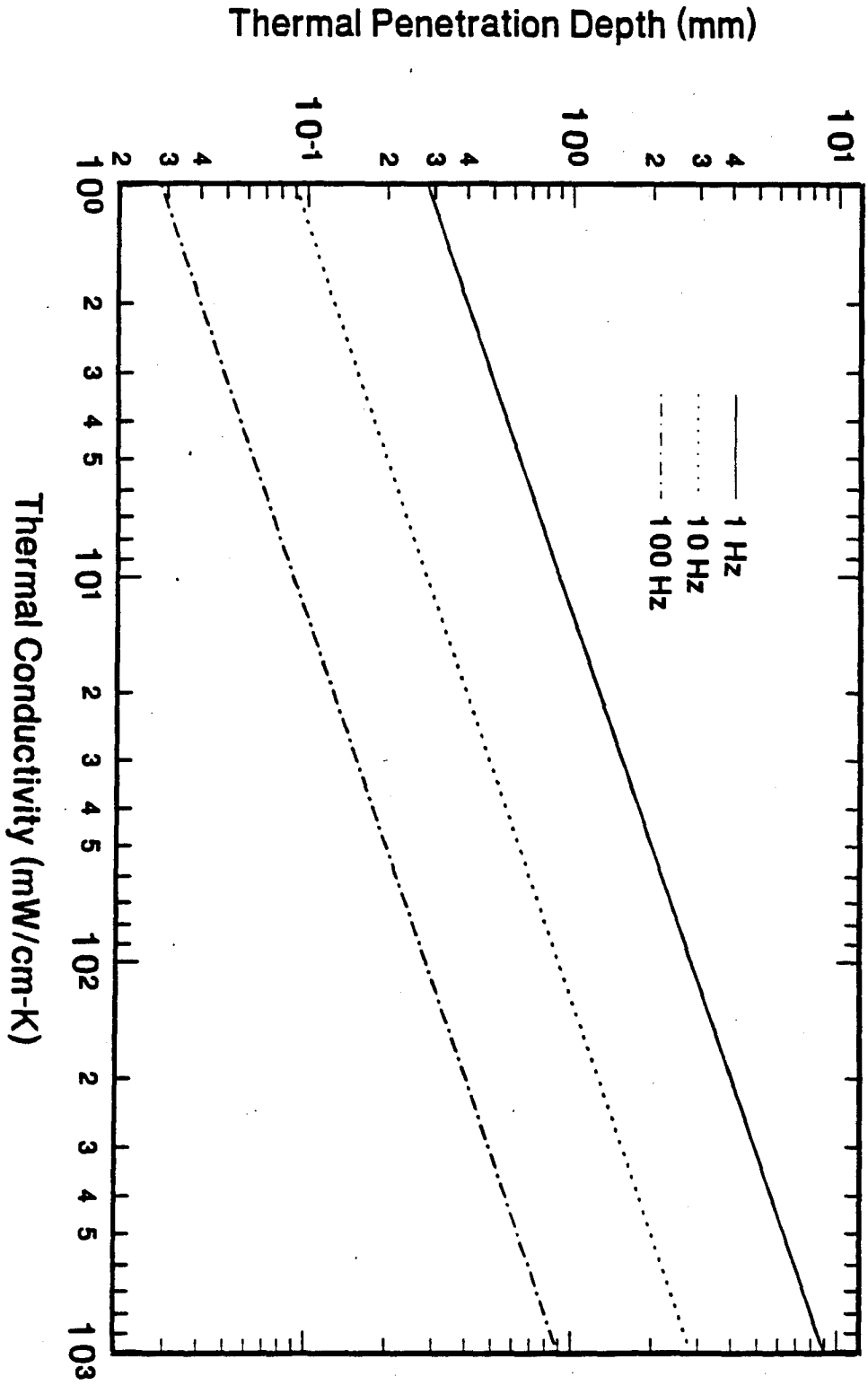

Fig. 5. Thermal penetration depth as a function of thermal conductivity for a matrix material with volumetric heat capacity of 0.4 J/(cm^3·K).

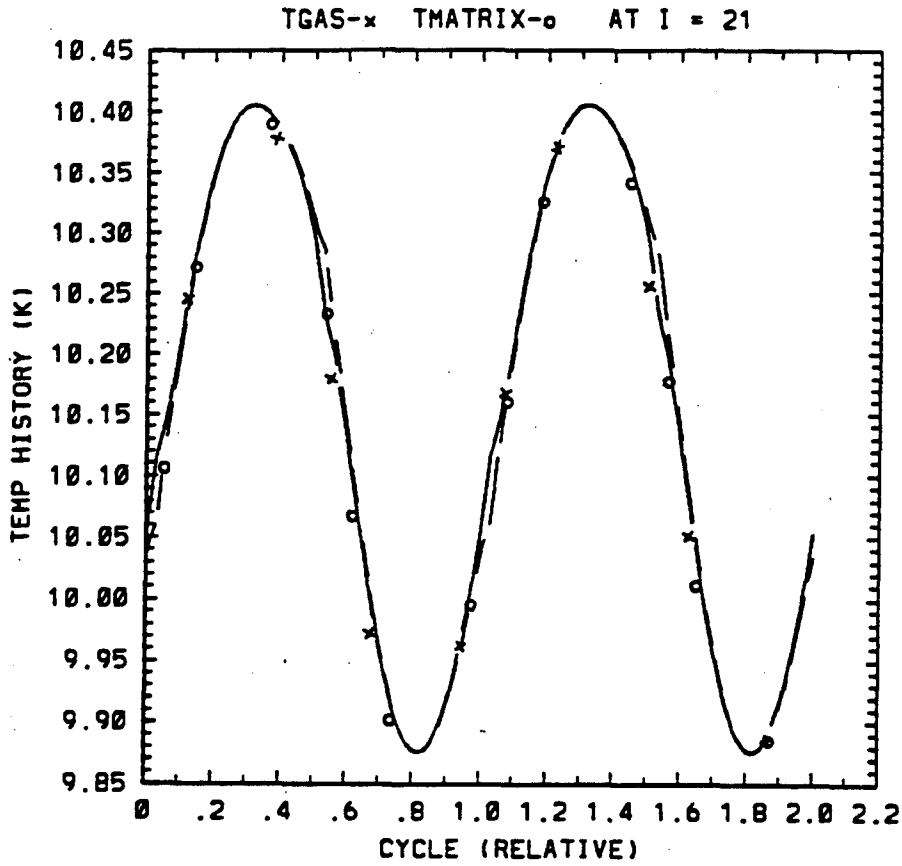

Fig. 6. Temperature of the gas and the matrix as a function of time at the center of the regenerator for Case A.

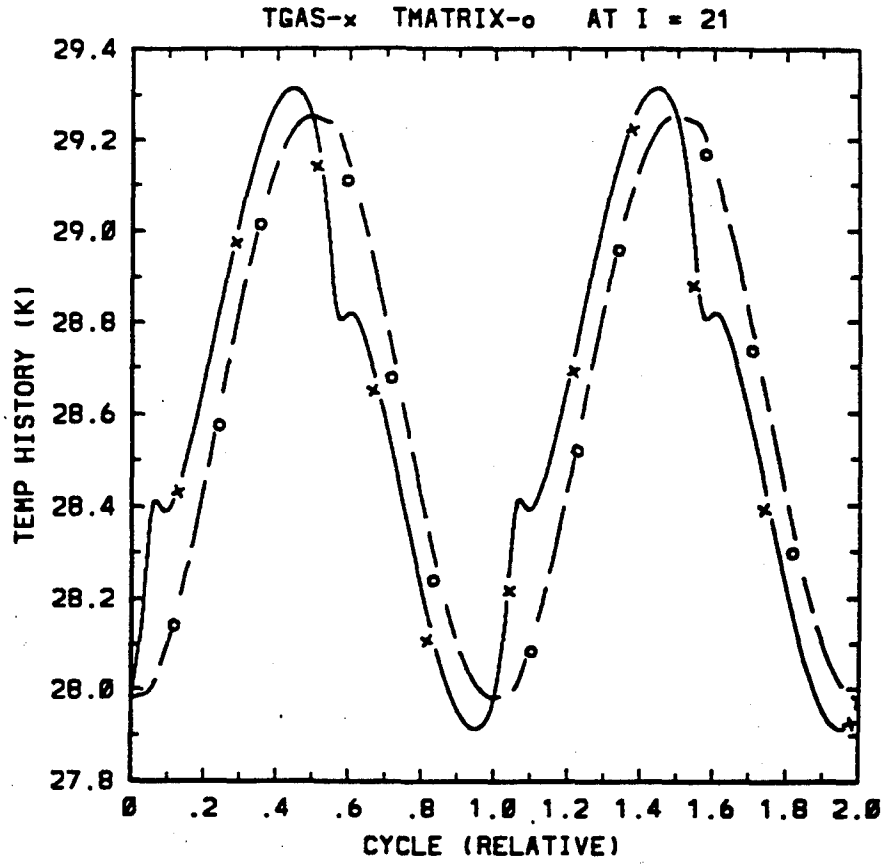

Fig. 7. Temperature of the gas and the matrix as a function of time at the center of the regenerator for Case D.

APPENDIX A
RELATIONSHIP BETWEEN GAS AND MATRIX TEMPERATURES

The conservation of energy equation for the matrix is given by

$$h_t A(T-T_m) = C_r \dot{T}_m, \tag{32}$$

where h_t is the heat transfer coefficient and A is the surface area for heat transfer between the gas and the matrix. The definition of the number of heat transfer units is

$$N_{tu} = \frac{h_t A}{\langle \dot{m} \rangle c_p}, \tag{33}$$

where $\langle \dot{m} \rangle$ is the mass flow rate averaged over a half cycle. When this equation is solved for $h_t A$ and substituted into Eq. (32) we have

$$\langle \dot{m} \rangle c_p N_{tu}(T-T_m) = C_r \dot{T}_m. \tag{34}$$

We now assume that the gas and matrix temperatures oscillate sinusoidally, which means that they can be represented by complex variables in the manner

$$T_m = T_{m1} e^{i(\omega t + \phi)}, \tag{35}$$

where T_{m1} is the amplitude of the temperature oscillation, ω is the angular frequency, and ϕ is the phase angle at $t = 0$. With this sinusoidal approximation we have

$$\dot{T}_m = i\omega T_m. \tag{36}$$

Substituting Eq. (36) into Eq. (34) yields

$$\langle \dot{m} \rangle c_p N_{tu}(T-T_m) = C_r i\omega T_m. \tag{37}$$

Equation (37) can be solved for T_m to give

$$T_m = \frac{T}{1 + \dfrac{i\omega C_r}{\langle \dot{m} \rangle c_p N_{tu}}}. \tag{38}$$

The term $\langle \dot{m} \rangle$ is given by

$$\langle \dot{m} \rangle = 2fm, \tag{39}$$

where m is the mass of gas moved in the half cycle. When Eq. (39) is substituted into Eq. (38) and $2\pi f$ is used for ω, we get

$$T_m = \frac{T}{1 + \dfrac{i\pi C_r}{mc_p N_{tu}}} = \frac{T}{1 + \dfrac{i\pi (C_r/C_f)}{N_{tu}}}. \tag{40}$$

This equation can be rewritten in the alternate form

$$T_m = \frac{Te^{-i\beta}}{\sqrt{1 + \left(\dfrac{\pi (C_r/C_f)}{N_{tu}}\right)^2}}, \tag{41}$$

where

$$\beta = \tan^{-1}\left(\frac{\pi (C_r/C_f)}{N_{tu}}\right). \tag{42}$$

Equation (41) shows that the amplitude of T_m is reduced from that of T by the factor in the denominator of Eq. (41) and that T_m lags T by the phase angle β. Both the amplitude and phase are determined by the ratio $(C_r/C_f)/N_{tu}$. For small values of this ratio it has the largest influence on the phase angle. Equations (41) and (42) show that $T_m \approx T$ whenever $(C_r/C_f)/N_{tu} \leq 0.05$.

APPENDIX III

Report on

PRELIMINARY FEASIBILITY STUDY OF FULLERENE THERMAL PROPERTIES FOR CRYOGENIC APPLICATIONS

performed for General Pneumatics Corporation
for the USAF Phillips Laboratory Contract No. F29601-93-C-0085

Preliminary Feasibility Study of Fullerene Thermal Properties for Cryogenic Applications

John B. Page and Otto F. Sankey

Department of Physics and Astronomy

Arizona State University, Tempe, Arizona 85287-1504

(August 25, 1993)

I. LOW TEMPERATURE SPECIFIC HEAT OF PURE SOLID FULLERENES

A. Solid C_{60}

In a classically vibrating system at high temperatures, each mode will contribute R/N_A to the specific heat, where R is the ideal gas constant (8.31 J/mol K) and N_A is Avogadro's number (6.02×10^{23}). Thus for a solid of C_{60} molecules, each molecule has $n_{DOF} = 3 \times 60$ vibrational degrees of freedom, and the high temperature specific heat will approach $n_{DOF} \times R = 180R$ for each mole (720 grams) of solid. This result (the law of Dulong-Petit) only holds for high enough temperatures that quantum effects are negligible.

The n_{DOF} modes of each C_{60} molecule can be classified into three categories - 174 "internal" vibrational modes within the ball, 3 rotational modes of the rigid ball, and 3 modes involving rigid translation of the ball. Because the bonds within the ball are so strong (2-dimensional graphitic bonds), all 174 internal vibrational modes have relatively high frequencies - the *lowest* on-ball frequency is 265 cm^{-1}, which translates into an energy in temperature units of $\Theta_{on\ ball} = 381$ K. As the temperature is cooled below this value, all of the internal modes freeze out (go into their quantum mechanical ground states), and their contribution to the specific heat decreases exponentially with decreasing temperature. Hence at the low temperatures of interest here (5 - 30 K), *all* 174 intra-ball modes are inactive and do not contribute to the specific heat.

Thus we immediately see a potential disadvantage of using a large molecule with strong internal bonds, such as C_{60}. This is that out of the n_{DOF} degrees of freedom available from each molecule to contribute to the specific heat, there remains only a small fraction not frozen out at temperatures well below room temperature. For C_{60}, this fraction is $f = 6/180 = 0.033$, so that 97 % of the modes cannot contribute.

The remaining modes, which *can* contribute to the low temperature specific heat, are the three vibrational and three rotational modes of each rigid ball. At low temperatures C_{60} forms a weakly bonded (van der Waals) solid. Since each ball's internal modes are frozen out as discussed above, one can regard the solid as being composed of very heavy ($60 \times 12 = 720$ amu) "atoms" which are weakly bound. Accordingly, we expect the low-temperature solid to have a spectrum of collective low-frequency vibrational and "librational" (twisting) modes – these are just the modes formed out of the translational and rotational modes for the individual C_{60} molecules. If the frequencies of the collective modes are sufficiently low, they could give rise to a substantial specific heat *per ball* at low temperature. We will see below that this is indeed the case. Unfortunately, however, the large size of each C_{60} molecule (7.1 Å diameter) results in the number of molecules per unit volume in the solid being rather low, such that the net low temperature specific heat/volume is less than that for some competing solids.

The crystal structure of solid C_{60} is face centered cubic (FCC), with the center-to-center distance between adjacent balls being $\approx 10\mathring{A}$. At low temperatures the structure is more accurately described as simple cubic (SC) with four molecules inside the unit cube. This SC solid still has the FCC arrangement of molecules, but the corner and 3 face molecules of the FCC arrangement are oriented differently, yielding the SC structure. At room temperature the molecules rotate freely, but at low temperature the rotations becomes collective librational modes, as discussed above.

We will now first qualitatively discuss the contribution to the specific heat of the vibrational and librational modes in low temperature solid C_{60}, and then discuss published experimental results of the low temperature specific heat.

Li, Lu and Martin [1] and Yildirim and Harris [2] have performed model calculations of the vibrational and libration modes of solid C_{60}. The results of Ref. [1] are shown in Fig. 1. The different panels show the mode frequencies vs. wavevector, for various high symmetry directions in the solid. In total, there are $6 \times 4 = 24$ branches, since there are 6 modes per ball and 4 balls per SC cell. These calculated results should be considered as semiquantitative, with errors possibly as large as 50%. Fig. 1b shows only the vibrational mode branches and Fig. 1c shows just the librational branches. The librations involve twisting oscillations of the molecules, and we note that their frequencies are in the 11 – 20 cm^{-1} range. In energy units this converts to a temperature range of 16 – 30 K. Hence the librational modes will contribute to the specific heat above this temperature range, and their contribution will exponentially decrease at temperatures below this range.

The vibrational branches (Fig. 1b) are of two types: acoustic and optic. The 3 acoustic branches (elastic waves) increase linearly with frequency from wavevector $k = 0$ (Γ-point), and they give rise to a Debye contribution to the specific heat. The 9 optic mode branches have frequencies in the range 20 – 45 cm^{-1}, corresponding to 30 - 65 K in temperature units. These branches give rise to an Einstein oscillator-like contribution to the specific heat, as do the librational mode branches. Unfortunately, neither the optic nor libration branches have energies corresponding to temperatures below the 5 – 20 K range. Hence these modes will contribute less than their Dulong-Petit values to the low-temperature specific heat.

The specific heat of solid C_{60} has been measured by a number of researchers over the last several years. [4]. The low temperature specific heat of solid C_{60} has recently been measured in the temperature range 2 – 20 K by Beyermann et al. [3]. These researchers successfully modeled their data assuming 3 acoustic vibrational branches with a Debye temperature $\Theta_D = 37$ K, 9 optic vibrational branches with an Einstein temperature $\Theta_E = 30$ K, and twelve 12 librational branches with an Einstein temperature $\Theta_L = 58$ K. They also used a very small linear term γT, of unknown origin. This simple model almost perfectly fits their data. In this analysis the vibrational Debye contribution is largest below

4 K, while the optic vibrations dominate from 4 K to over 20 K. The resulting volume specific heat is shown in Fig. 2(a), along with data on other materials for comparison [Fig. 2(b)]. We note that in the 5 – 30 K range, the volume specific heat of solid C_{60} is not particularly large compared to other materials. *Thus pristine C_{60} solid does not have an overly high specific heat per unit volume in the 5 – 30 K temperature range.*

We can then ask why the specific heat at low temperatures is not especially large, and how we might increase it. The reasons for the relatively small low-temperature volume specific heat are threefold: (1) Only 6 of the 180 modes (3%) of each ball can contribute at temperatures well below room temperature, as discussed earlier. (2) The low-frequency collective modes, which *could* contribute, have Debye frequencies (acoustic vibrations) and Einstein frequencies (optic vibrations and librations) that are relatively high for our purposes: in temperature units they are 37 K, 30 K, and 58 K respectively. As a result, for temperatures in the 5 – 30 K range, the collective modes are being frozen out. (3) Owing to the large size of each C_{60} molecule, the number of balls per unit volume in the solid is very low compared with the number of atoms/volume in "ordinary" solids. To illustrate, we note that the Debye temperatures for a soft heavy solid, Lead, and for a soft light solid, Argon, are 88 K and 85 K, respectively, which are larger than for C_{60}. Nevertheless, from Fig. 3 we see that both Pb and Ar have significantly larger low temperature specific heats, *per unit volume*, than solid C_{60}. The dominant effect is that the numbers of atoms/volume for solid Pb and Ar are much larger than the number of balls/volume in solid C_{60} – the volumes occupied by Pb and Ar atoms in the solids are 30 $Å^3$ and 36 $Å^3$, respectively, compared with the $\approx 710 Å^3$ occupied by each ball in solid C_{60}. Thus the number of atoms/volume for these solids is more than 20 × the number of balls/volume for solid C_{60}. This factor strongly overcomes the effect of their higher Debye temperatures, leading to much higher volume specific heats than for solid C_{60}.

If, on the other hand, we plot the low temperature specific heats of these three solids *per unit mass*, the situation is quite different, owing to the very different mass densities of solid Ar and Pb. As seen in Fig. 4, the mass specific heat of C_{60} is now about a factor of

two greater than that of lead over the range 10 K – 15 K, while that for Ar is much larger than for either of these materials.

B. Solids formed from larger icosahedral fullerenes

We now briefly speculate on how the low temperature specific heat of solid C_{60} might be changed by increasing the number of atoms per ball. There is believed to exist a whole family of ball-like fullerenes (e.g. icosahedral C_{60}, C_{80}, C_{140}, C_{180}, C_{240}, etc.). In solid C_{60} the balls interact through Van der Waals bonds comparable with those in planar graphite, and the distance between adjacent ball-ball surfaces is about 3 Å, similar to the interplanar separation in graphite. Accordingly, we now consider FCC fullerene solids composed of the larger balls listed above, with the surface-surface spacing between adjacent balls maintained at its 3 Åvalue for C_{60}. The dynamical effect of the larger balls should be to lower the Debye and Einstein frequencies for the collective vibrational and librational modes; these frequencies should be proportional to $1/\sqrt{n_{ball}}$ for the vibrations and to $1/n_{ball}$ for the librations. These decreases will result in the specific heats falling off with decreasing temperature more slowly for the larger fullerenes, as shown in Fig. 5. Thus for our hypothetical solid C_{240}, we see that the estimated volume specific heat does not begin to fall off until below 10 K. Unfortunately, however, the number of C_{240} balls/volume is only 20 % that for solid C_{60}, and this results in our computed volume specific heat being lower than that for solid C_{60}, for temperatures above 7 K. The mass densities for these hypothetical fullerene solids are within 80 % of that for solid C_{60}, so that our computed mass specific heats for these solids show analogous behavior.

II. LOW TEMPERATURE SPECIFIC HEAT OF C_{60} ENCAPSULATED ATOMS

We next consider the possibility of using C_{60} molecules as relatively large-volume cages encapsulating atoms or molecules. The existence of such so-called "endohedral" fullerenes has been established both experimentally and theoretically over the last few years ([5]);

for instance, the existence of endohedral fullerene complexes with He and La is well established. Moreover, the strong C-C bonds in the cage render the individual balls very incompressible [8] and also should allow efficient transmission of thermal energy into endohedral fullerenes.

In general, the specific heat of a confined particle will approach its maximum value (Dulong Petit) for temperatures such that the thermal average energy becomes comparable with the quantum mechanical level spacing. Hence, small level spacings will enhance the low-temperature specific heat. The uncertainty principle results in the level spacing scaling inversely with the confining volume, and because the volume of C_{60} is large on an atomic scale, a fullerene-encapsulated particle may well be able to maintain its Dulong-Petit specific heat at relatively low temperatures.

As a crude estimate of this effect, we consider the simple problem of a free particle of mass m in a cubical box of volume $V = L^3$. The energy levels are given by

$$E_{n_x,n_y,n_z} = \frac{1}{2m}\left(\frac{\hbar\pi}{L}\right)^2(n_x^2 + n_y^2 + n_z^2), \tag{1}$$

where $n_\alpha = 1, 2, 3, \ldots$. The level spacing scales as $V^{-2/3}$. It is straightforward to evaluate the heat capacity C using the general expression

$$\frac{C}{k_B} = \left(\frac{1}{k_B T}\right)^2 \left\{ \frac{Z \sum_n d_n E_n^2 \exp(-\beta E_n) - [\sum_n d_n E_n \exp(-\beta E_n)]^2}{Z^2} \right\}, \tag{2}$$

for a system with a set of energy levels $\{E_n\}$ having degeneracies $\{d_n\}$. The quantity Z is the partition function, given by $Z = \sum_n d_n \exp(-\beta E_n)$ and $\beta = 1/(k_B T)$.

If we evaluate this using the energy levels of Eq. 1 for the case of a Helium atom (mass 4 amu) inside a cubical box of volume equal to that for a C_{60} molecule [$V = (5.64\mathring{A})^3$], we obtain the curve given in Fig. 6. We note that even for this light atom, C/k_B is slightly *above* its Dulong-Petit value (3/2) over the entire temperature range 5 - 30 K. This may be viewed as encouraging, but our crude estimate has of course overestimated the volume likely to be available to an endohedral atom, thereby overestimating the heat capacity.

To be more realistic, we turn to published estimates of the entrapped atom's potential energy function in endohedral fullerenes. [6,7] The few existing papers on this topic deal

mostly with closed-shell encapsulated ions, which are found to stabilize the endohedral fullerenes energetically. In Ref. [6], it is predicted that the equilibrium position of Na^+ in C_{60} is displaced by $\approx 0.7\AA$ from the cage center, with an energy lowering of 0.04 eV relative to the center. The potential energy is found to have little angular dependence. Qualitatively similar behavior is predicted for other guest ions, i.e. F^-, Mg^{2+}, and Al^{3+}. Hence for such systems it appears that as a first approximation one can regard the trapped particle as moving freely on a spherical surface; for Na^+, the radius would be 0.7 Å. For this model, the energy levels are given by

$$E_n = \frac{\hbar^2}{2I} n(n+1), \tag{3}$$

with $I = mr^2$ and $n = 0, 1, 2, \ldots$ The degeneracy is $d_n = 2n + 1$.

Using this formula in Eq.(2) to estimate the heat capacity for Na^+ (m = 23. amu) moving freely on a sphere of radius $r = 0.7\AA$, we obtain the results shown in Fig. 7, and again it is seen that the Dulong-Petit value is maintained over the temperature range (5 -30 K). (The value of C/k_B is 1 for this case, since there are now two degrees of freedom available to the particle.)

So the attainment of the Dulong-Petit value for the low-temperature heat capacity appears to be readily attainable for individual endohedral fullerene molecules. The basic reason is that the encapsulated ions have a relatively large amount of "room" in which to move, resulting in closely spaced energy levels. Unfortunately, this is not the whole story since, by the same token, the net contribution to the overall specific heat *per unit volume* decreases with increasing fullerene volume, as previously noted. Hence, to determine the range of possibilities, we next use the observed volume and mass densities of solid C_{60} at atmospheric pressure (and at 20 GPa [200 kbar]) to estimate the maximum attainable specific heats (the Dulong-Petit values), with respect to both volume and mass, for several possible degrees of freedom that might be available to encapsulated particles in solid C_{60}. These maximum values are are (per ball): 1) $3k_B/2$ for a freely translating particle, 2) k_B for a particle confined to move freely on a sphere – this is the same as for a small,

freely rotating "dumbell" molecule), 3) $5k_B/2$ for a trapped molecule which can rotate *and* translate, 4) $3k_B$ for a bound particle behaving as a 3-dimensional simple harmonic oscillator. The results are given in Table I, where we have also included the volume and mass specific heats of solid C_{60} at 5 K and 20 K.

We see that the inclusion of encapsulated particles can indeed increase the volume and mass specific heats of solid C_{60}, especially at low temperatures. The case of an encapsulated 3-dim. oscillator appears to be favorable, but it might be difficult to achieve in practice: to retain 80 % of its Dulong-Petit heat capacity at, say 10 K, its frequency would have to be $\approx 12cm^{-1}$, which is quite low. However, the table values for the rotor case (or for a combination of translation/rotation) are probably attainable over the whole 5 K – 30 K temperature range, for simple encapsulated ions like Na^+, K^+, etc. Again, the basic physics is that the encapsulated particles effectively add degrees of freedom to each ball, and the large available volume in each ball is such that these new degrees of freedom produce heat capacities which maintain their Dulong-Petit values down to very low temperatures. However, just as for the case of pure solid C_{60}, the relatively low number of fullerene molecules/volume results in volume specific heats which are less than those for other pure solids, such as Argon and Lead, as discussed in Section I.

III. SUMMARY

Based on the foregoing discussion, it appears that a solid formed from endohedral C_{60} molecules, each of which contains an ion which is displaced from the ball center and moves on a "spherical" orbit of $\approx 0.7\AA$, is probably the most attractive fullerene system. The specific heat of such a system would be enhanced by nearly a factor of 3 at 5 K over that for the pristine solid, and by substantially more at lower temperatures. However, our discussion also shows that even encapsulated solid C_{60} would not have an overly high specific heat per unit volume over the *entire* 5 – 30 K temperature range, when compared with other solids.

REFERENCES

[1] X.-P. Li, J.P.Lu and R.M.Martin, Phys. Rev. B **46**, 4301 (1992).

[2] T.Yildirim and A.B.Harris, Phys. Rev. B **46**, 7878 (1992).

[3] W. P. Beyermann, M. F. Hundley, J. D. Thompson, F. N. Diederich and G. Grüner, Phys. Rev. Lett. **68**, 2046 (1992); Phys. Rev. Lett. **69**, 2737 (1992).

[4] J.R.Olson, K.A.Topp and R.O.Pohl, Science **259**, 1145 (1993); T.Atake, T.Tanaka, H.Kawaji, K.Saito, S.Suzuki, I.Ikemoto and Y. Achiba, Physica C **185-189**, 427 (1991); E.Grivei, B.Nysten, M. Cassart, A. Demain and J.P.Issi, Solid State Commun. **85**, 73 (1993).

[5] See, for instance, Y.Chai, T.Guo, C.Jin, R.E.Haufler, L.P.F.Chibante, J.Fure, L.Wang,J.M.Alford and R.E.Smalley, J. Phys. Chem. **95**, 7564 (1991); M.M. Alvarez, E.G.Gillan, K.Holczer, R.B.Kaner, K.S.Min and R.L.Whetten, J. Phys. Chem. **95**, 10561 (1991); M.Kolb and W.Thiel, J. Comp. Chem. **14**, 37 (1993); J. Cioslowski, J. Am. Chem. Soc. **113**, 4139 (1991); and references therein.

[6] J. Cioslowski and E. D. Fleischmann, J. Chem. Phys. **94**, 3730 (1991).

[7] J.L.Ballester and B.I.Dunlap, Phys. Rev. A **45**, 7985 (1992).

[8] R.S.Ruoff and A.L.Ruoff, Nature **350**, 663 (1991). These authors use phenomenological arguments to estimate that the bulk modulus of a C_{60} molecule is 843 GPa. This reflects the strong C-C bonding and is much larger than the value 18 GPa measured for the *solid*, [9] where the balls interact through weak Van der Waals forces.

[9] S.J.Duclos, K.Brister, R.C. Haddon, A.R. Kortan and F.A.Thiel, Nature **351**, 380 (1991).

TABLES

TABLE I. Maximum attainable (Dulong-Petit) values for the specific heats per unit volume and per unit mass for various configurations of fullerene-encapsulated atoms or molecules. Also given are estimates of the maximum volume specific heat at 200 kbar pressure. For comparison, the table also gives the specific heats for pure solid C_{60} at 5 K and 20 K.

	1 Atmos.		200k Atmos.[a]
	$J/(cm^3K)$	$J/(gmK)$	$J/(cm^3K)$
"free particle"	0.029	0.017	0.043
rotor	0.019	0.011	0.028
translatable rotor	0.048	0.029	0.071
3-dim. oscillator	0.060	0.036	0.088
pure C_{60} solid at 5 K	0.0066	0.0039	-
pure C_{60} solid at 20 K	0.079	0.047	-

[a]For these estimates we used the measured room temperature fractional lattice constant decrease of 12 % at 20 GPa, reported in Ref. [9]. It was also reported there that the radii of the fullerene balls were not observed to change at this pressure.

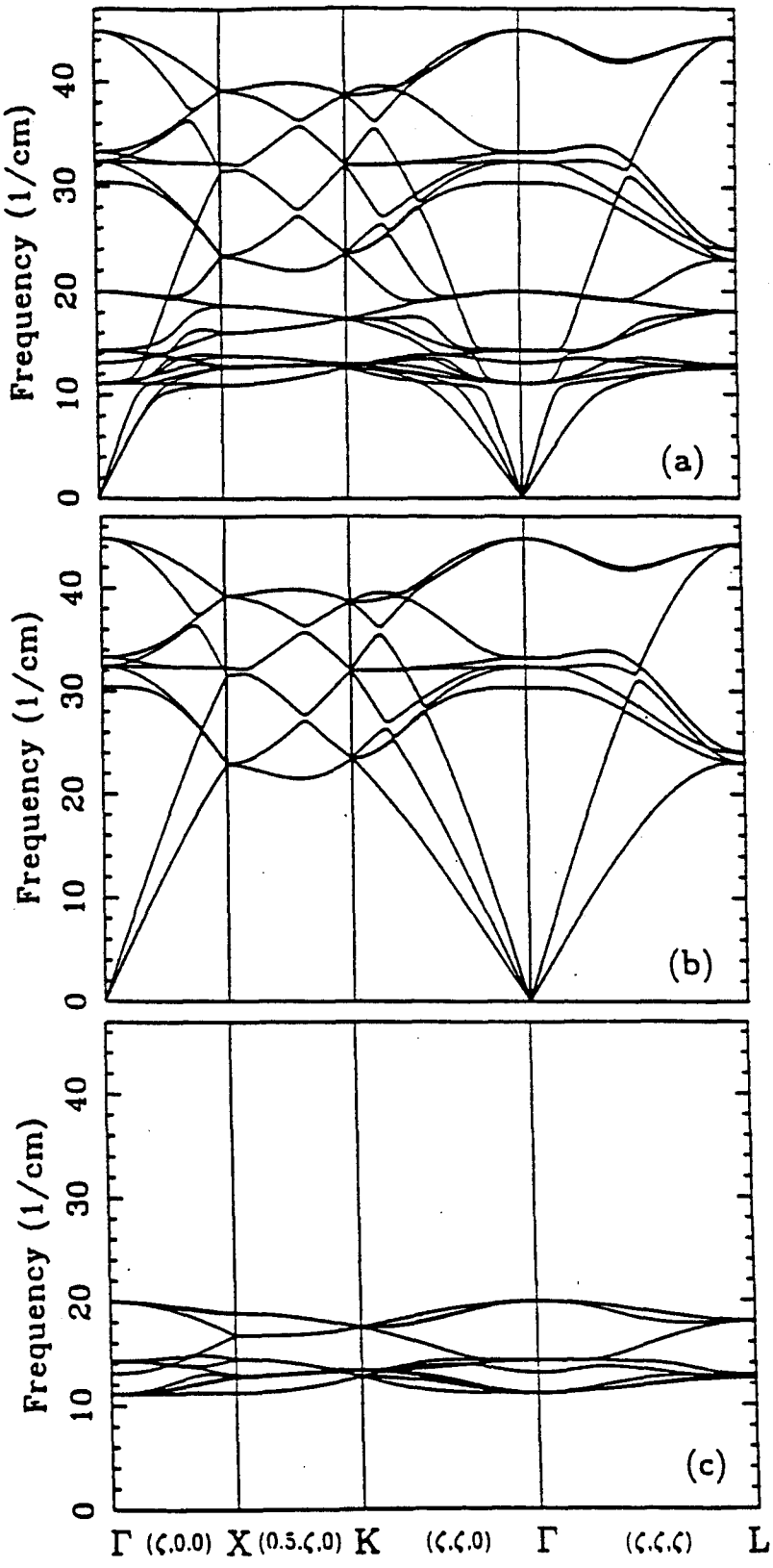

FIGURE 1 (FROM REF. 1)

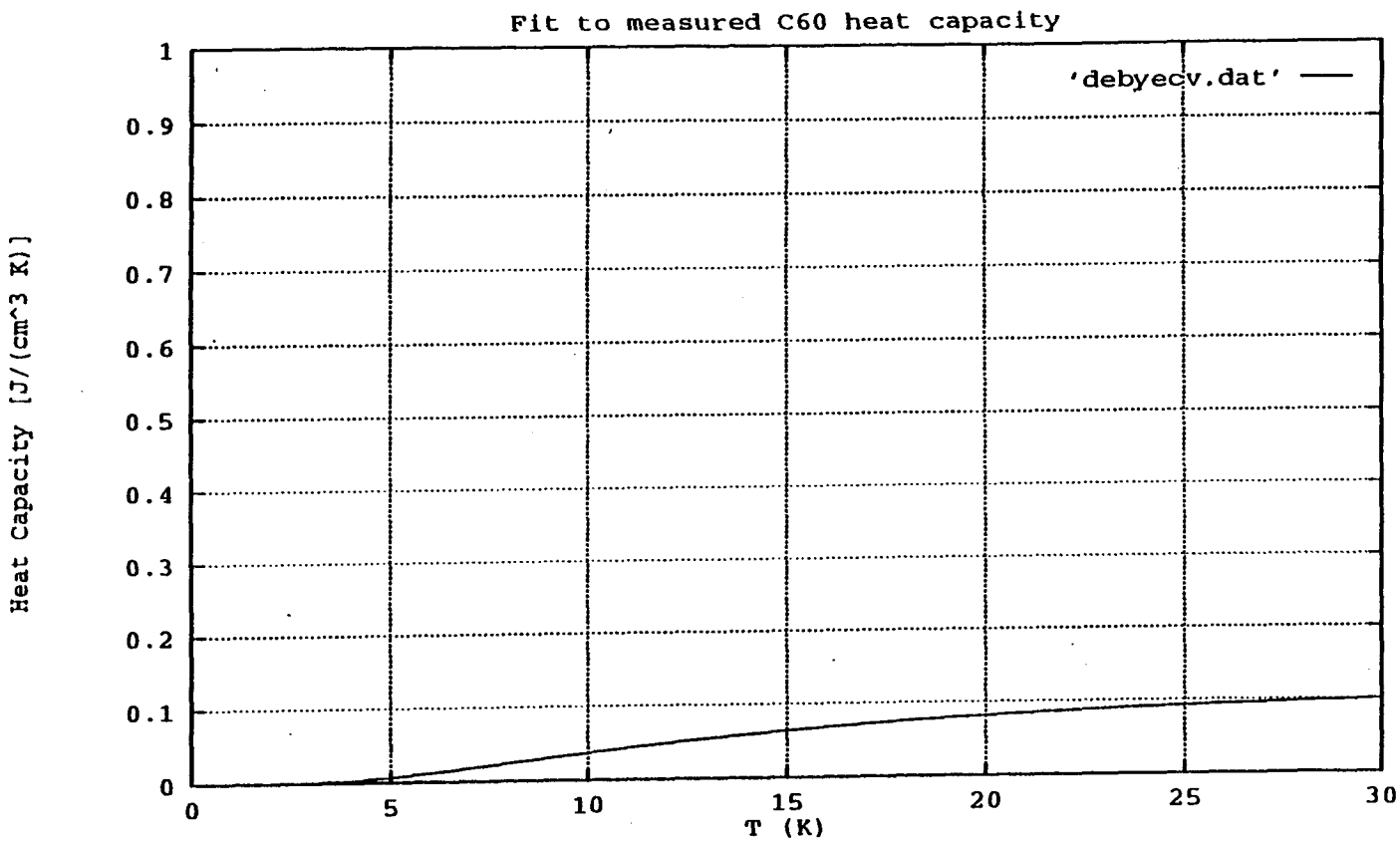
Fit to measured C60 heat capacity
'debyecv.dat'
Heat Capacity [J/(cm^3 K)]
T (K)
0
0.1
0.2
0.3
0.4
0.5
0.6
0.7
0.8
0.9
1
0
5
10
15
20
25
30

FIGURE 2(a)

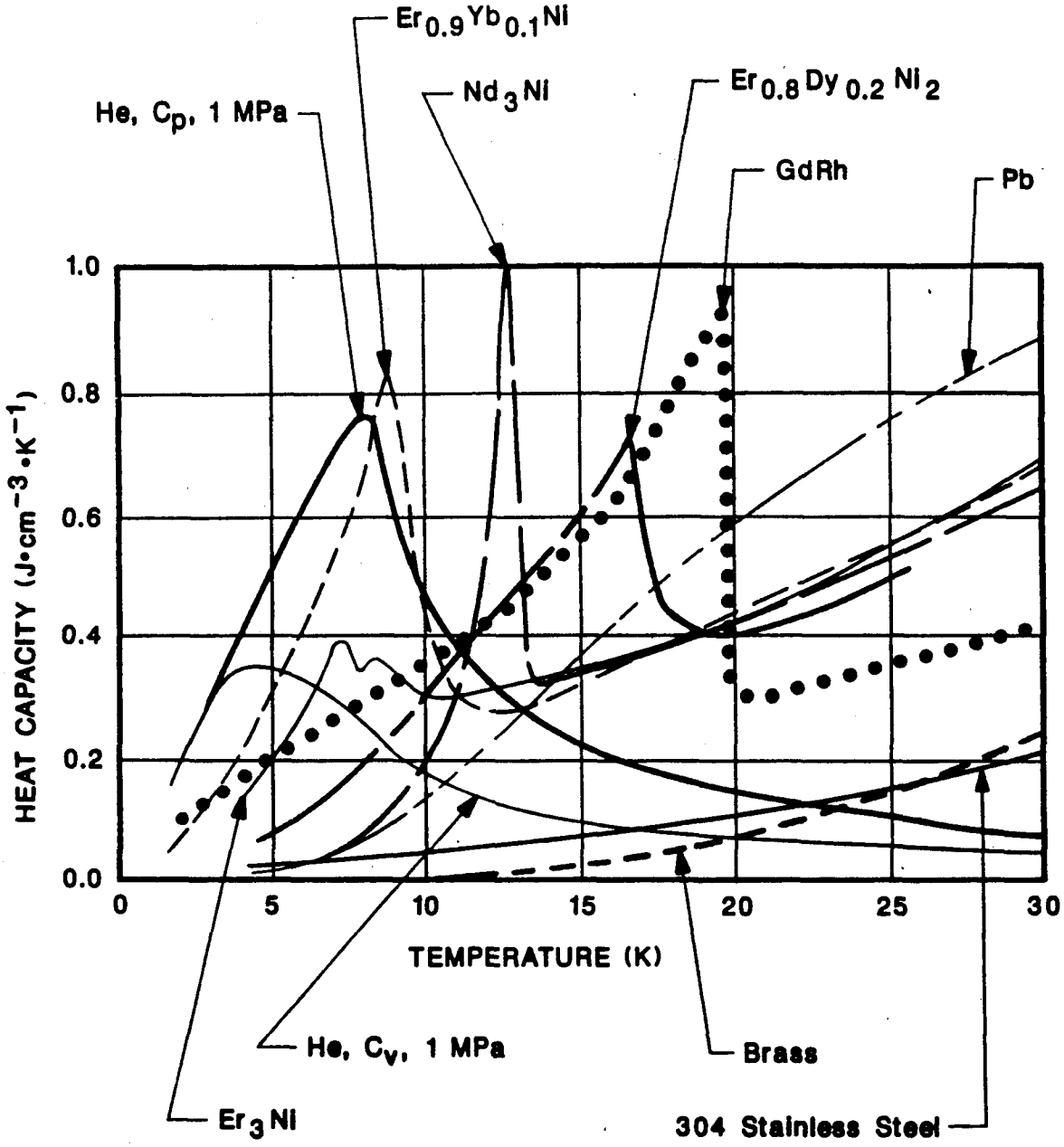

FIGURE 2. VOLUMETRIC HEAT CAPACITIES OF VARIOUS MATERIALS

FIGURE 2(b)

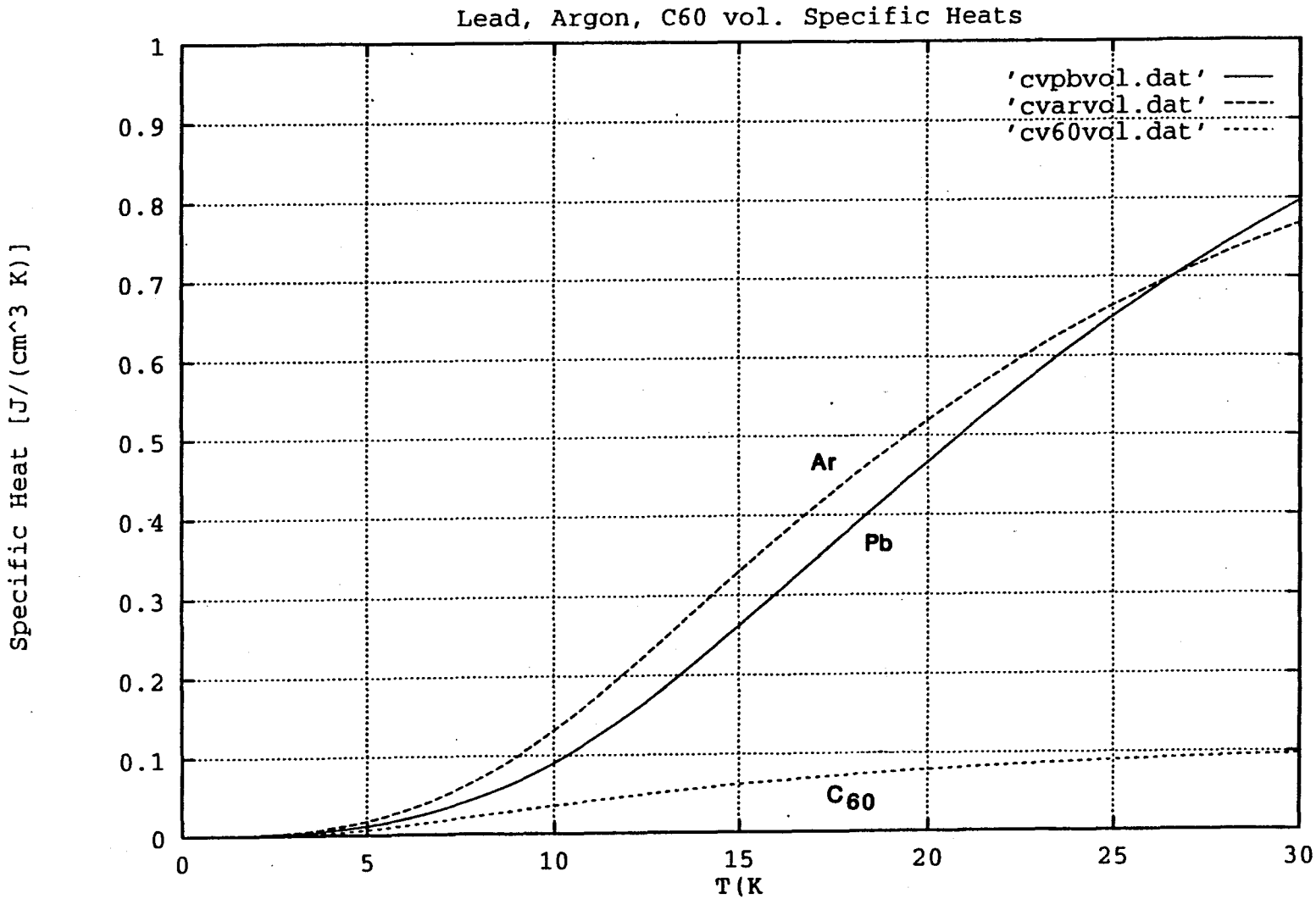
Lead, Argon, C60 vol. Specific Heats
'cvpbvol.dat'
'cvarvol.dat'
'cv60vol.dat'
Ar
Pb
C60
Specific Heat [J/(cm^3 K)]
T(K
0
0.1
0.2
0.3
0.4
0.5
0.6
0.7
0.8
0.9
1
0
5
10
15
20
25
30

FIGURE 3

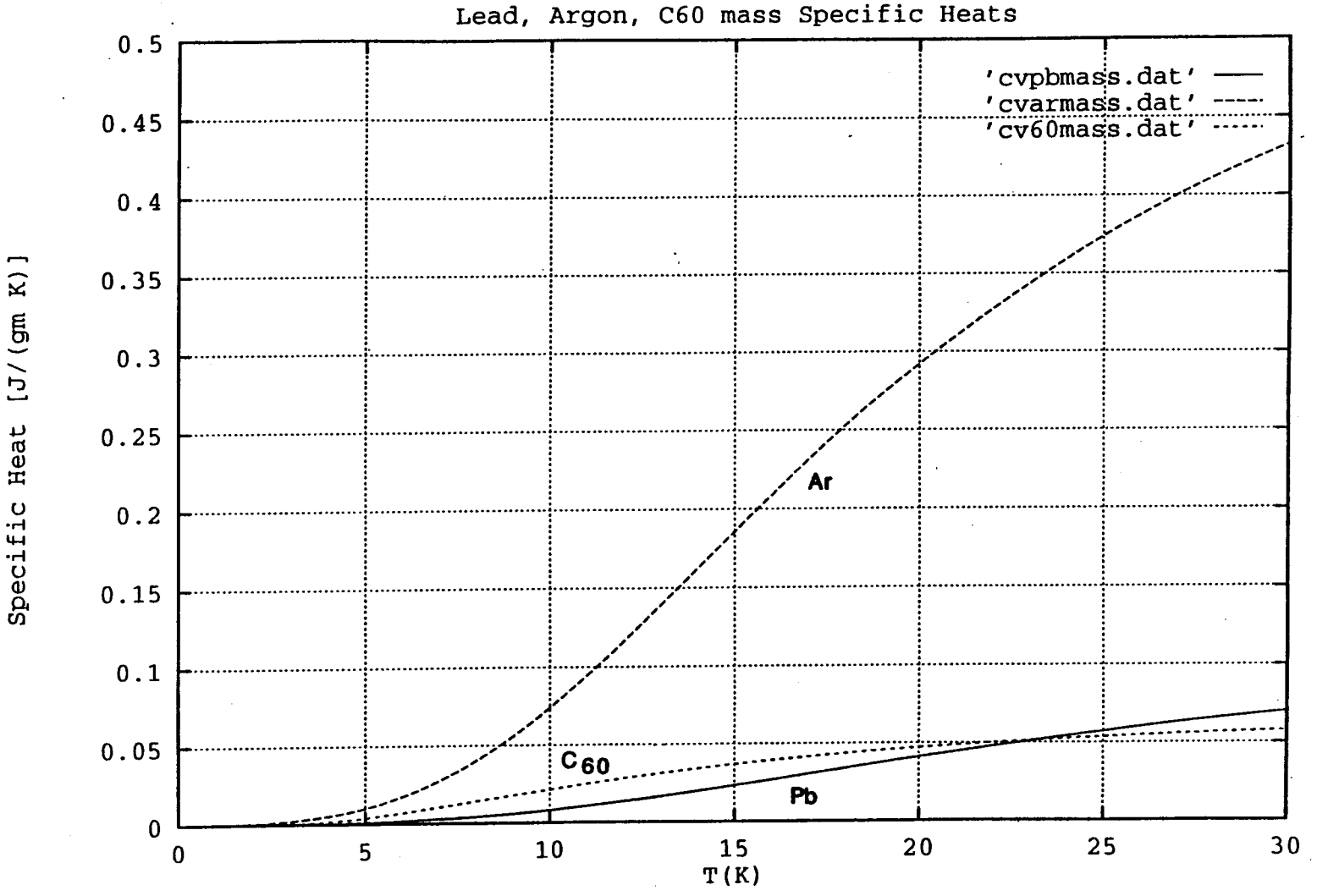
Lead, Argon, C60 mass Specific Heats
'cvpbmass.dat'
'cvarmass.dat'
'cv60mass.dat'
Specific Heat [J/(gm K)]
T(K)
Ar
C60
Pb
0.5
0.45
0.4
0.35
0.3
0.25
0.2
0.15
0.1
0.05
0
0
5
10
15
20
25
30

FIGURE 4

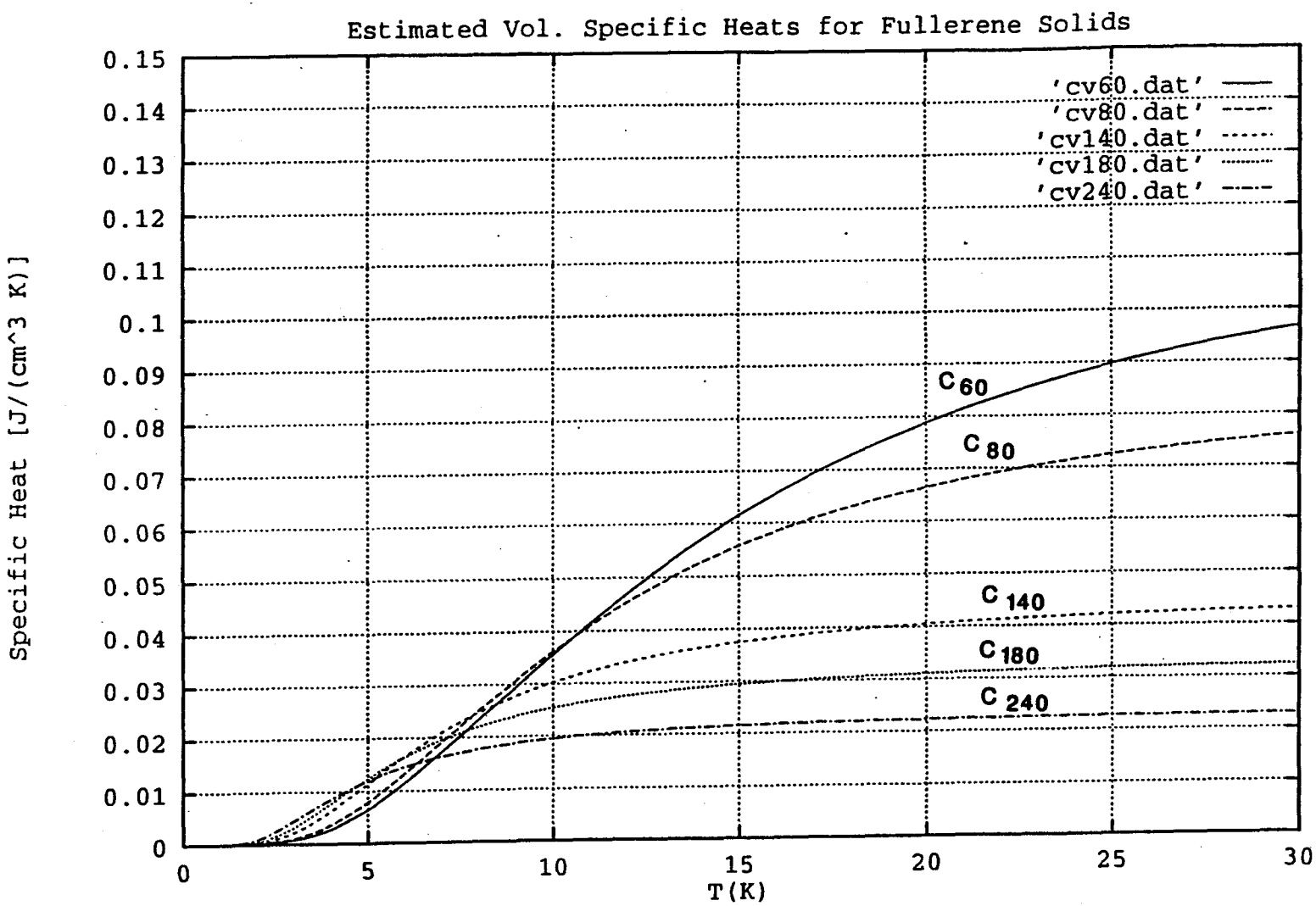
Estimated Vol. Specific Heats for Fullerene Solids
Specific Heat [J/(cm^3 K)]
T(K)
'cv60.dat'
'cv80.dat'
'cv140.dat'
'cv180.dat'
'cv240.dat'
C60
C80
C140
C180
C240
0.15
0.14
0.13
0.12
0.11
0.1
0.09
0.08
0.07
0.06
0.05
0.04
0.03
0.02
0.01
0
0
5
10
15
20
25
30

FIGURE 5

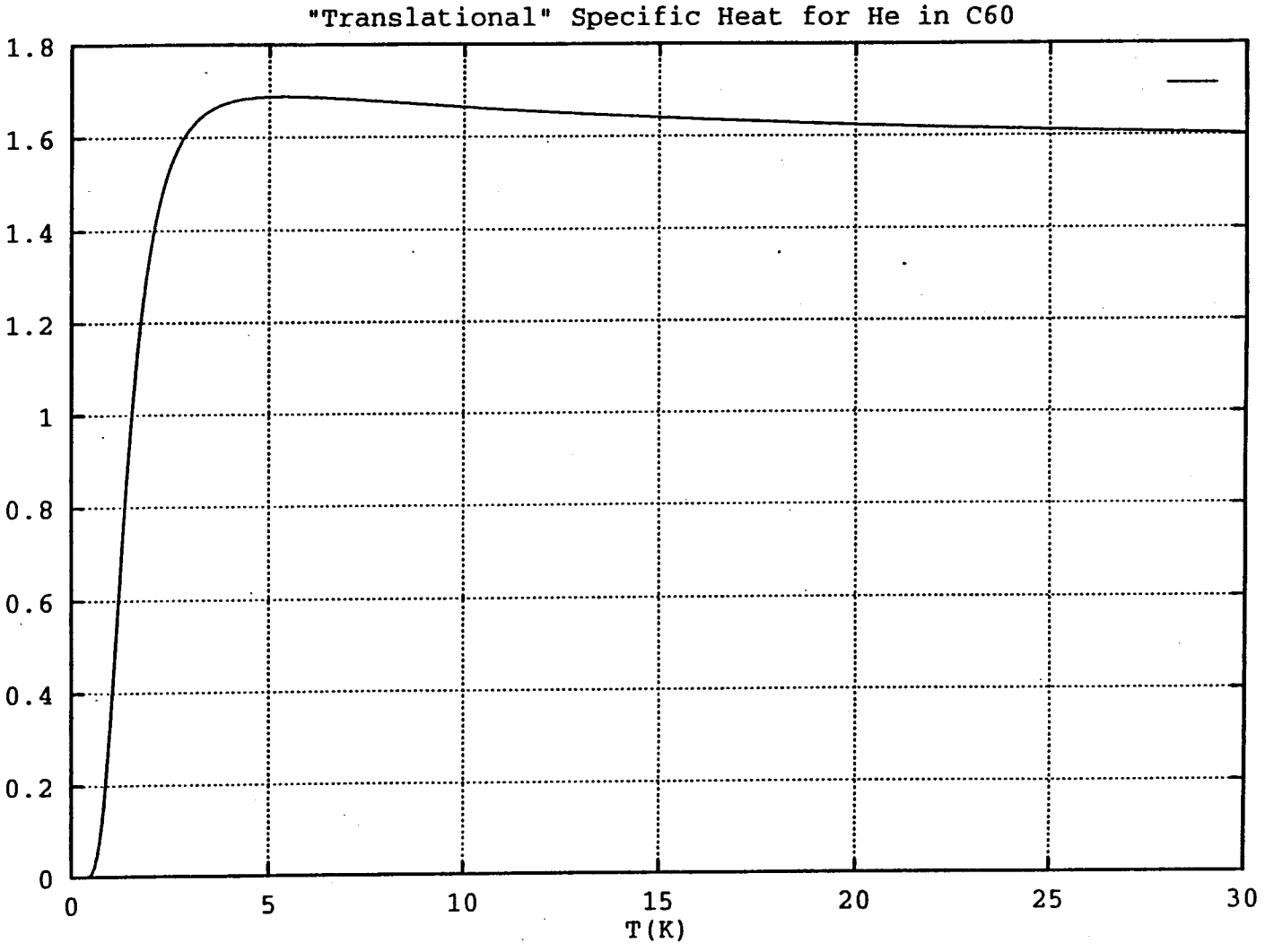
"Translational" Specific Heat for He in C60
C/kB
T(K)
0
0.2
0.4
0.6
0.8
1
1.2
1.4
1.6
1.8
0
5
10
15
20
25
30

FIGURE 6

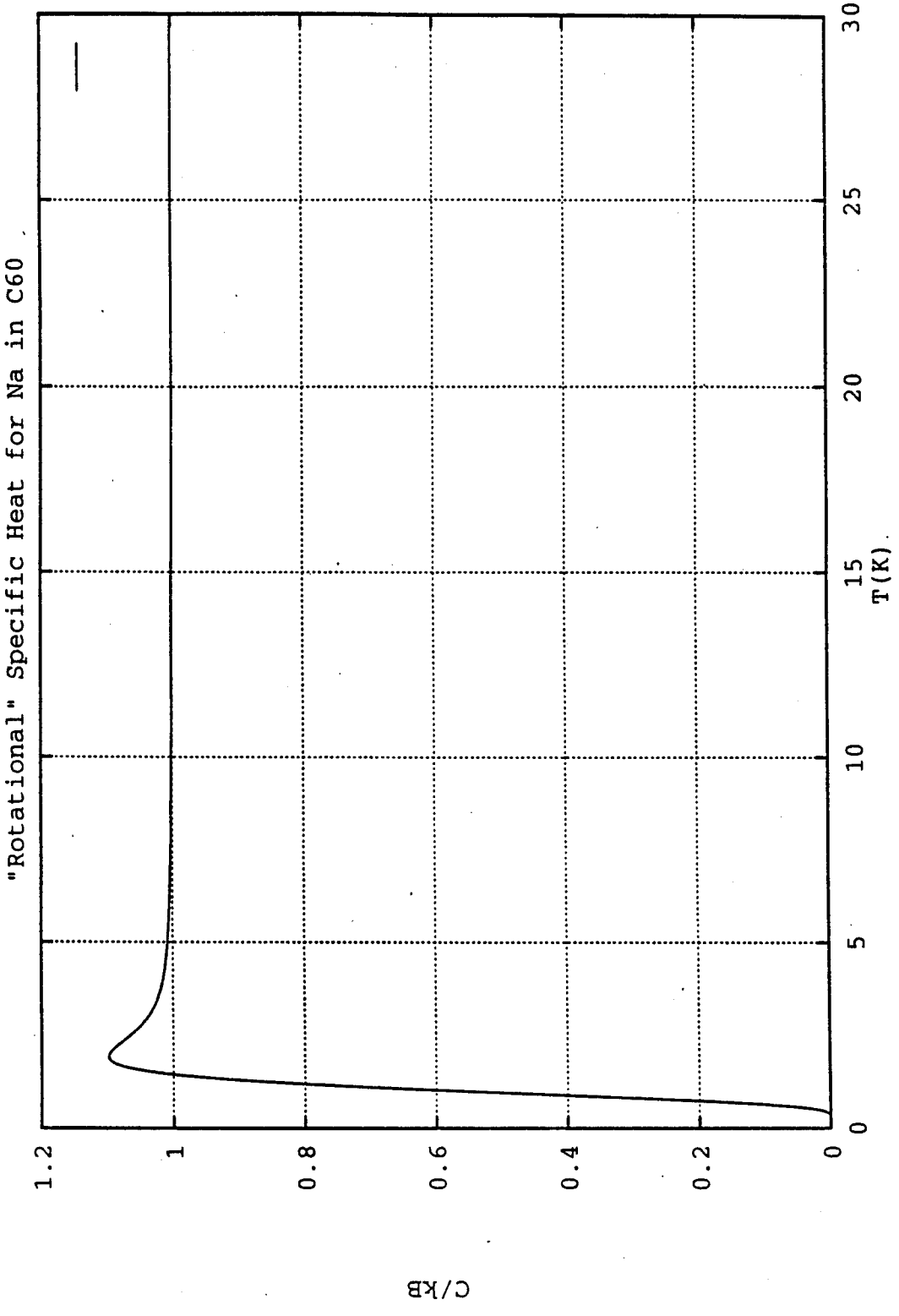
"Rotational" Specific Heat for Na in C60
C/kB
T(K)
0
0.2
0.4
0.6
0.8
1
1.2
5
10
15
20
25
30

FIGURE 7

APPENDIX IV

Report on

TECHNOLOGY FOR PRODUCING AND CONFIRMING CANDIDATE FULLERENES

performed for General Pneumatics Corporation
for the USAF Phillips Laboratory Contract No. F29601-93-C-0085

A. INTRODUCTION:

Fullerenes are closed caged pure carbon molecules with unqiue and unprecedented properties. Their unique closed caged structure permits synthesis of novel molecules with exceptional properties (1). One such novel class of molecules has been synthesized by encapsulating elements within the fullerene cage - for instance $He@C_{60}$. The encapsulation shields the element inside the cage from the outer environment - both from chemical and mechanical view point. Furthermore, these encapsulated molecules are predicted to have physical properties (such as heat capacity and thermal conductivity) that are more than mere combination of the properties of the encapsulated element and the unique three dimensional cage structure of the fullerenes. Therefore, these novel materials are ideal candidates for applications where some particular element needs to be used but has to be positioned and shielded away from the application environment. One such application is advanced high performance cryogenics where the candidate cryogenic media (stationary helium) needs to be isolated from the heat transfer fluid (flowing helium).

Furthermore, C_{60} - the most prominent and abundant member of the fullerene family - has a unique lattice structure with C_{60} molecules rotating rapidly in the crystal lattice [1]. Within the lattice and at room temperature, the mean cage diameter is 6.83 Å and the mean cage outer diameter is 10.18 Å. The tetrahedral site radius in the lattice is 1.12 Å and the octahedral site radius is 2.07 Å [2]. Based on the above data, the theoretical voidage for C_{60} is about 48% and the minimum lattice porosity is about 12% (based on mean cage diameter). These features bestow C_{60} with fluid flow properties that are ideally suited to the fluid flow issues in cryogenics.

Together, the unique closed cage structure and the high lattice porosity, make C_{60} an ideal candidate material basis for cryogenic applications. This report describes the methods that can be used to produce candidate fullerene materials, the various techniques for determining whether helium or other elements have been encapsulated, procedures for forming and shaping of bulk material so as to determine the bulk properties and a preliminary plan for producing and verifying fullerene samples for testing in Phase II.

B. PRODUCTION OF CANDIDATE FULLERENES IN MACROSCOPIC QUANTITIES.

There are many methods of producing macroscopic quantities of candidate fullerenes. These methods can be grouped into two categories:

[1] In-situ Production Methods
[2] Synthetic Production Methods

Both these methods are discussed below:

[1] In-situ Production Methods

In-situ methods produce the candidate fullerenes while regular fullerenes are being synthesized. Although there are numerous methods to produce fullerenes (for instance: RF plasma, Induction heating etc.), there are two efficient and economical methods to produce practical quantities of candidate fullerenes. These are:

a) The Graphite Vaporization Process
b) The Flame Process

THE GRAPHITE VAPORIZATION PROCESS:

The graphite vaporization process was discovered by Huffman and Krätschmer (2). The process consists of electrically arcing electrodes that are rich in graphite, in an inert sub-atmospheric environment. The arc produces carbon vapor and the vapor anneals to form the stable closed caged molecules - fullerenes. If the graphite electrode used in the graphite vaporization process is packed with other compounds, then the arc produces a high temperature vapor that is rich in carbon and other elements. These elements get entrapped during the carbon cage formation process resulting in novel materials such as encapsulated fullerenes. Another factor that leads to the formation of encapsulated fullerenes is the presence of an inert environment. From purely statistical arguments, the presence of helium gas amongst the vaporized carbon atoms creates the opportunity for helium to get entrapped within the cage when the carbon atoms anneal to form a closed cage. This mechanism of formation for helium encapsulated fullerenes ($He@C_{60}$) has already been established by the ingenious experiments of Schwarz et al (3). In summary, the first production method for formation of candidate fullerenes is to co-vaporize carbon with candidate elements of interest and annealing this vapor under conditions that yield practical quantities of candidate fullerenes. MER has already demonstrated this technology by encapsulating numerous elements inside C_{60}.

THE FLAME PROCESS:

The flame process was discovered at M.I.T. by Howard et al (4). This process involves burning benzene with oxygen under fuel-rich conditions in presence of an inert such as helium. The fuel-rich flame yields soot that is rich in fullerenes. The fullerenes so found are expected to entrap helium with statistical probability as discussed above.

The flame process is not convenient if one wants to produce practical quantities of other encapsulated candidate fullerenes. This is so because the flame is a reducing environment. This causes the candidate elements to pre-react and form complexes that are difficult to encapsulate. The flame process also produces many other side products such as poly-aromatic hydrocarbons. The poly-aromatic hydrocarbons are difficult and expensive to separate. For these reasons, the flame process appears unsuited for the needs of this program.

[2] Synthetic Production Methods

Synthetic production methods are an alternative method of producing candidate fullerenes. These methods begin with pure C_{60} and modify C_{60} to desired encapsulated candidate fullerenes. There are two general synthetic production methods for fullerenes:

a) The High Energy Beam Method
b) The Thermal Window Method

a) The High Energy Beam Method

The high energy beam method was discovered by Schwarz et al (3) in 1991. The method involves first producing C_{60} cations, then accelerating these cations into a beam, impacting the beam in a helium cloud, and then finally neutralizing the cation products. The high energy ion beam provides the activation energy required for the helium to pass through the electronic cloud of C_{60} (3,5,6).

The high energy beam method is capital intensive and therefore an expensive production method.

b) The Thermal Window Method

The thermal window method was discovered by Saunders et al (7) in 1993. The method involves heating purified C_{60} with helium. At high temperatures there is reversible break of one or more bonds of C_{60}. The reversible break of bonds opens a window in the fullerene cage which lets helium (and other candidate elements) enter C_{60}. These thermally created windows close when the vapor is cooled. Therefore by properly heating and cooling helium rich C_{60} vapor, candidate fullerenes such $He@C_{60}$ can be produced. Saunders et al (7) report experimental evidence that even at 600 C, a few ppm levels of $He@C_{60}$ can be produced by this method.

The thermal window method is a less expensive method of producing $He@C_{60}$. However, the ppm level yield per pass is very low. Therefore, the thermal window method is practical only when it is coupled with a concentration and purification technology described next.

C. TECHNIQUES FOR VERIFICATION AND CONCENTRATING DESIRED COMPOSITION OF FULLERENE PRODUCED

VERIFYING $He@C_{60}$:

The purity of $He@C_{60}$ and other candidate molecules can be established by mass spectrometric techniques such as Electron Impact (EI) mass spectrometry and Laser Desorption (LD) mass spectrometry. EI mass spectrometry is the most economical method of verifying the composition, but sometimes EI mass spectrometry leads to erroneous results

because of molecule fragmentation. LD mass spectrometry is expensive, but is gentle and provides reliable results.

CONCENTRATING $He@C_{60}$:

The candidate fullerene molecules produced by methods described above are a mixture of fullerenes and encapsulated fullerenes. The large scale purification of encapsulated fullerenes from fullerenes is as yet unknown. However, small amounts of encapsulated fullerenes are routinely separated and purified during verification by mass spectrometric techniques. MER plans to economically scale up the principles of mass spectrometer for separating and purifying practical amounts of $He@C_{60}$ and other candidate fullerenes. The details of the plan is discussed below.

D. PHASE II TECHNICAL APPROACH

MER's technical approach for production will be to sequentially couple the best of the two alternate processes for producing $He@C_{60}$. That is, MER will sequentially couple the in-situ graphite vaporization production method described above with the thermal window method also described above. The graphite vaporization production method has already been demonstrated to produce $He@C_{60}$ (5). The products so obtained from the graphite vaporization reactor will next be processed in a thermal window reactor so as to increase the yield of $He@C_{60}$.

MER's technical approach for purification will be to economically scale up the principles of mass spectrometry so as to purify the $He@C_{60}$ from other fullerenes. This approach will be used because it has the lowest risk of failure (this purification method has been routinely demonstrated for microscopic separation).

E. PHASE II RESEARCH OBJECTIVES

The objective is to produce and verify the candidate fullerenes ($He@C_{60}$) for testing in Phase II. The objective includes establishing the best and the most economical technology for bulk production of the candidate fullerenes. The questions that the Phase II program will seek to answer so as to meet the above Phase II research objectives are as follows:

1. How does $He@C_{60}$ yields change with changes in the helium pressure in the graphite vaporization reactor?

2. What is the relationship between the rate of graphite rod burn to the yield of $He@C_{60}$ in the graphite vaporization reactor?

3. How does total $He@C_{60}$ yields change with changes in the temperature and the pressure of the thermal window reactor?

4. What purification rates and what purities can be achieved in

a commercially available mass spectrometer?

5. What will an economical scale up of a mass spectrometer design?

6. How does the $He@C_{60}$ purity and production rate change with changes in the magnetic field, the ionization rate and the ion beam velocity?

The answers to these questions will establish a reliable bulk production method and will provide sufficient quantities of purified $He@C_{60}$ that will be used for testing.

E. PHASE II RESEARCH PLAN

To achieve the above mentioned technical objectives, MER will conduct a systematic research plan described below. The activities that will be carried out to produce and purify $He@C_{60}$ will consist of:

1. Complete a detailed critical path experimental plan
2. Produce $He@C_{60}$
3. Scale up purification system
4. Purify $He@C_{60}$
5. Determine properties of $He@C_{60}$

Each of these activities are described in detail below.

1. Complete a detailed critical path experimental plan.

Figure 1 shows an overall tentative plan for this program. This tentative program will be supplemented with a more detailed plan that will include each individual task and subtask; and which will have timing and manpower allocated and put into a critical path schedule to aid in accomplishing the ambitious amount of work that is necessary to demonstrate the cited objects and answer the listed questions. We will utilize computer management software Time Line 3.0 to produce Gantt and Pert chart tracking. The output of the program plan is a valuable tool to the effective use or resources and effective planning of scientific programs.

ACTIVITIES	MONTHS 0 4 8 12 16 20 24 26
Complete a detailed critical path experimental plan. (1*)	0 1 ---
Produce He@C_{60} (34*)	0 16 ----------
Scale up purification system (16*)	2 10 ----------
Purify He@C_{60} (24*)	10 20 ----------
Determine the properties of He@C_{60} (18*)	14 20 ----------
Prepare final report (7*)	20 22 -------

(*): Relates percentage of program efforts.

Figure 1

The production and the purification experiments will be statistically designed. This is the most efficient experimental program design and will permit this program to carry out the ambitious objectives and the parallel activities planned in Figure 1. As appropriate, both partial and full factorial designs will be utilized to optimize the production and purification system.

MER has used this program planning and execution in several other SBIR Phase I and II programs, and commercial development programs and thus can take full advantage of this efficient program design and management without development of computerized program management itself. Because of our experience of program planning for the development and production of fullerene molecules that includes buckyballs, buckytubes, doped buckyballs and buckytubes, custom fullerene molecules, we are confident that we can effectively plan the experimental program to produce and purify candidate fullerenes.

2. Produce He@C_{60}

MER will produce the candidate fullerenes in a two step process. First, He@C_{60} will be produced in a helium environment based graphite vaporization process. The product so obtained will be heated in helium in a high pressure, high temperature reactor. The high temperature, high pressure reaction will open thermal windows in C_{60} allowing for helium to migrate inside the cage - facts which have been demonstrated by the work of Saunders et al (7).

MER is well equipped to accomplish this part of the plan. MER pioneered the design and the optimization of a computer controlled fully automated reactor (Figure 2). The reactor has in built provisions to introduce helium during graphite vaporization. The reactor has successfully produced bulk quantities of quality fullerenes for MER's numerous customers. MER's cumulative technical experience with fullerene reactors exceeds 10 man years and therefore, MER is confident of its ability to deliver the candidate fullerenes required by this project.

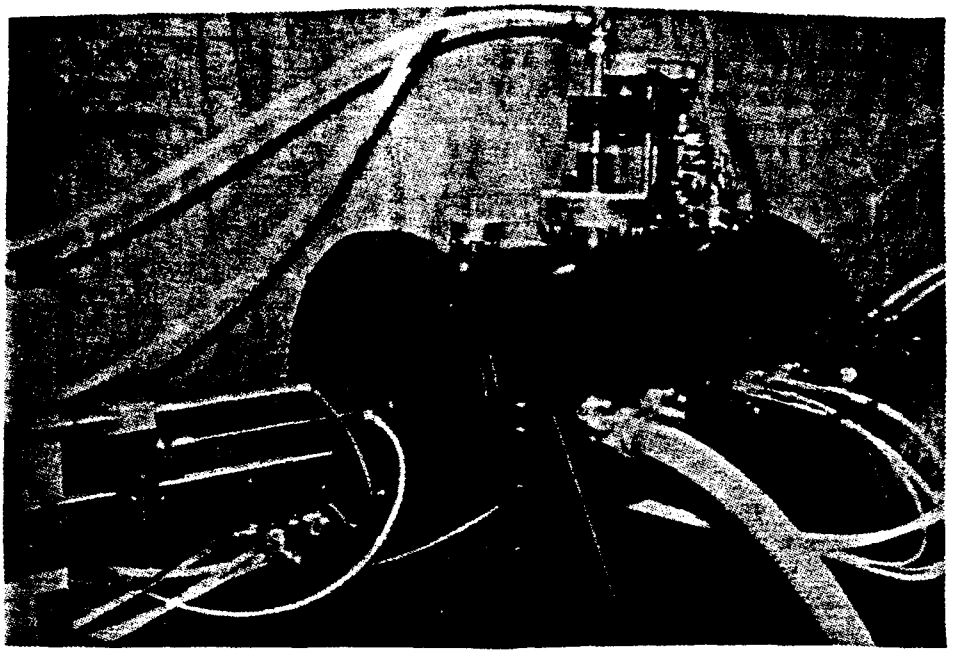

Figure 2. Computer Controlled Fullerene Reactor

For step 2 (thermal window) of the $He@C_{60}$ production process, MER has a state of art, high temperature, high pressure reactor that will be used for the thermal window reaction. This reactor has the capabilities to process large quantities of fullerenes and is therefore ideally suited for the Phase II work.

3. Scale up Purification System

MER will scale up the basic design of mass spectrometer so as to build an economical molecular weight separator. The design equation to be used for the scaling up will include:

1. The force balance equation:

$$mv_f^2/r = Bqv_f$$

where, m: mass of the species to be purified
v_f: velocity of the species
r: radius of the magnetic disc (equipment)
B: magnetic field available, perpendicular to the direction of ions
q: charge of the species that is being purified

2. The energy balance equation:

$$W = qV$$

where, W: Electrical energy required
q: charge of the species that is being purified
V: Ionization Potential of the species being purified

3. The momentum balance equation:

$$v_f = qEt/m$$

where, v_f: design velocity of the species entering the magnetic disc
E: accelerating electrical field
t: acceleration time

MER has the necessary equipment (corona discharger, large magnets, equipment fabrication facilities) to accomplish this part of the plan. The results obtained here will be cross-checked independently by SRI International's SALI mass spectrometry on a purchase order basis.

MER has built and scaled up numerous equipment including the computer controlled fully automated fullerene reactor system and fullerene purification system. The design and scaling up of mass spectrometric principles so as to build molecular weight separator will not be difficult for MER.

4. Purify $He@C_{60}$

MER will purify $He@C_{60}$ in the scaled up molecular weight separator. The quality and the purity of the purified material will be independently re-established using a laser ionization mass spectrometer on a purchase order basis. To keep the experimental expenses low, MER will recycle and repolish unconverted C_{60} so as to produce the desired candidate fullerenes.

5. Determine the properties of $He@C_{60}$

The candidate fullerenes after being purified will be formed into select geometries such as discs, pellets or other shapes. MER has demonstrated the production of fullerene shapes of different diameters, thicknesses and sizes by a unique consolidation of fullerene powder. This technique of forming cohesive solid will be optimized so as to ensure that a controlled density, highly permeable fullerene solid can be reproducibly produced from the candidate fullerene powders. Next, Phase II work at MER will measure various thermochemical and mechanical

properties of the candidate fullerene solid. The density of candidate fullerene powder and formed samples will be measured by Archimedes' principle in accordance with ASTM C373-72 (reapproved 1982). These results will also be confirmed by pycnometric studies uses the helium, argon or nitrogen as the process gas.

The mass density of C_{60} has been reported as 1.72 gm/cc and the volume coefficient of thermal expansion has been reported to be 6.2 x 10^{-5} /K [9]. The thermal conductivity for C_{60} has been measured to be 0.4 W/mK (at 300K).

The permeability of helium through C_{60} solids have not been measured and will depend on the pressure drop available at the cryogenic conditions. MER has a permeability measuring cell and will use it during Phase II to obtain this data for solids formed out of candidate fullerenes. Even though no data is available for helium diffusion through fullerenes, hydrogen and oxygen diffusion through the interstitial sites of fullerenes has been reported by Assink et al [8]. They conclude that oxygen and hydrogen molecules readily diffuse into the interstitial sites of C_{60} and C_{70} fullerenes. Since helium is inert and is smaller than oxygen or hydrogen molecule, the interstitial transport of helium is expected to be superior to either of these gases.

One of the important aspects of developing fullerenes for cryogenic applications is the accurate measurement of thermophysical and mechanical properties in the temperature range of interest.

Cohesive strength is the theoretical summation of different binding energies at the grain boundary. The cohesive strength can be calculated by assuming different arrangement of atoms, interstitial and charge distribution at the grain boundaries and integrating the binding energies involved with each of these arrangement over the total grain boundary area.

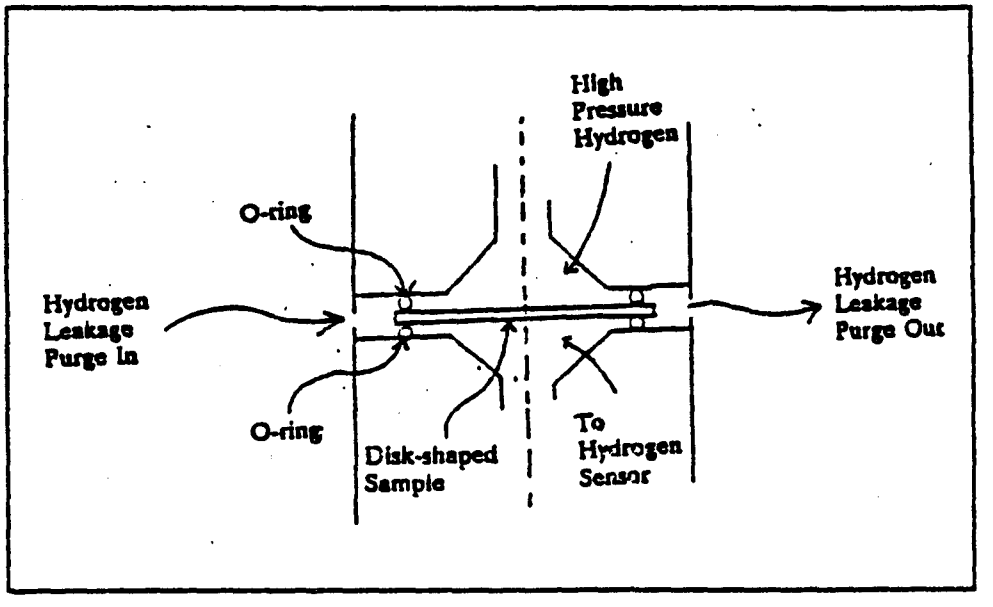

Figure 3. Schematic of helium transport cell.

Permeability of C_{60} will be investigated utilizing a transport cell. The apparatus is built from thick stainless steel (capable of handling >2000psi) and uses disk shaped samples to separate high pressure helium region from an atmospheric region which can be tested for the helium content. The apparatus is shown in Figure 3.

Since there is a possibility of leakage around the o-rings, the apparatus allows for a purge gas to sweep away any leaking gas. The helium transport cell is hooked up to a GC with a detection limit of 100ppb. Permeability of different gases can also be investigated by hooking up the permeation cell to a GC detection unit.

Coefficient of thermal expansion will be measured by a vitreous silica push rod dilatometer assembly in accordance with ASTM-E228-85 (reapproved 1989). The sample will be cooled at a rate of 3°C/min by controlled addition of liquid helium and the linear charges in dimension will be measured by a linear-variable differential transformer.

Thermal conductivity, being a transport property, is more difficult to determine reliably. Direct measurement of thermal conductivity can be made by comparative techniques involving contacting and coupling it with a standard samples in the temperature range of -150°C to around 300°C. However direct thermal conductivity measurement is not very accurate, so the data is generally obtained indirectly from experimental measurement of thermal diffusivity and specific heat. The thermal diffusivity is measured by supplying a high intensity, short duration pulse of thermal energy to one face of the specimen followed by measuring the resulting temperature rise as a function of time on the other face. The thermal diffusivity has been measured using a laser flash at VPI and Xenon lamp flash at ORNL at temperatures ranging from RT to 1200°C. The specific heat of the sample will be measured utilizing a standard differential scanning calorimeter at VPI. The thermal conductivity, K, can thus be calculated from the measurements of thermal diffusivity α, specific heat Cp, and bulk density S, by using the relationship $K = \alpha \rho Cp$.

References:

1. Kroto, Smalley, et al. *Nature*, 318, 162 (1985).
2. Krätschmer et al. *Nature*, 347, 354 (1990)
3. Schwarz et al. *Angew. Chem. Int. Ed. Engl.*, 30, 884 (1991)
4. Howard et al. *Nature*, 352, 139 (1991).
5. Caldwell et al. *J. Am. Chem. Soc.*, 114, 3743 (1992)
6. Ross and Calahan, *J. Phys. Chem.*, 95, 5720 (1991)
7. Saunders et al. *Science*, 259, 1428 (1993)
8. Assink et al, J. Mater. Res., Vol 7, No 8 (August, 1992)
9. Dresselhaus et al, J. Mater. Res., Vol 8, No 8 (August, 1993)

DISTRIBUTION LIST

AUL/LSE Bldg 1405 - 600 Chennault Circle Maxwell AFB, AL 36112-6424	1 cy
DTIC/OCC Cameron Station Alexandria, VA 22304-6145	2 cys
AFSAA/SAI 1580 Air Force Pentagon Washington, DC 20330-1580	1 cy
PL/SUL Kirtland AFB, NM 87117-5776	2 cys
PL/HO Kirtland AFB, NM 87117-5776	1 cy
Official Record Copy	
PL/VTPT/Brian Whitney	2 cys
Dr. R. V. Wick PL/VT Kirtland, AFB, NM 87117-5776	1 cy